Doctoral Dissertation

On relationships between lightning and observed phenomena and activities in thunderstorms, typhoons and volcanoes

(雷放電と積乱雲、台風、および火山活動の関係に関する研究)

A DISSERTATION
SUBMITTED TO THE DEPARTMENT OF COSMO SCIENCES
ON GRADUATE SCHOOL OF SCIENCE OF HOKKAIDO UNIVERSITY
IN PARTIAL FULFILLMENT OF THE REQUIREMENTS
FOR THE DEGREE OF THE DOCTOR OF SCIENCE

Purwadi

Planetary and Space Group
Department of Cosmoscience
Graduate School of Science
Hokkaido University

September 2020

Dedication

to my parents

Kartini and Zainuri

to my wife

Puji Utami

and to my sons

Delta and Theta

Abstract

Thunderstorm clouds may cause hydro-meteorological hazards such as torrential rainfall causes flood, hail, tornadoes, and CG lightning stroke. However, the existing thunderstorms observation method, such as weather radar, cannot grasp the physics behind heavy precipitation. A previous study mentioned that lightning is a good proxy for thunderstorm clouds severe weather[4]. Zipser, 1994, mentions that the occurrence of lightning in a thunderstorm requires strong updraft (7 m/s) at a temperature colder than 0°C to -20°C[27]. Observing the early thunderstorms cloud evolution at a temperature colder than 0°C can be conducted from space and possible to use to predict the final result of thunderstorm clouds. So, the combination of ground-based lightning detection networks and thermal infrared sensor(TIS) sensor cameras from space is suggested. This study evaluates the correlation between lightning and other thunderstorm parameters and suggests a precise methodology for those combination thunderstorm observations.

During the Understanding of Lightning and Thunderstorm (ULAT) Project and e-Asia Joint research Project, 2017 to 2020 FSY, some VLF receiver called V-POTEKA has been manufactured by Meisei Company-Japan and developed together with Hokkaido University. During this period, V-POTEKA was deployed to observe cloud to ground (CG) lightning in Asian countries called AVON. Moreover, V-POTEKA was deployed in Philippines to cover lightning observation in that country called Nationwide Network. V-POTEKA networks has been test and operated and shows the ability to detect the lightning phenomena in the target area. The comparison of the lightning geolocation estimate by the V-POTEKA lightning detection networks and Blitzortung shows the relative distance 35km and 37 km for the Nationwide Network and AVON.

The relationship between lightning and other thunderstorm cloud characteristic such as cloud top temperature (CTT), cloud top height (CTH), and precipitation has been conducted using AVON lightning data and static grid method. The result shows that CTT, CTH, rain rate, and precipitation volume (PV) is logarithmic function of CG lightning event. The result also agree with the previous work which mention that the total lightning is exponential function of CTH. During the operation, the V-POTEKA Nationwide Network in Philippines detects the lightning produce by Taal Volcano eruption on January 12th, 2020. The development of Taal Volcano eruption cloud ash is detected using Himawari 8 band 15 (12μm) and performed in 2D and 3D. The temporal evolution of the cloud ash shows the maximum cloud growth speed is ~50 m/s at around 07:00 to 07:10 UTC which closed to big explosion time ~15:00LT (07:00 UTC). The first CG lightning detected by V-POTEKA Nationwide Network occur at 07:47:25.15725 UTC. 34 CG lightning are detected by V-POTEKA Nationwide Network during the Taal Volcano eruption on January 12th, 2020.

Moreover, The study of correlation between lightning and maximum sustainable wind speed has been conducted using new technique for the first time in the world. The lightning is assumed to be proportional to the energy and the wind to be the carrier of the energy input. We did the back-tracing of the 60 point in radius 100 km to the typhoon eye. The speed and direction is taken from the ERA5 reanalysis at the pressure level 1000 to 400 with spatial resolution 0.25°x0.25°. We calculate new point with interval time 30 minutes with the speed and direction updated to be the closest place and time. The lightning data detected by Blitzortung is counted using the back-tracing point windows with interval time 6 hours. The result of this study shows, the wind in level 900 Mb is to be the most reasonable path to carry the energy to the typhoon Trami from place with the distance-time 36 hours to 48 hours from the typhoon Trami eye. The lag time in the maximum cross-correlation value between reaching center time and increasing maximum wind speed is 6-12 hours, which is assumed to be the conversion time of energy from latent heat to the kinetics energy.

Thermal infrared sensor (TIS) camera has been developed by Hokkaido University and will be installed in LAPAN-A4 micro satellite. The LAPAN-A4 micro satellite is planned to be launched in third quarter of 2020 and orbit the earth at 500 km height. In LAPAN-A4 orbit, the Hokkaido University (HU) TIS camera will have better earth surfaces spatial resolution than existing geostationary satellite and the early formation of thunderstorm cloud can be conducted more detail than before.

Acknowledgments

Many people have been supported to finish this dissertation, and all of them deserve many thanks.

First, I would like to thank Professor Yukihiro Takahashi for the opportunities to join his e-Asia research team. I would like to express my great appreciation for his respectful guidance with boundless enthusiasm during this study. The great thanks also for my boss, Dr. Tri Handoko Seto, and Mr. Erwin Mulyana, who had selected me to take this challenge.

The special thanks to Mrs. Eriko Momota, who have supported me since I was in Indonesia and during the study in Japan. I would also like to express my appreciation to Dr. Mitsuteru Sato and Dr. Hisayuki Kubota for quality discussion and suggestions on this study. I would like to thank Dr. Kozo Yamashita for the first guidance to estimate the lightning geolocation. Furthermore, I would like to give heartfelt thanks to Dr. Junichi Kurihara and Mr. Shigeyuki Komatsubara for their help in thermal infrared sensor camera testing and calibration.

I give heartfelt thanks to Mr. Findy Renggono, Dr. Halda A. Belgaman, and BPPT team for the kind support from Indonesia. I would also like to express my sincere appreciation to Mr. Arif Saefudin and his team for warm communication.

The special thanks to my friend Yuuki Sato for supporting me since I come to Sapporo.

Finally, I would like to say many thanks to everyone who cannot I mention one by one on this page.

PURWADI

Sapporo, Hokkaido

This research was supported by Japan Society for the Promotion of Science (JSPS), Core-to-Core Program, B. Asia-Africa Science Platforms, by Japan Science and Technology Agency(JST) together with Technology and Higher Education(RISTEKDIKTI) of the of Indonesia under the e-ASIA Joint Research Program, and by Japan International Cooperation Agency (JICA) and JST, SATREPS.

Contents

List of Tables

List of Figure

Chapter 1
Introduction

1.1. General

Hydrometeorological disaster is a natural phenomenon related to atmospheric layers, hydrology, and oceanography. This disaster can endanger, damage, and cause loss of life. This hydrometeorological disaster is a disaster that includes floods, landslides, whirlwinds, hail storms, snowstorms, drought disasters, torrential rains, very heavy snowfalls, and others. Due to global climate change, these natural hazards are expected to rise. Floods affect every country and cause more fatalities and property damage than any other type of sudden-onset hazard. In addition to causing injuries and deaths, floods can disrupt water purification and sewage disposal systems and cause toxic waste sites to overflow. Floods affect some hundred millions of people and their livelihoods and claim thousands of lives annually worldwide. Hurricanes, cyclones, and typhoons are severe storms that form over tropical water. Windstorm-related events worldwide cause an average of 30,000 deaths and US$ 2.3 billion in damage each year[1].

Thunderstorm cloud is one of the natural phenomena which can cause the torrential rainfall to cause flooding and SST, which is the majority disaster in Indonesia, as explained in figure 1.1. Not only torrential rainfall and SST, but the thunderstorm cloud is also dangerous because of its cloud to ground (CG) lightning stroke, causes strong wind, and hail. The dangers of the thunderstorm cloud not only happen in Indonesia, but it can happen in other places in the world. Brooks, 1925, estimated around 1,800 thunderstorms are occurring at any one time around the world[2].

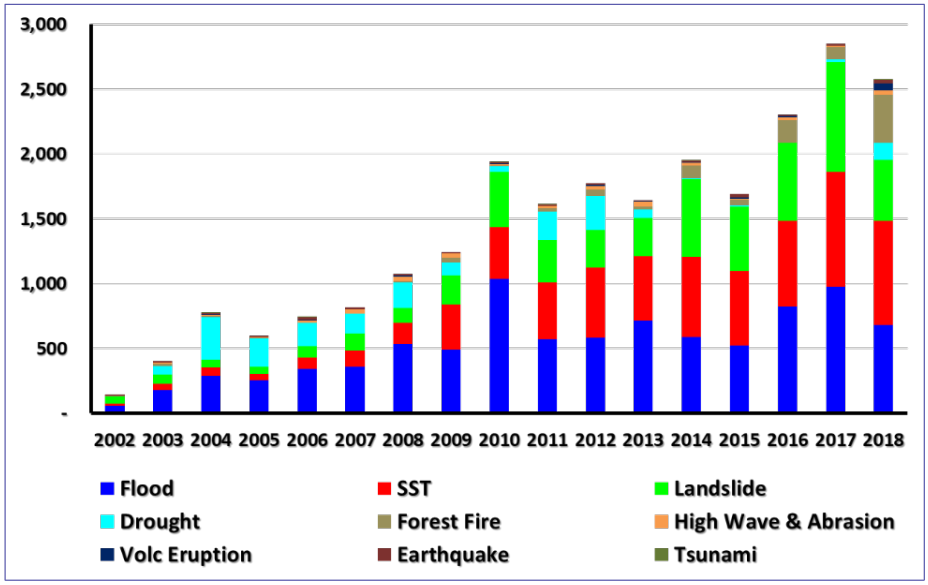

Figure 1.1. Disaster trend in 2002 - 2018 in Indonesia.
(source: National Disaster Management Agency (BNPB) of Indonesia, dibi.bnpb.go.id)

Generally, the thunderstorm cloud, also known as cumulonimbus, is described by the largest and most convective vigorous in the atmosphere [3]. Previous research has been conducted to understanding the behavior of thunderstorm cloud, namely the formation, dynamical processes, and the hazardous of the thunderstorm cloud [3-7]. Many study also has been conducted to characterize the thunderstorm cloud based on location, and seasonal variation[7, 8].

Most of the previous thunderstorm study has been conducted using weather radar [8]. A weather radar is a useful instrument for observing the clouds particle, such as precipitation, hail, snow, and motions. However, the physics behind how radar works, called range folding and attenuation, causes the limitation to grasp the thunderstorm parameter behind the heavy precipitation inside the thunderstorm cloud[9]. So, through this study, we are going to propose a new methodology for understanding the thunderstorm clouds.

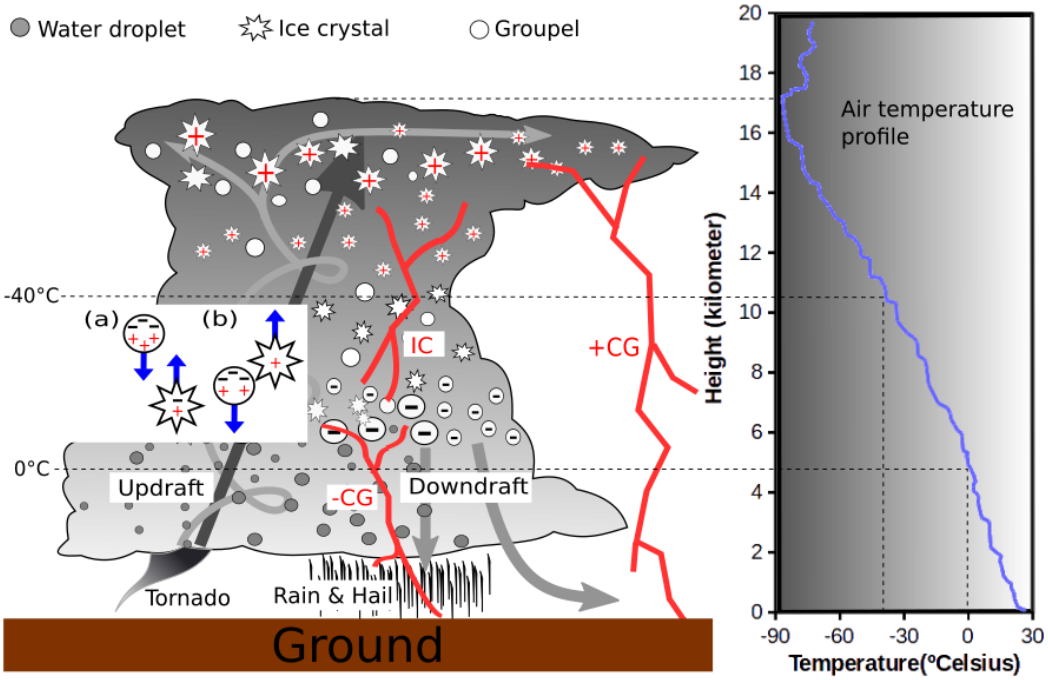

Figure 1.2. Schematic of thunderstorm cloud parameter and its severe weather's

Lightning is one of the characteristics of a thunderstorm cloud that can be detected from far away, either from other parts of the earth or space[10-13]. The lightning produce by the thunderstorm cloud emits electromagnetic waves in broadband. Very low frequency (VLF; 3-30kHz) is one of the electromagnetic bands emitted by lightning cloud-to-ground (CG) lightning return stroke, which can be propagated using radio instrumentation in the distance thousands of kilometers[12,13]. Previous researchers denoted a significant proportional correlation between lightning activity frequencies and heavy rainfall [14-16]. Seity et al., 2003, concluded that the number of CG activities had a good correlation with hail and graupel events, and that was indicated by weather radar echo more than 35dBZ[17]. Some studies also mention that the peak of CG lightning activity occurs a few minutes before the surface rainfall [8,14]. Other related researches re-emphasized a notable correlation between lightning activities (Intra cloud/IC+CG) to severe weather such as high wind, hail, and tornado [18-20]. The number of lightning

around hurricanes (typhoons) has a strong correlation with maximum sustainable wind speed with the lag time 1 or 2 days[21,22].

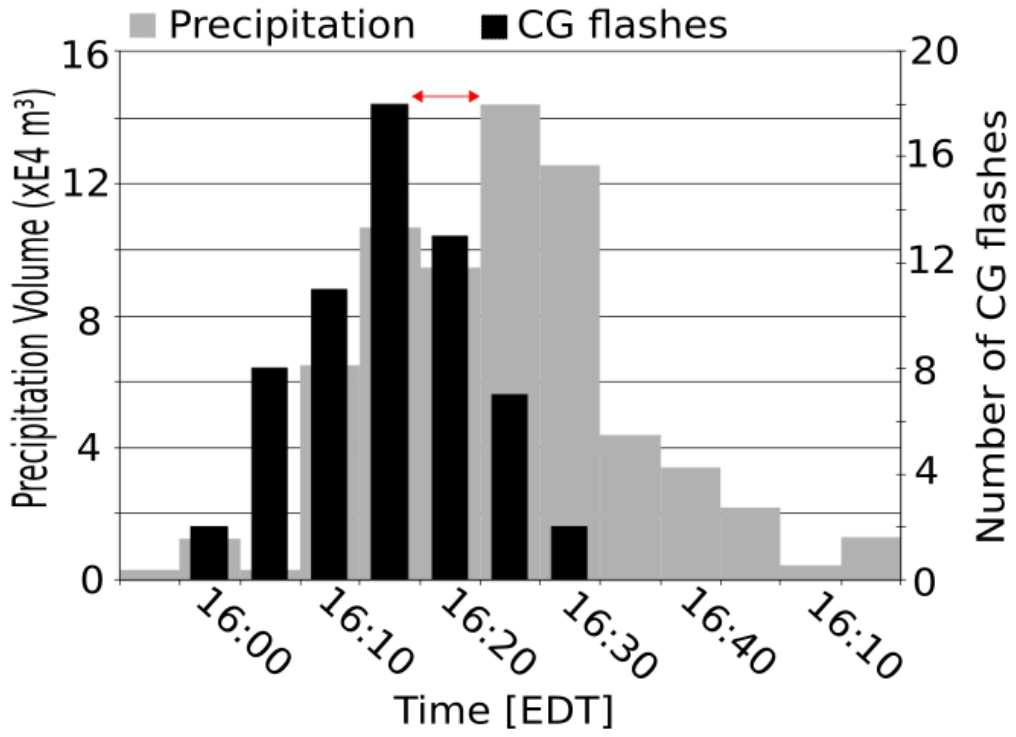

Figure 1. 3. Peak CG lightning leading the peak of surface rainfall. Gungle et al., 2010.

Lightning sometime also occurs in some phenomena such as during volcanic erruption. Volcanic Lightning is common for the volcanic during eruptions, which has potential information about the physical processes taking place during explosive eruptions, especially at under-monitored volcanoes. Volcanic plumps differ from thunderstorm clouds in the presence of tephra volcanic, aerosol, and gas content, as well as temperature profiles and convection methods. The addition of silicate particles plays another electrification mechanism. Besides, initially higher temperatures, seen in the close ventilation section of volcanic fur, inhibit the development of graupels. Then, the mechanism of ice filling becomes important to

boast of lightning, which develops in the upper regions of the volcanic plume, where sub-freezing temperatures can increase ice formation [23-25].

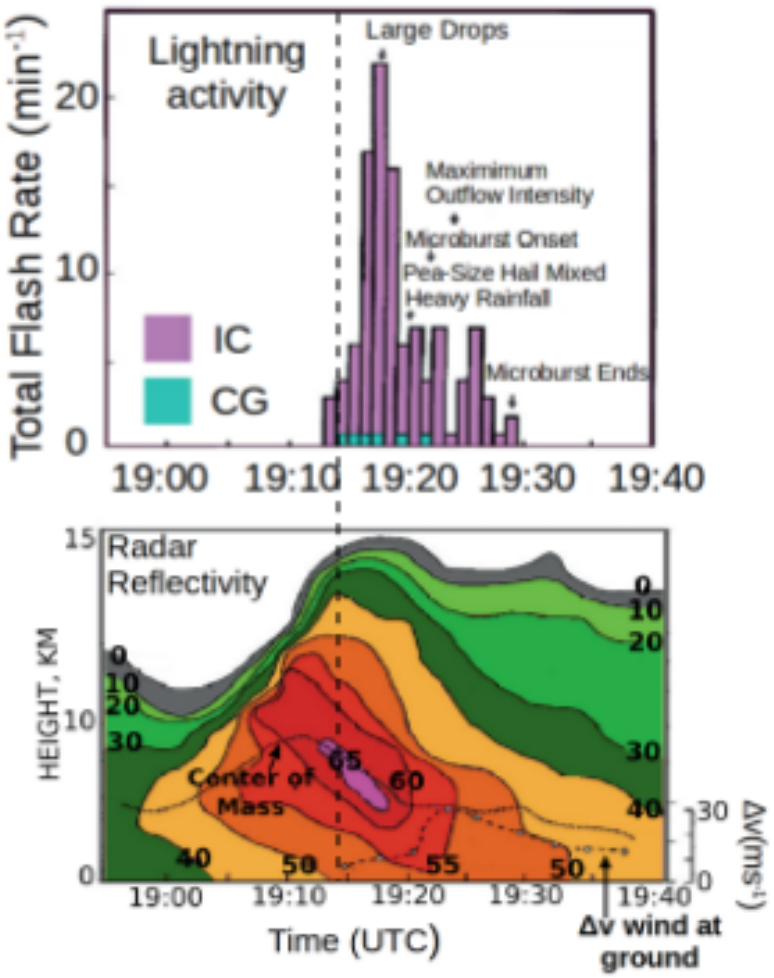

Figure 1.4. Lightning activities are related to thunderstorm updraft intensities, storm growth, and decay. The CG lightning start occurs when the growth of the thunderstorm cloud almost reach the maximum height. Gatlin et al., 2010.

A thunderstorm cloud can be identified as a large and tall cloud. Some study has been done to classify and estimated the height of the clouds using the meteorological satellite image[26-29]. The thermal infrared sensor (TIS) image was

proposed to identify the cloud top height (CTH) using brightness temperature different (BTD)[29]. However, we use a simple method to estimate the CTH using the TIS data for this study. Assuming the surface temperature of the cloud will create an equilibrium with the surrounding temperature which the temperature drops in the troposphere. Thus, the surface temperature of a cloud can reflect its height. The colder clouds mean the higher clouds. So, by measuring the surface temperature and assuming that the cloud surface follows the atmosphere temperature profile, the cloud height could be estimated. Cloud growth speed can be estimated using CTH estimation in some interval time. By estimating the growth speed in the early formation, the thunderstorm cloud can be differentiated to other cloud types such as the cirrus cloud. Moreover, additional lightning data could make the thunderstorm cloud easy to identify. So, the combination observation, lightning, and thermal infrared camera, is suggested to be the alternative or complimentary for the general thunderstorm observation method.

Existing the thermal infrared camera onboard on geostationary satellite such as Himawari 8, with time resolution 2.5 minutes for Japan Area and 10 minutes for full disk, and the 2 km spatial resolution is enough to study the thunderstorm cloud. Nevertheless, 2 km spatial resolution is not enough for thunderstorm hazard alert application, because of the detail information in the early thunderstorm cloud formation in the size of 4-5 kilometers cannot be well extracted. Micro satellite in low earth orbit (LEO) could provide better spatial resolution than existing geostationary satellite. So in this study, we are going find some suggestion method for the next application thunderstorm observation using ground lightning detection network and thermal infrared camera onboard on a microsatellite.

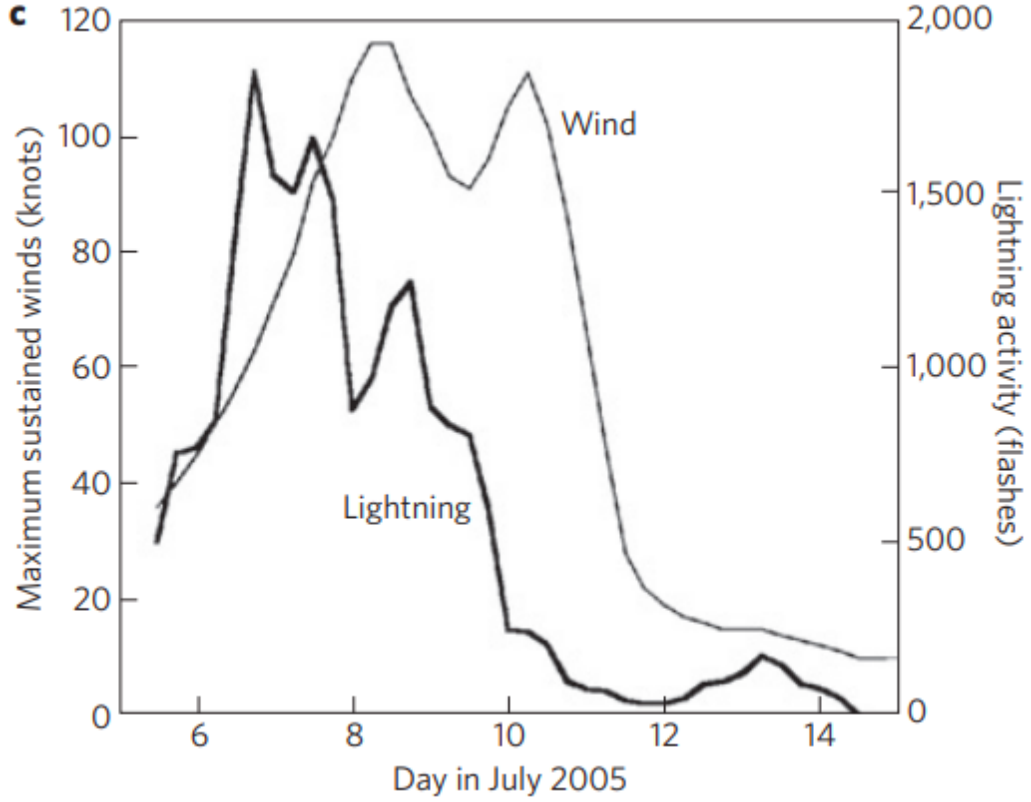

Figure 1. 4. The maximum sustained winds (solid thin curve) and the observed lightning frequencies within a 10◦ ×10◦ gridbox centred on the eye of the storm (solid bold curve). Price et al., 2009.

1.2. Thunderstorm cloud and Lightning

A cloud is a result of a condensation process described as a collection of drops of water or small ice crystals. The process of cloud formation and precipitation is a series of processes consisting of dynamic processes and microphysical processes. The dynamic process includes air motion, which provides general conditions for cloud formation. In contrast, the micro-physical process is the process of forming individual grains through steam condensation and growing by interactions between

individuals. Moisture content in the atmosphere depends on the evaporation process with the requirement that there is a source of water vapor on the surface; there is an energy source for the removal process and atmospheric conditions. The temperature difference in the air package and its environment will affect the density of the air parcel, affecting the buoyancy. When the air moves up and decreases the air pressure, the air expands, and the temperature drops. Clouds form when an air packet containing water vapor moves vertically and experiences cooling and condensation. The point at which clouds form is known as the lifting condensation level (LCL), which is the basis of the cloud.

Generally, the LCL is within 1000 m of the Earth's surface, and substantially lower than the altitude of the 0ºC isotherm, typically 4000-5000 m above ground. Consequently, the vast majority of clouds form at temperatures above freezing and consist entirely of liquid droplets. The weight of the evidence shows that such clouds are not strongly electrified and rarely produce lightning[6].

Numerous observations in many geographical locations disclose that thunderstorm clouds must extend at least 2-3 km into the sub-freezing portion before the first lightning is observed[6]. This observation is consistent with the thunderstorm cloud electrification mechanism. The fiction and collision between ice crystal and cloud droplet or other smaller particles are suggested to be the source of the electrification mechanism. Therefore, cloud dynamics has thus an important role and can be correlated within the electrification process. [3] stated that the cloud's electrification process occurs when the cloud reaches the freezing level, with cloud growth speed reaching more than 8 m/s. Zipser, 1994, mentions that the occurrence of lightning in a thunderstorm requires strong updraft (7 m/s) at a temperature colder than 0 to -20 C[30]. Deierling and Peterson [2008] show that time series of updraft volume in charging zone with vertical velocities higher than either 5 or 10 m/s have a clear relationship with total lightning activity (IC and CG) for 11 thunderstorms in United State (r=0.93)[31].

Lightning occurs due to static displaced that is large enough on certain sides of the cloud, giving rise to different potential on several sides of the cloud, both with

several sides inside the clouds, clouds against other clouds, also clouds against the earth. Generally, lightning is divided into three categories, namely: intra-cloud (IC), cloud-to-cloud (CC), and cloud-to-ground(CG). The negative cloud to ground (-CG) is 90% of global CG lightning, meanwhile positive cloud to the ground is 10%[32].

Lightning emits different electromagnetic waves due to different processes in the discharge, which can either be low or high the scale of which is from the Hz scale to several hundred MHz [33, 34]. The process that started the lightning is much like ladder steps in finding the release path. In this process, lightning emits Very High Frequency (VHF) electromagnetic waves, and the lashed-out lightning happened when the electromagnetic potential difference reached the released target, either be it the earth's surface or another cloud. The last few steps of the stepped-leader, the onset of a connecting discharge, and the beginning of a return stroke. The return stroke of CG lightning emits electromagnetic radiation in range VLF(Very Low Frequency, 3kHz-30 kHz), LF (Low Frequency, 30 kHz-300kHz), and ELF (Extremely Low Frequency, 3Hz-3 kHz). This range of frequency determines the distance of propagation and the type of antenna. Higher frequency is more attenuated, resulting in the weak signal in far from source and may cause difficulty in detecting it by radio instrumentation.

VLF electromagnetic wave emitted by lightning cloud-to-ground (CG) lightning return stroke can be propagated using radio instrumentation in the distance up to thousands of kilometers[12,13]. Two components of electromagnetic waves, namely vertical (electric field) and field horizontal (magnetic field) can be propagated using a dipole antenna and loop antenna, respectively. The estimated location of lightning using electromagnetic propagation can be determined by Direct Finding (DF), Time of Arrival (ToA), of the combination[4, 5, 6], while DF needs two component of magnetic field data. For this study, we will use the dipole antenna to detect the electric field emitted by CG lightning stroke in the VLF range and estimate the lightning location using ToA method.

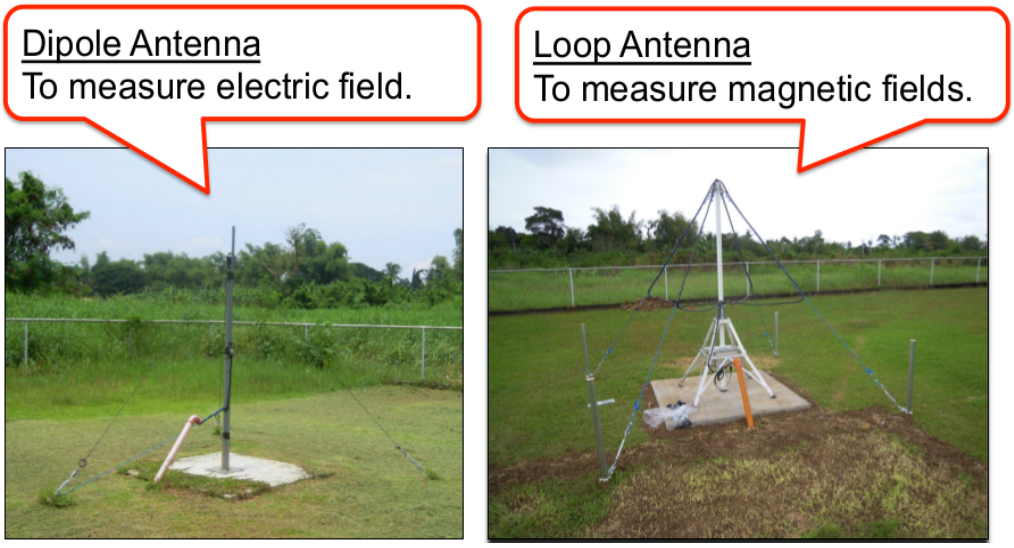

Figure 1.. Dipole anttenna (left panel) and lood antenna (right one) installed in Los Banos, Phillippines[35]

1.3 Cloud imaging

General important topic in analyzing the meteorological satellites data is detection of the cloud, cloud classifying, and estimating the cloud physical parameter. Cloud top temperature and height is the cloud physical parameter which important to detecting the thunderstorm clouds. Thunderstorm cloud are characterize as the tall clouds with the rapid changing of height before reach the maximum height. Lutz, 2003, suggest to use TIR and brightness temperature different to estimate CTH[26]. Hamada et. al., 2008 used split-window and probability density function (PDF) method to determine cloud type from infrared image at 10.8 μm and at 12 μm wavelength using fifth Geostationary Meteorological Satellite (GMS-5) [22]. Further, Hamada et. al., 2010 estimated cloud height using same wavelength but from different satellite which is Geostationary multifunctional transport satellite (MTSAT-1R) [26]. Meanwhile [27] measured cloud height using infrared image from Feng Yun 2 (FY2) satellite and compared it with weather radar data.

1.4. Purpose of this thesis

Previous researches show that the lightning is a good proxy of severe weather such as torrential rainfall, hail, microburst, and the lightning it self [19]. Some studies also show that lightning data is possible to use to predict the maximum wind speed of tornadoes. However, the actual observation of the thunderstorm clouds evolution method has some limitations. Range folding causes the phenomena behind high particle density inside the thunderstorm cloud can not be seen by the Doppler radar. Recent satellite imagery technology has been rapidly developed to contribute to thunderstorm observation but still not find established methodology. The combination observation using a ground-based lightning detection network and thermal infrared camera sensor (TIS) onboard micro satellite is suggested as an alternative or complementary of the existence thunderstorm observation method. TIS onboard micro-satellite is suggested to improve the spatial resolution of the geostationary satellite.

In this study, we evaluate the relationship between CG lightning with other thunderstorm characteristics such as the cloud top temperature (CTT), cloud top height (CTH), and rainfall. This evaluation is intended to get suggestion methodology which applicable for real-time thunderstorm monitoring using ground lightning detection network and thermal infrared camera onboard on a microsatellite. For this study, we use the lightning data estimated by AVON. AVON data provides lightning location data, which can be used to estimate the thunderstorm cloud's location. The Himawari 8 band 15 (12μm) provides CTT data, which can be converted to CTH using the radiosonde data. Meanwhile, we use TRMM precipitation data standard V7 to indicate the final result process of thunderstorm clouds. We use the grid method to process the whole data.

The Taal volcano in Batangas, Philippines, erupted on January 12th, 2020. During the eruption, the Taal volcano cloud ash produces lightning. The V-POTEKA Nationwide network, established during Understanding Thundestorm and Lightning (ULAT Project) and eAsia Joint Research Project (eAsia JRP) in the Philippines,

detects the VLF signal emitted lightning produce by Taal volcano cloud ash. We use the Himawari 8 band 15 (12μm) to get the evolution information of the clouds to ash, such as the growth speed and the size of the cloud ash. The study case of this Taal volcano eruption on January 12th, 2020 gives brief explanation of the cloud growth evolution related with CG lightning occurrence.

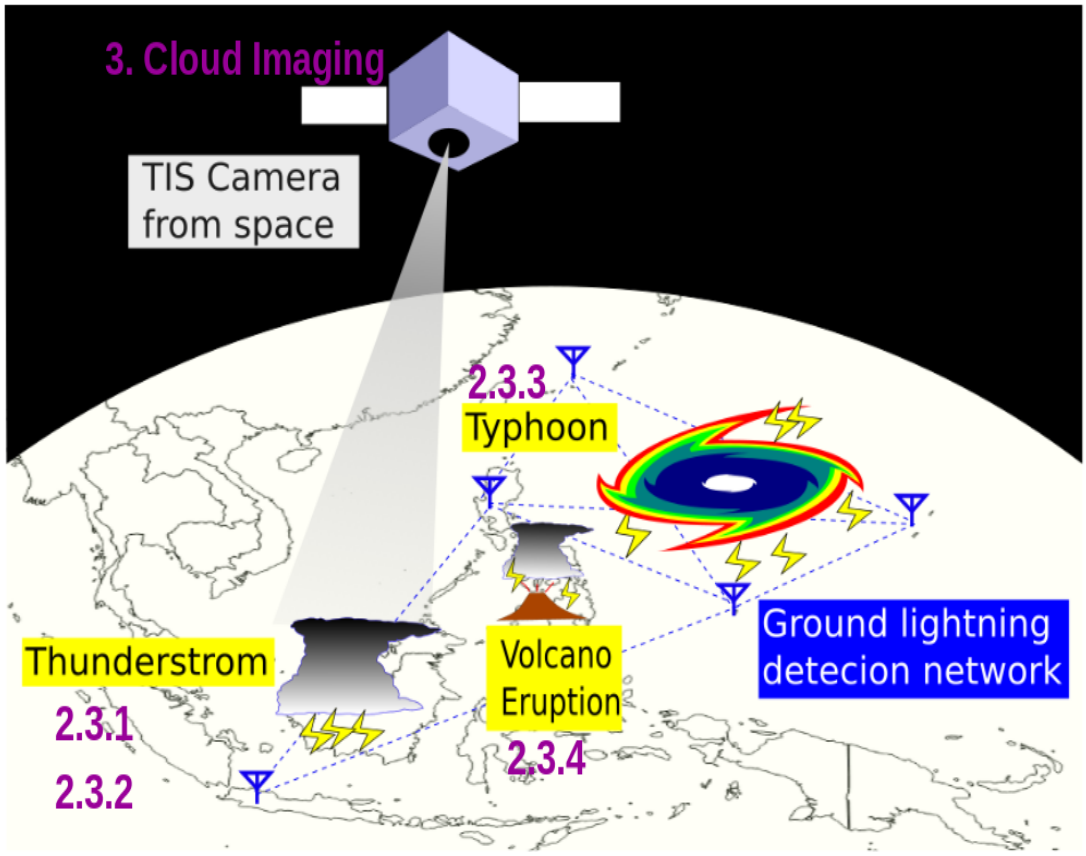

Figure 176. Schematic of the scope of this study

We also introduce the new methodology in understanding the correlation between lightning and the maximum sustainable wind speed using the back-tracing technique. Typhoon Trami, which occurred from September 20th to October 1st, 2018, is taken as a case study. We use the Blitzortung lightning data, which is

assumed to be proportional to latent heat energy. The ERA5 reanalysis data in different pressure levels is assumed as the energy carrier. In this study, we will search for the best level of the wind to be the carrier of latent heat energy. The purpose of this study also to search the most reasonable energy source location of the typhoon.

On the other hand, we develop the thermal infrared sensor (TIS) camera with the specs to understanding the early formation of the thunderstorm cloud, which will be installed in the LAPAN-A4 microsatellite. Some environmental testing, namely vibration test, vacuum chamber test, thermal chamber test, and EMC, is applied to the TIS camera. The environmental test is to represent the real condition during the storing, launching, and operation. Surviving against this test shows the TIS camera will survive in the real condition, which will be passed. The LAPAN-A4 is planned to launch in the third quarter of 2020. The LAPAN-A4 will be used in the real-time monitoring of thunderstorm clouds combine with the ground lightning detection network. So, overall of this study becomes the initial study to create some proposal method to apply in the real-time monitoring of thunderstorm cloud applications using ground lightning detection networks and thermal infrared camera onboard on micro-satellite.

Chapter 2

Lightning

2.1. Introduction

In this study, we used the VLF receiver manufactured by Meisei Company-Japan and developed together with Hokkaido University to detect the electromagnetic field emitted by CG lightning. Based on the sampling frequency, there are two types of VLF receivers produced by Meisei company, namely 100µs dan 10µs, as shown by figures 2.1 and 2.3, respectively. Besides that, both types also have different data formats, which will be explained in sub chapter 2.2. The VLF receiver can be and mostly combined with automatic weather stations (**Po**int **Te**nki **KA**nsoku = POTEKA), so it is called V-POTEKA.

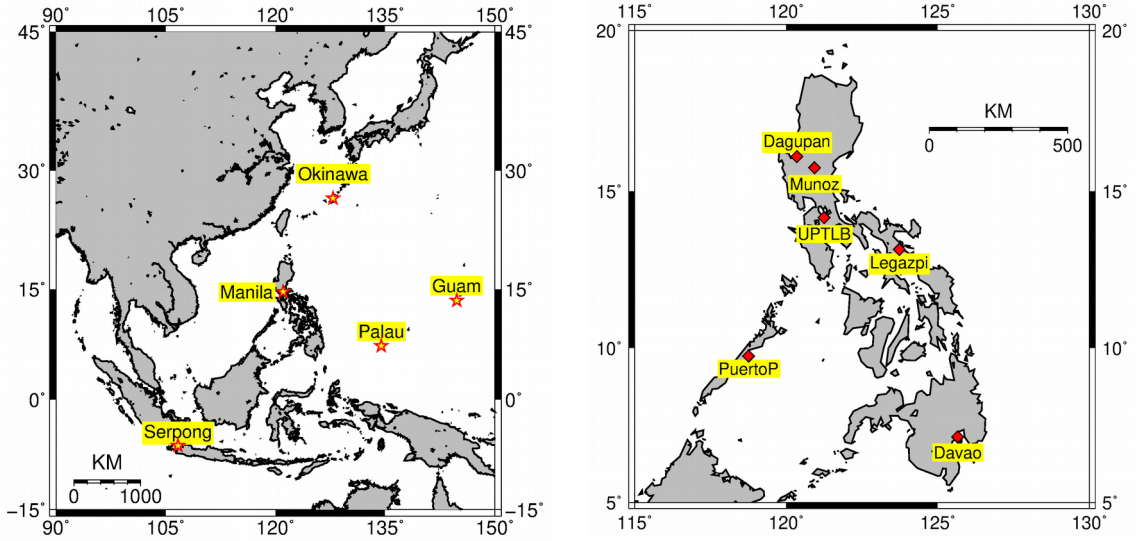

Figure 2.0. AVON with V-POTEKA instrument (left) and Philippines Nation-wide Network (right)

Generally, the VLF receiver-type of V-POTEKA consists of a dipole antenna, solar panel, and power and communication box. It has 3G communication for sending the data to the server every minute. Furthermore, every instrument is synchronized by the GPS clock, which makes the data sent to the server have standard time. This will increase the accuracy in carrying out the geographic estimation location of lightning.

During the ULAT Project and e-Asia Joint Research Project (2017 to 2020 FSY), V-POTEKA has been installed in the northwest Pacific, the Philippines, and Indonesia. We have evaluated the performance of several devices installed, including the number of files sent, the number of signals detected, the ratio of amplitudes between stations, and the attenuation of the signal as a function of distance. The statistical study comparing with the clouds' position show that the results of the geolocation of lightning have the best accuracy of ~ 30 km for the AVON V-POTEKA. By the simulation, we also show that geolocation error and sensitivity are different for each place due to systematic problems.

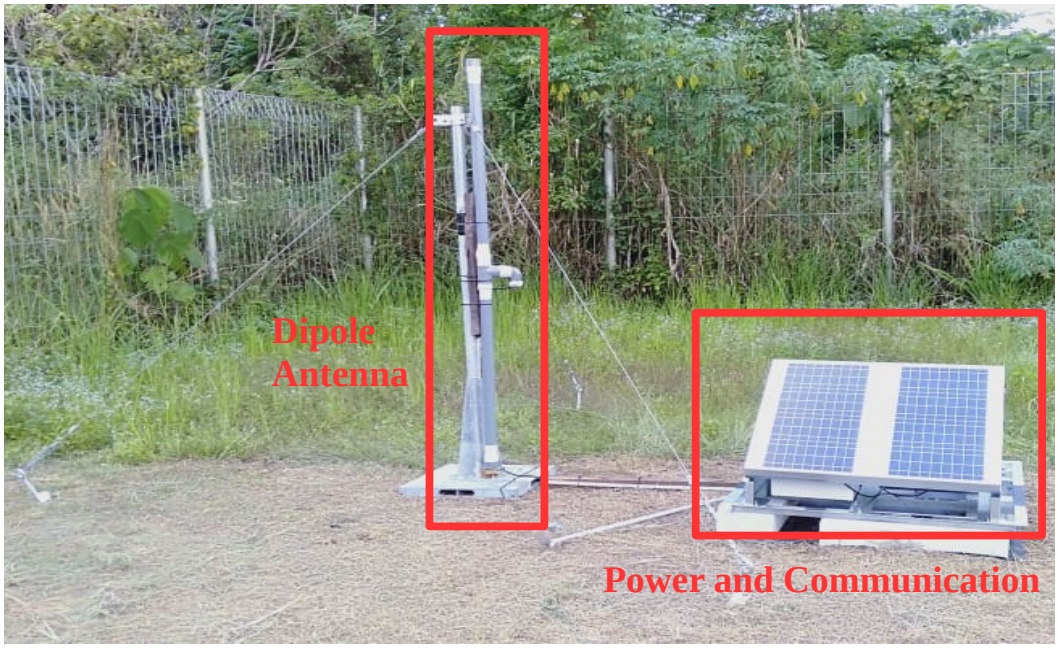

Gambar 2.1. V-POTEKA installed in Serpong

Several natural phenomena analysis has been carried out using the AVON lightning network and Philippines Nation-wide networks. In this study, we have used the lightning geolocation estimation results for several analyzes, such as the correlation between lightning, cloud growth, and rain intensity, diurnal lightning variations in Kalimantan, Taal volcano eruptions, and typhoons analysis.

2.2. Instrumentation

2.2.1. AVON (V-POTEKA-100µs)

The AVON instrument, manufactured by Meisei Company-Japan, uses dipole antennas to detect electric fields emitted by return stroke of CG lightning. This type is now intended to cover the Asia region. So, this lightning detection network is called the **A**sia **V**LF detecti**o**n **N**etwork (AVON). This instrument works with a bandpass filter with a frequency range of 1 to 40 kHz and sampling data frequency 100µs. For the data storage efficiency, when the signal exceeds the threshold, it takes some parameters, namely amplitude positive peak (APP) at the time positive peak (TPP) and negative amplitude peak (APN) at the time negative peak (TPN), as illustrated by figure 2.2. The event trigger threshold of each station is set as a fixed value.

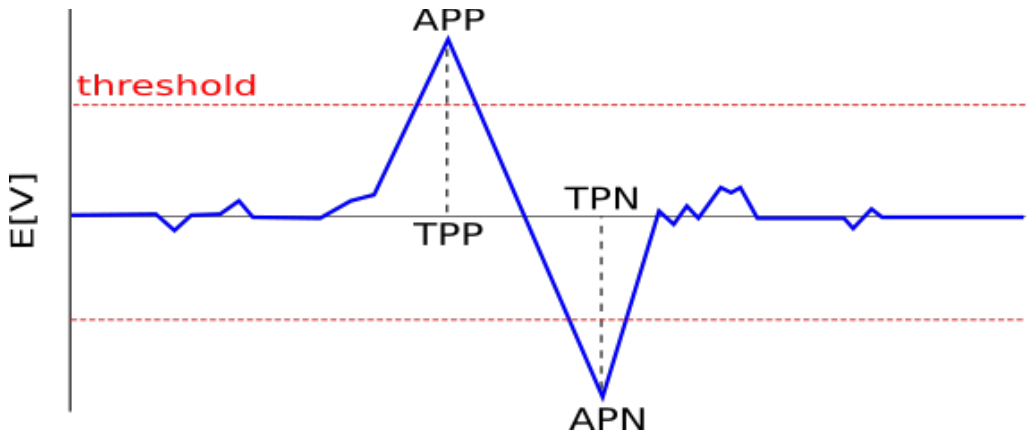

Figure 2.2. Schematic AVON V-POTEKA sampling data illustration

The parameters is recorded every minutes in a file with the file format name "*event_stationNumber_yyyymmddHHMM.csv"* (example: event_00064919_202004040938.csv). Format of the event data in the file is as follow:

stationNumber,EVNT,AMECA_01,yyyymmddHHMMSS,01,E,TPP value,APP value,TPN value,APN value,PTP 1,GPS 1,VTR 000200

example:

00064919,EVNT,AMECA_01,20200302014959,01,E,TPP 04384,APP 000362,TPN 04388,APN -000434,PTP 1,GPS 1,VTR 000200

The data is sent to the server in Meisei company-Japan every minutes.

2.2.2. Philippines Nation-wide Network (V-POTEKA- 10μs)

Figure 2.3. Example of V-POTEKA installed on roof top building of Hokkaido University. This kind of V-POTEKA is distributed to Philippines as Philippines Nation-wide Network

Like the AVON instrument, the V-POTEKA for the Philippines Nation-wide Network also uses dipole antennas to detect electric fields emitted by CG lightning. This type of V-POTEKA also use bandpass filter 1-40 kHz but has sampling frequency 10μs. Different from AVON, it takes more parameters, as shown in figure 2.4. The upper panel shows the example of the VLF signal. When the signal amplitude exceeds the threshold, the data processing unit onboard V-POTEKA picks up the six parameters (TPS, TPP, TPZ, TPN, APP, APN). Besides, the computer automatically calculates the time-integrated VLF signal, as shown in the bottom panel, which is proportional to the lightning current waveform. Then, the computer picks up the two more parameters, APC and APP. APC is the peak amplitude of the time-integrated VLF signal (amplitude at TPZ). APF is the amplitude of the time-integrated VLF signal at TPP (the positive-peak time of the triggered VLF signal in the top panel). Then, the parameters are written in the file every minute with the file and data format.

File name format:
"vlf_stationNumber_yyyymmddHHMM.csv"
(example:vlf_00173477_202004040938.csv).

The data format is as follow:

stationNumber,EVNT,V-POTEKA,yyyymmddHHMMSS,01,E,TPS value,TPP value,TPZ value,TPN value,APP value,APN value,APF value,APC value,NFT 2,SPE 0,GPS 1,VTR 0091

example:

00173477,EVNT,V-POTEKA,20200404093804,01,E,TPS 051997,TPP 052006,TPZ 052003,TPN 052001,APP 014837,APN -016568,APF -016568,APC -00035,NFT 2,SPE 0,GPS 1,VTR 0091

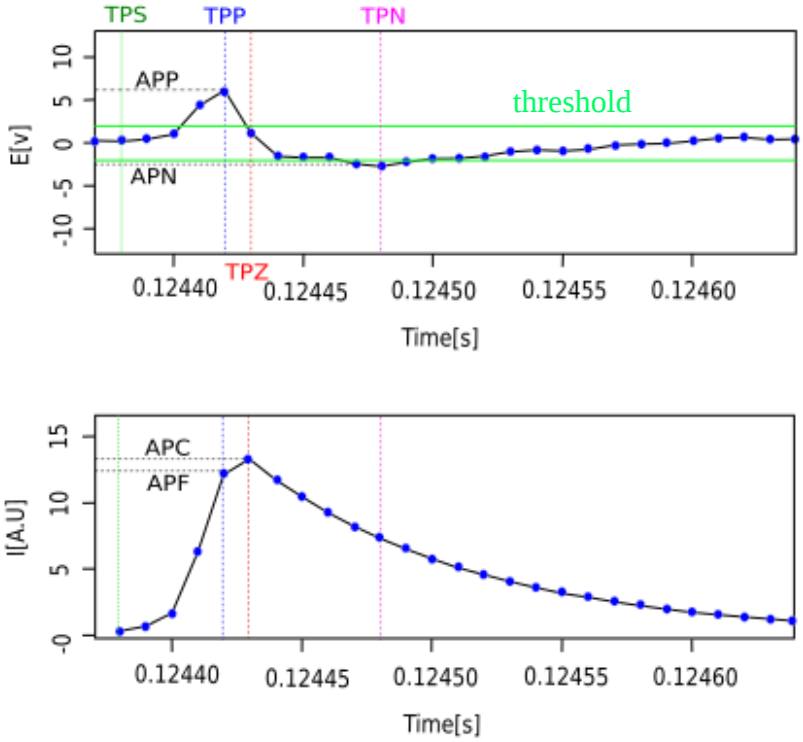

Figure 2.4. Schematic Nation-wide Network V-POTEKA sampling data.

2.3. Lightning data

2.3.1. Data performance

2.3.1.1. AVON instrumentation

The number of files and events in the file sent to the server indicates the signal detected by AVON stations. The number of files and data per hour is plotted to indicate the detection sensitivity of the instrument. Figure 2.5 shows the plotting number of files and data for Manila, Palau, Guam, and Okinawa. The maximum number of the files is 60 per hour, which means one file is sent to the server per minute. From the results shown in Figure 2.5, the data transmission pattern for each

station is almost similar. During the day, the number of files and the number of events detected is small. Less detection in the day time may have some problems. We suspect that the problem is due to changes in the ionosphere D region height or system interference on the device.

Meanwhile, when viewed hourly data in figure 2.5, it does not show the same value. It shows that the sensitivity of each installed instrument is not the same. However, the problem is still unsolved in this study. Thus, analyzes using lightning data still have errors caused by mentions problem.

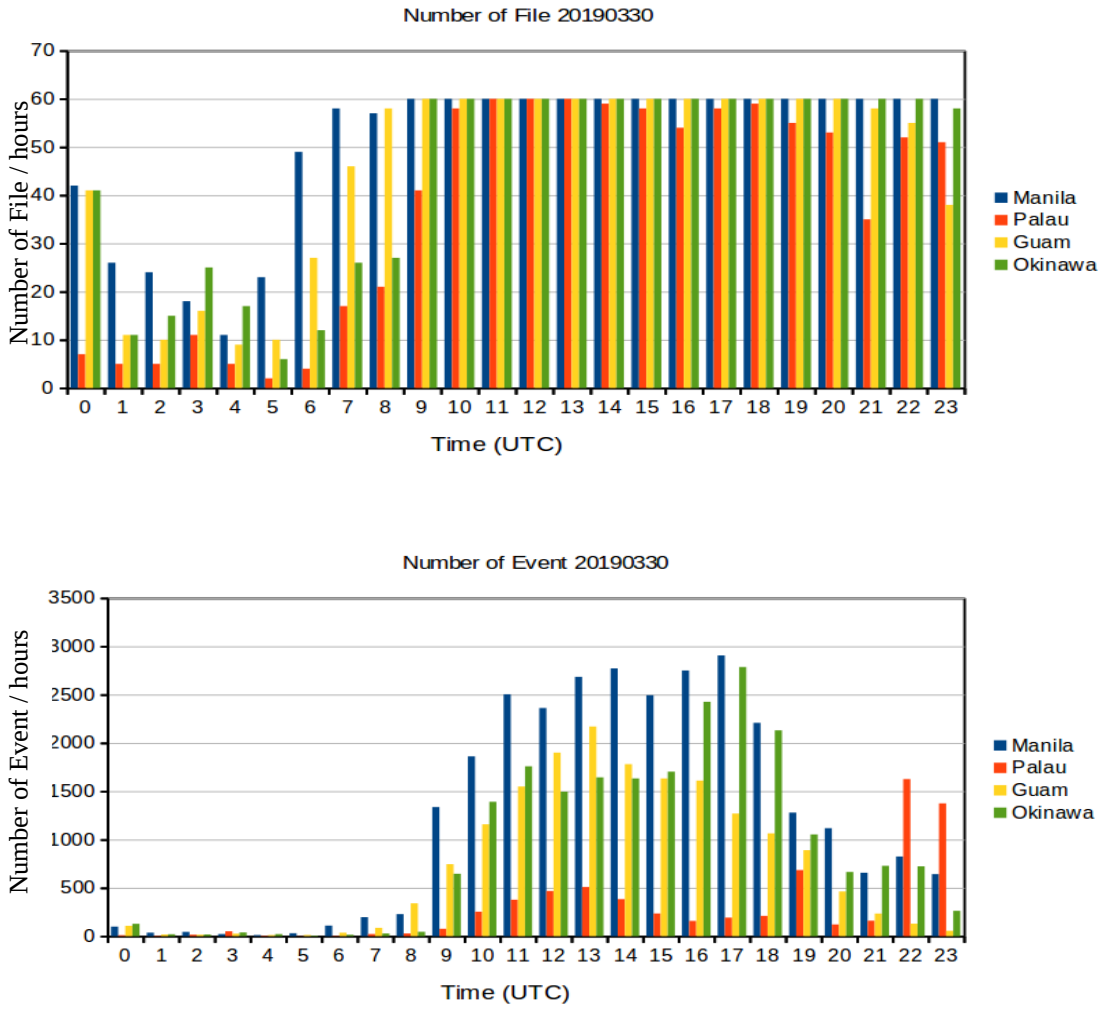

Figure 2.5. Detection sensitivity of Manila, Palau, Guam, and Okinawa

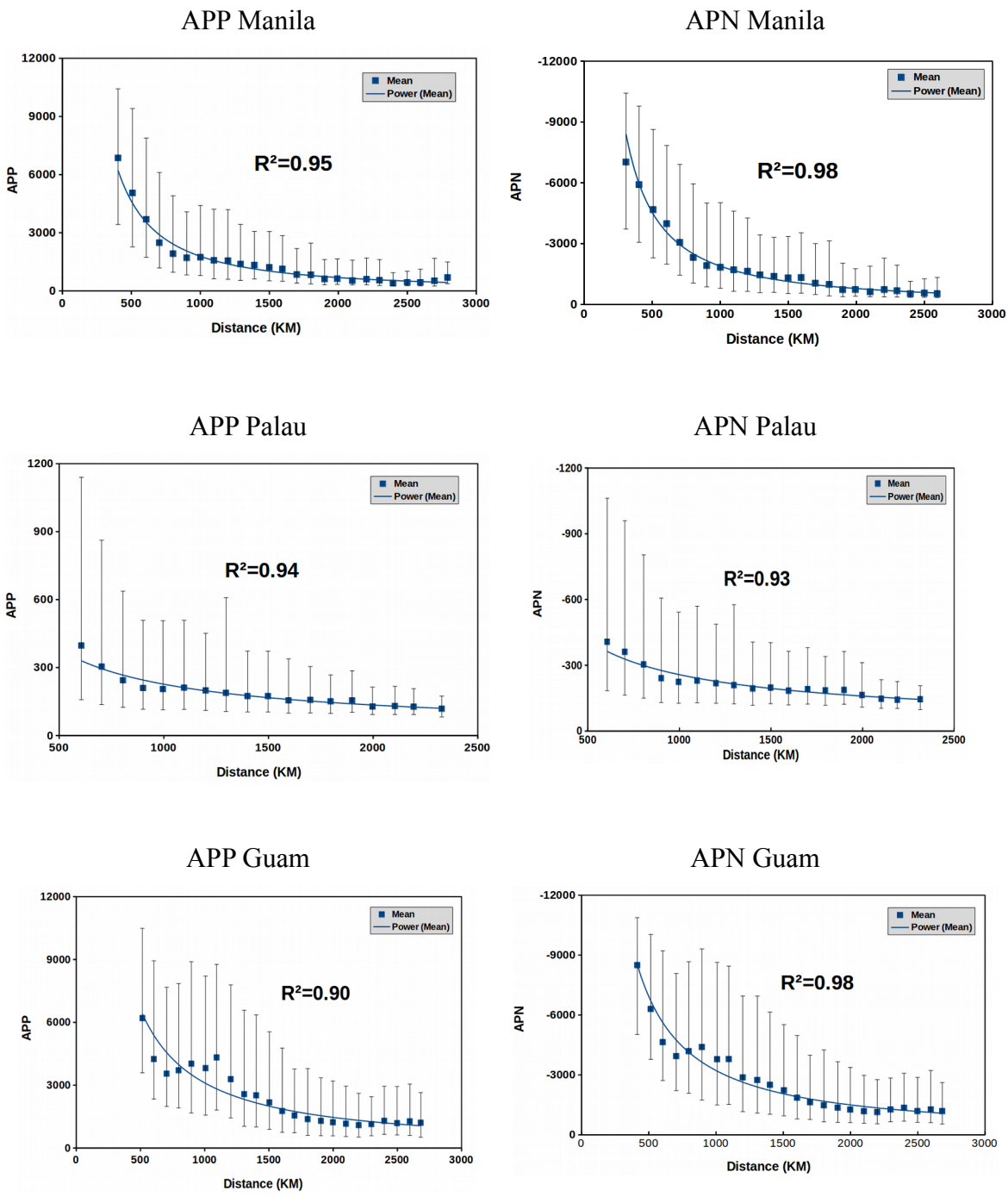

Figure 2.6. VLF signal attenuation with an interval of 100 km for Manila, Guam, and Palau. Error bar shows the upper and lower standard deviation.

VLF Electric field emitted by CG stroke is attenuated with the distance. The distant lightning will detect as a small signal. In this study, we plot the APP and APN as a function of distance for the Manila, Palau, and Guam stations using the 19440 events on July 27 – August 10, 2018. We take the average amplitude value for an interval distance of 100 km. The error bar shows the positive and negative standard deviations of every interval distance. From this work, we find that both APP and APN for three stations are attenuate and fit with the power function of distance, as shown in figure 2.6. The scale of Palau shows quite small compare to Manila and Guam. So from figure 2.5 and figure 2.6, we can conclude that Manila and Palau are the AVON instruments that are the most sensitive and less sensitive, respectively.

2.3.1.2. Nation-wide V-POTEKA - 10μs

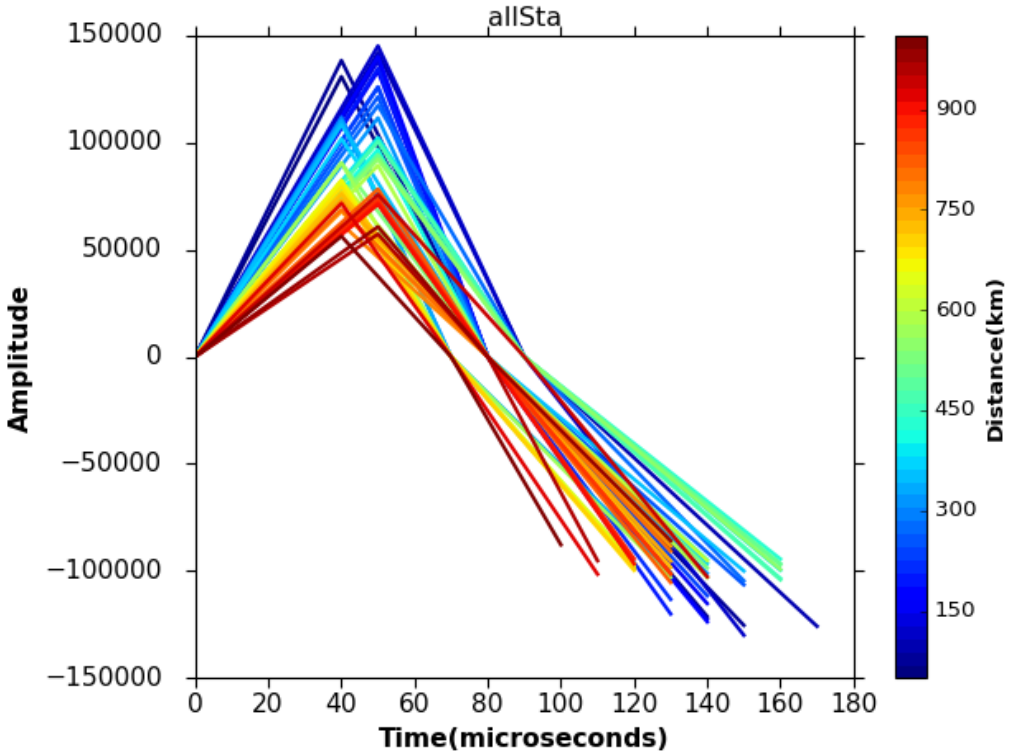

Figure 2. 7. Average negative cloud to ground (CG) lightning signal was detected by V-POTEKA with an interval distance of 20 km.

As explained in sub-chapter 2.2.2, V-POTEKA takes six parameters (TPS, TPP, TPZ, TPN, APP, APN). In this sub-chapter, we make an average of the six parameters for every interval distance 20 km, which is performed by figure 2.7. We use observation data form October 1 st, 2019 to March 31 st, 2020. We select the data which has positive APP value, negative APN Value, and different time of TPS to TPP and TPP to TPZ must be less than 250µs. During that period, we get 16735 samples that fulfill the requirement. The result of the plot, figure 2.7, shows that the APP is decreasing as an increase in the distance. The first half-wave shows the average frequency around 5-7 kHz. The peak of APP and APN decreases as increase the distance. The slope of zero amplitude at TPZ to APN becomes sharp as increase the distance, which agrees with the waveform bang created by Said et al, 2010 [12].

The average data, in figure 2.7, also can be represented as figure 2.8 and 2.9. Figure 2.8 is the APP as a function of distance. The APP graph is looked fit with the power trend line with r2 0.92. Similar to APP, APN in figure 2.9 also decrease as a distance. For the APN, the graph is not smooth as APP, but it still acceptable with r^2= 0.62.

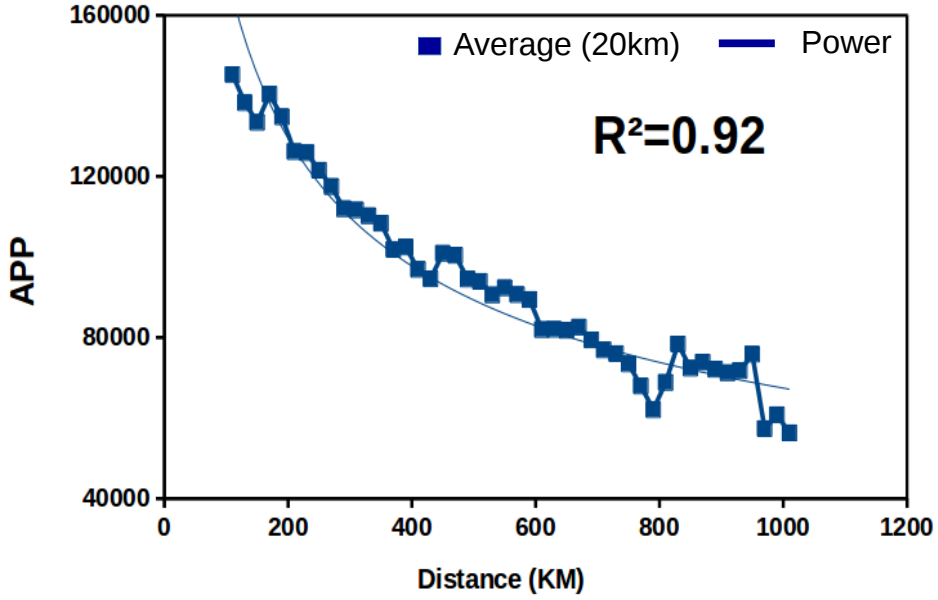

Figure 2.8. APP average of negative cloud to ground (CG) lightning as a function of distance.

V-POTEKA instrument is also designed to estimate charge moment change (CMC) of the lightning. The detection sensitivity uniformity of the V-POTEKA instrument is an important parameter to estimate the CMC correctly. To see the instrument's performance uniformity, we make a signal ratio between two stations with a distance similarity < 10 km. Figure 2.10, 2.11, and 2.12 plot the ratio between Davao to Legazpi, Legazpi to PuertoP, and PuertoP to Davao, respectively. The average signal ratio of APP and APN signal is shown in table 2.1. Table 2.1 shows that Legazpi is the most sensitive, and the PuertoP is the less sensitive one.

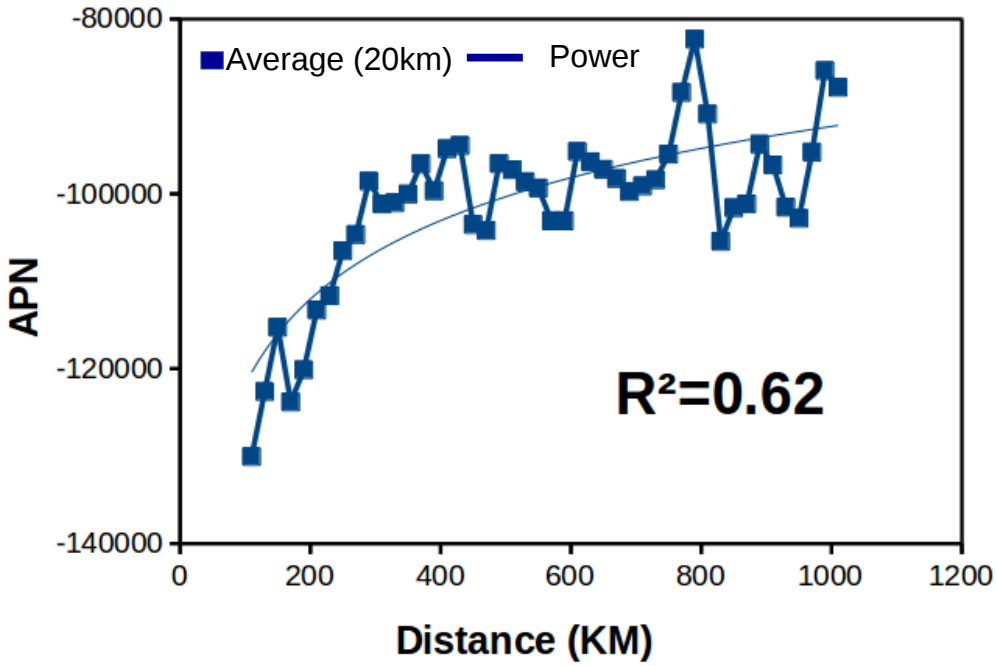

Figure 2.9. APN average of negative cloud to ground (CG) lightning as function of distance.

Table 2.1. Average of signal ratio

	APP	APN
Davao / Legazpi	71:100	64:100
Legazpi / PuertoP	100:59	100:56
PuertoP / Davao	79:100	64:100

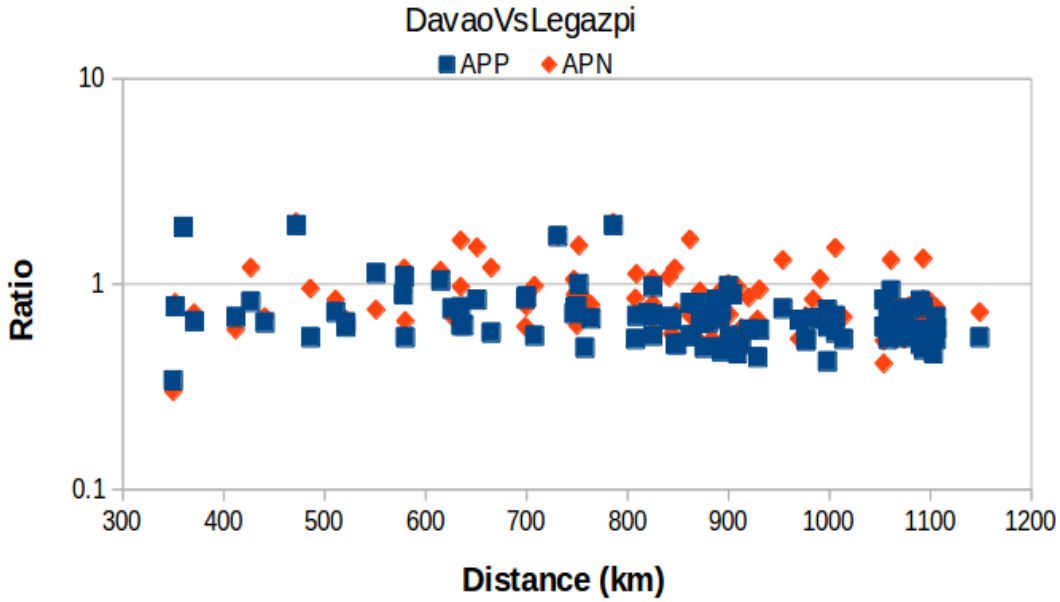

Figure 2.10. Signal amplitude ratio Davao to Legazpi with distance similarity < 10 km with number of sample 109.

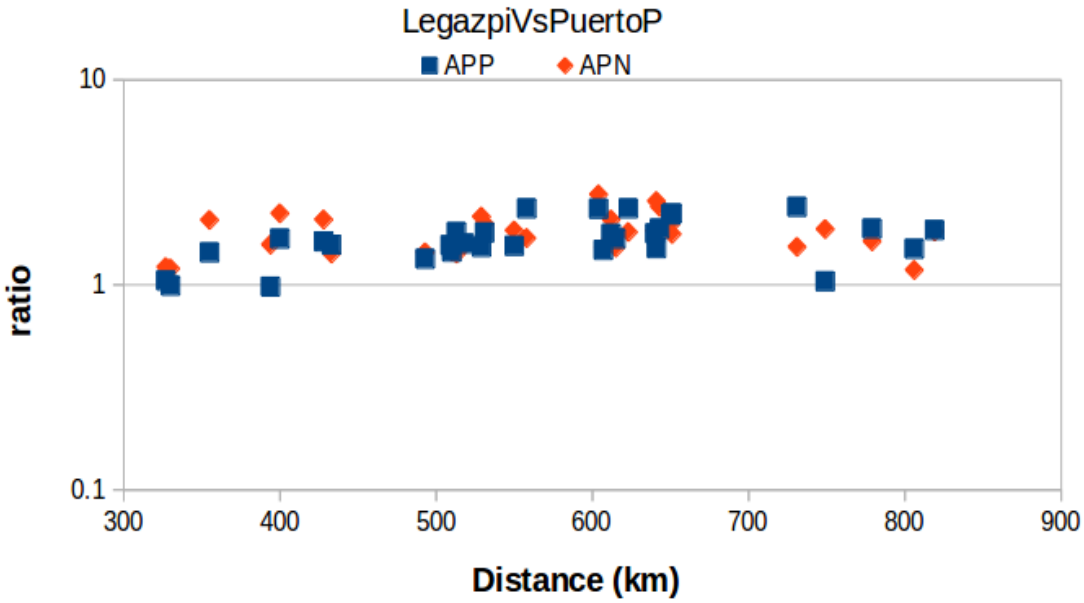

Figure 2.11. Signal amplitude ratio Legazpi to PuertoP with distance similarity < 10 km with umber of sample 32.

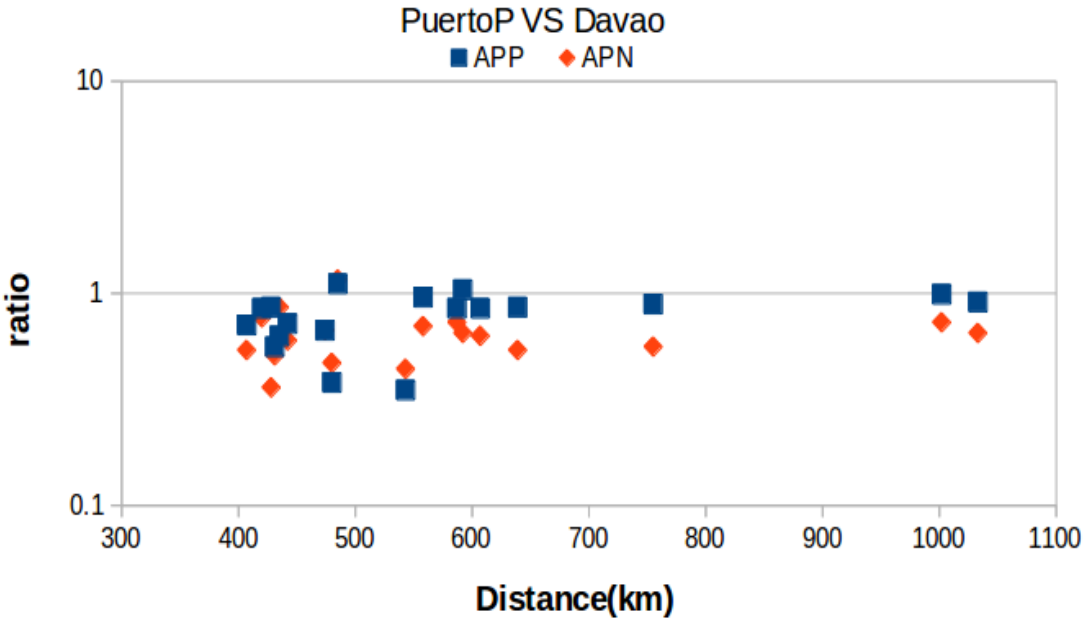

Figure 2.12. Signal amplitude ratio PuertoP to Davao with distance similarity < 10 km with number of sample 19.

2.3.2. AVON lightning geolocation estimation

ToA is the time difference received between 2 (two) stations. As shown in Figure 2.13, t_0 is the time the lightning occurred. Within a certain interval, the electromagnetic waves emitted by lightning will reach station A and station B in time t_A and t_B, respectively. Thus, the difference in the time of receiving an electromagnetic wave from stations A and B is t_A & t_B and can be represented as t_A-t_B.

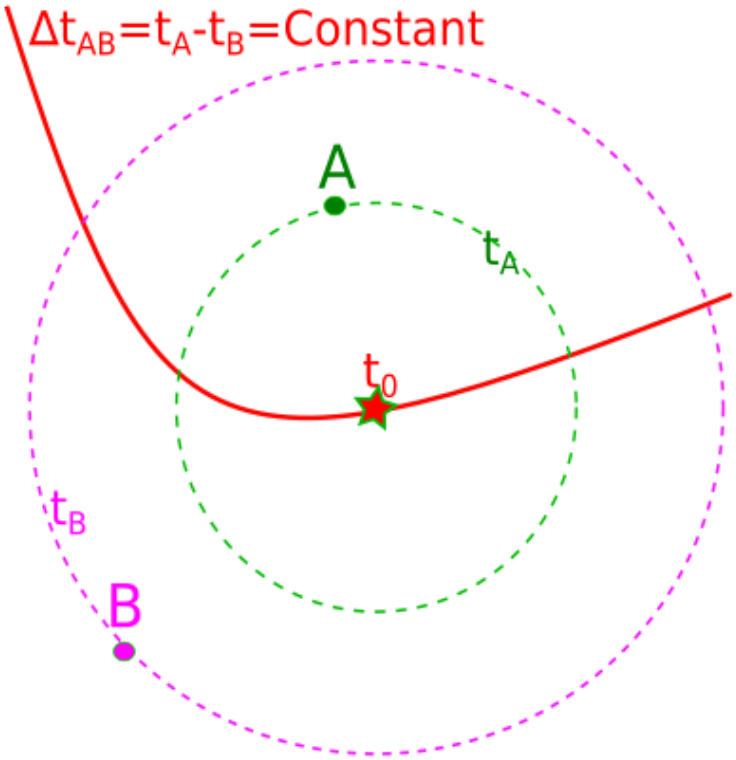

Figure 2.13. Illustration of time of arrival (ToA).

The location of lightning with a difference in time t_A and t_B is many points that can be described as a red line. So, it can be said that the red line is a possible location of lightning that occurs with a time difference Δt_{AB} called ToA lines. In this study, we found that the thick of the ToA line is not constant. Here, make geographic grid 0.03° x 0.03° in the area, which covers northwest pacific. The VLF signal's speed is assumed to be light (3 x 10^8 m/s). Light travel time from every point of grid to the AVON stations is calculated as ToA. In this study, the ToA is rounded to the GPS clock resolution unit (100μs). Different of ToA is counted by subtracting ToA of AVON station to other stations. We did it for each grid to Manila stations and Guam stations. Then, we count different times of arrival of each grid to both stations and perform it in a map, as shown in figure 2.14. The color shows the constant different times of arrival. From the map in figure 2.14, we can see that the ToA line is not

constant but depends on the distance and position of the grid. The different wide of the ToA line will make a systemic error of geolocation estimation different in every place.

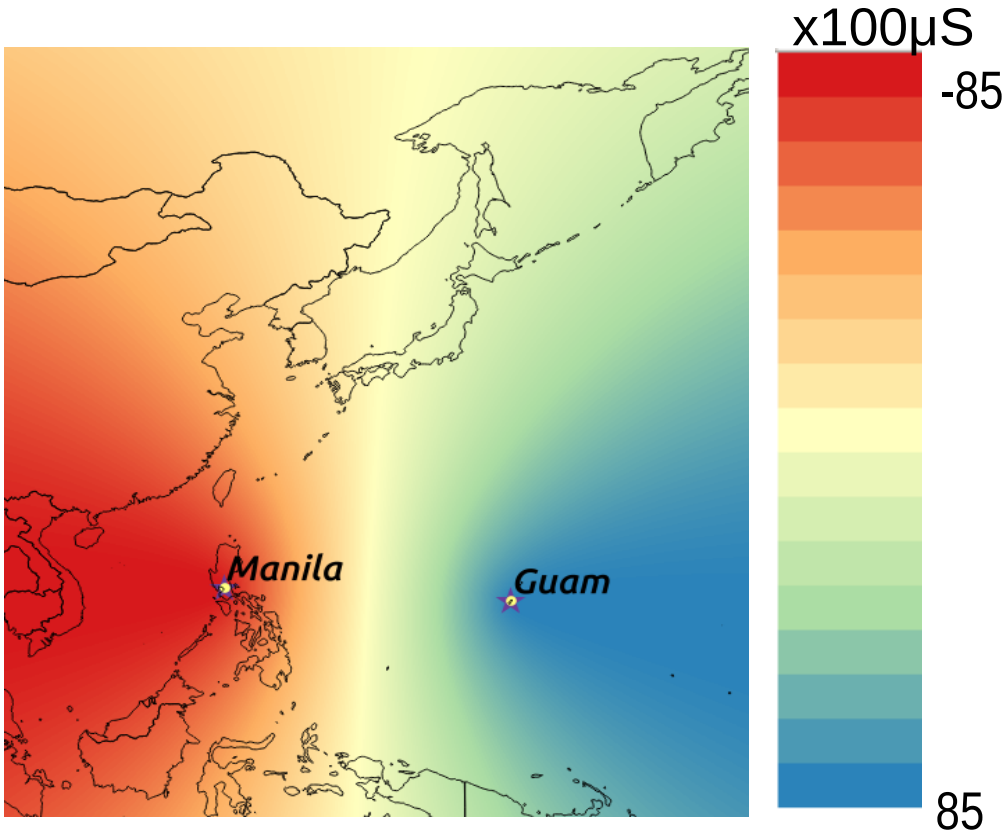

Figure 2.14. Different time of arrival (ToA) map for Manila and Guam.

At least using three ToA line, lightning geolocation can be estimated. Figure 2.15 is the example of the geolocation estimation using Manila, Palau, and Guam stations. Blue, green, and red are the toa line created by Manila to Palau, Palau to Guam, and Guam to Manila, respectively. These three ToA lines make cross-sections on the east coast of Mindanao Island. The result of the cross-section is a group of grids point, as shown in figure 2.15 (right). The area formed by the grids point is the possibility of the CG lightning locations. The area also has a constant different time of arrival to every station, making the ambiguity of lightning geolocation estimation. In this work, we define lightning geolocation as the median value of the ToA line

cross-section. We also define the radius ambiguity error as the farthest grids point of cross-sections to the lightning geolocation estimation.

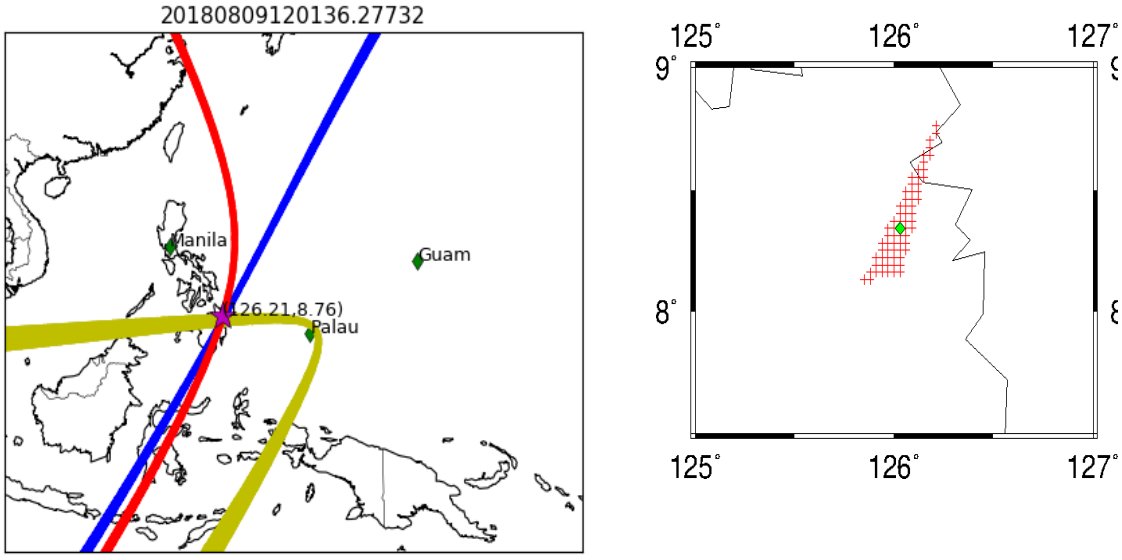

Figure 2.15. Lightning geolocation estimation using Manila, Palau, and Guam stations for August 9th, 2018 12:01:36.27732 (left). The zoom of cross-section (right). The red cross is the grid point of cross-section and grind is the median value as the lightning estimation.

2.3.2.1 Geolocation error simulation

As explained in sub-chapter 2.3.2, the ToA line cross-section is the area created by the grid point. The area size can be the ambiguity error of lightning geolocation. We use this idea to estimate the ambiguity map of lightning geolocation estimated by AVON detection networks. Similar work has been done by Hidayat et al. (1996) for the time-difference and direct (TDD) technique. He estimated the lightning location utilizing data of arrival time difference and direction of electromagnetic waves from 2 or 3 stations. He simulates the lightning geolocation error on the map, and the contour of error is seen[37].

Similar to Hidayat et al. (1996) we estimate lightning geolocation errors created by AVON detection networks. Five AVON instrument is deployed in five places, namely, Manila, Palau, Guam, Okinawa, and Serpong. We make a geolocation grid point with size 0.3° x 0.3°, which covers the area with longitude 100° E to 150°E and Latitude 30°N and 10°S. We estimate the lightning geolocation error for every combination of 3 stations for every grid point. Then we take the best lightning geolocation error and put the error value on the map. The final result of the error map can be seen in figure 2.16. Based on the map in figure 2.16, the best majority error is around 30 kilometers.

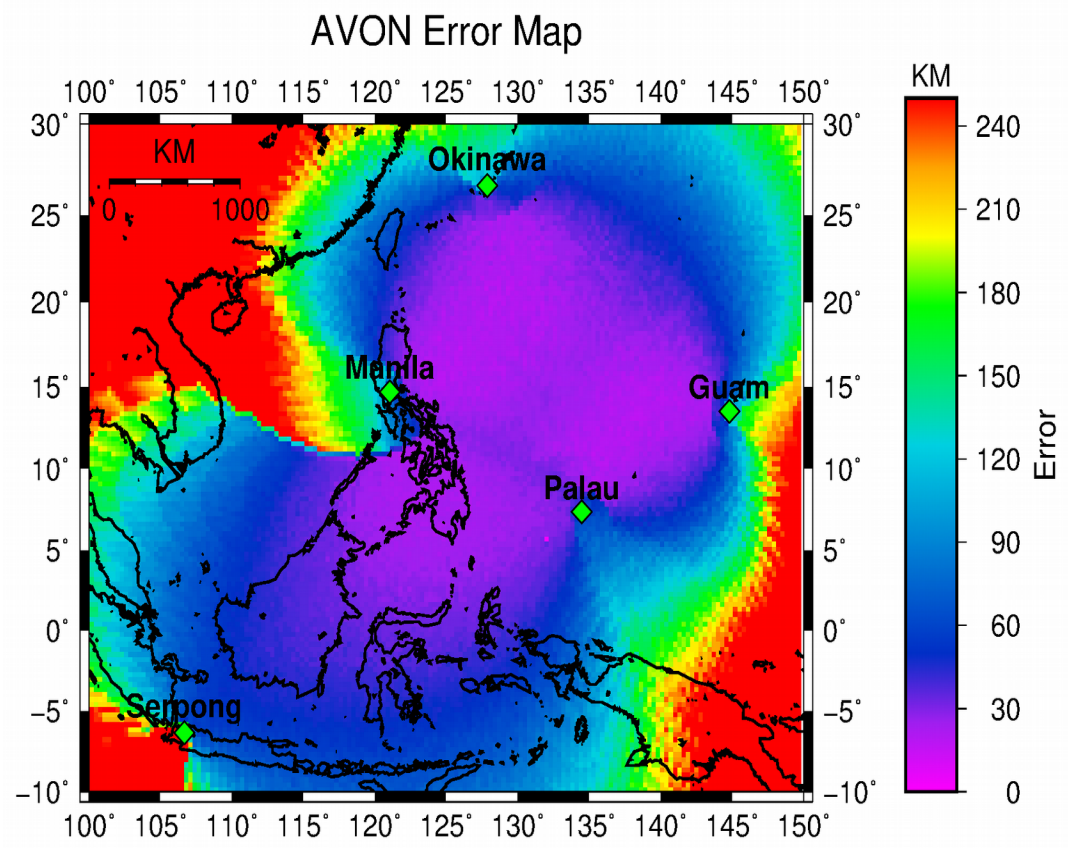

Figure 2.16. Lightning geolocation error simulation using the ToA method for AVON lightning detection networks deploy in Manila, Palau, Guam, Okinawa, and Serpong.

The reliability of this simulation result is confirmed using the statistical method. The lightning geolocation estimation, which touching the high cloud indicated by the low temperature of Himawari 8 Band 15 (wavelength 12 μm) brightness image, is assumed to have the more probable right of geolocation compare to untouchable one. In this study, we tested the 29.768 lightning geolocation estimated by Manila-Palau-Guam from July 27 – August 10, 2018. The sample is in a random location, which is also placed randomly in different simulation contour error. The simulation contour error for Manila, Guam, Palau is shown in figure 2.17.

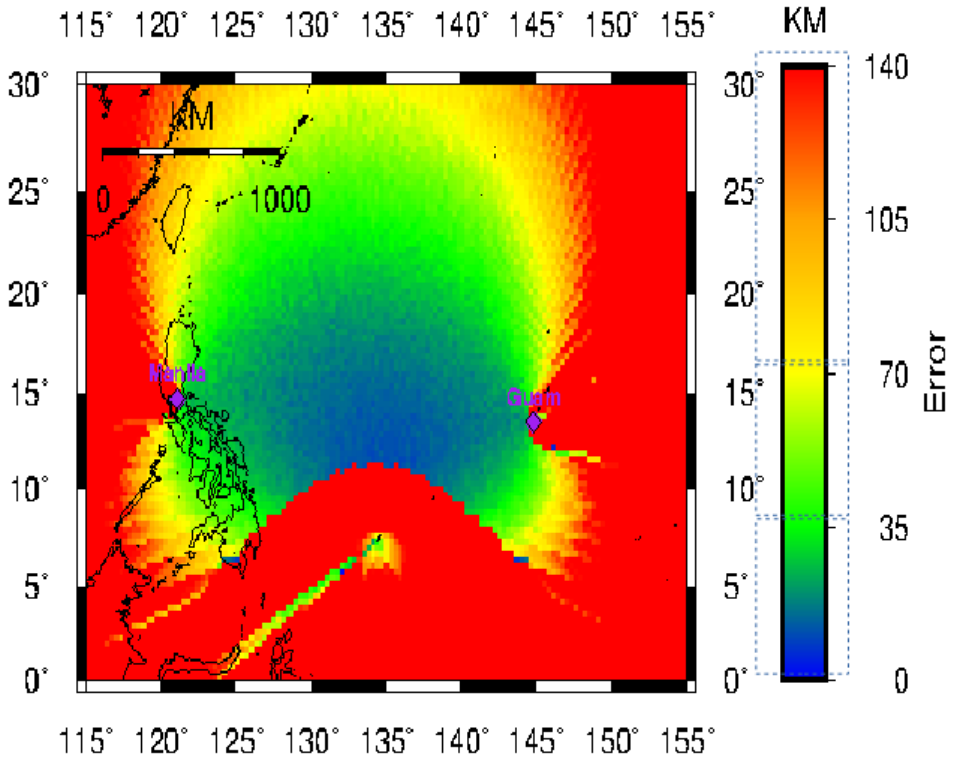

Figure 2.17. The simulation contour error for Manila, Guam, Palau

Then, we pick up the brightness temperature measured by Himawari 8 band 15 (12μm) on the exact location of lightning geolocation estimation. Then, we make it category based on the distance (<35 km, 35-70, 70-140, >140). For every distance category, we categories it into three temperature categories (<218 K, 218-273 K, >

275 K) and perform it as a graphic in figure 2.18. The number of lightning in the radius 0 kilometers category or precisely in the lightning geolocation estimation, which touching the cloud top temperature (CTT) < 218, decreases gradually as increase the error estimation; meanwhile, CTT > 273 gradually increase. Then, we take the lowest CTT with the radius 30km, 50km, and 70km to the lightning geolocation and plot it to the graph, shown in figure 2.18. Based on figure 2.18, the profile of the graph significantly changes in radius 30 km. Based on this statistical study, the majority error of AVON geolocation created by Manila, Guam, and Palau is ~30km.

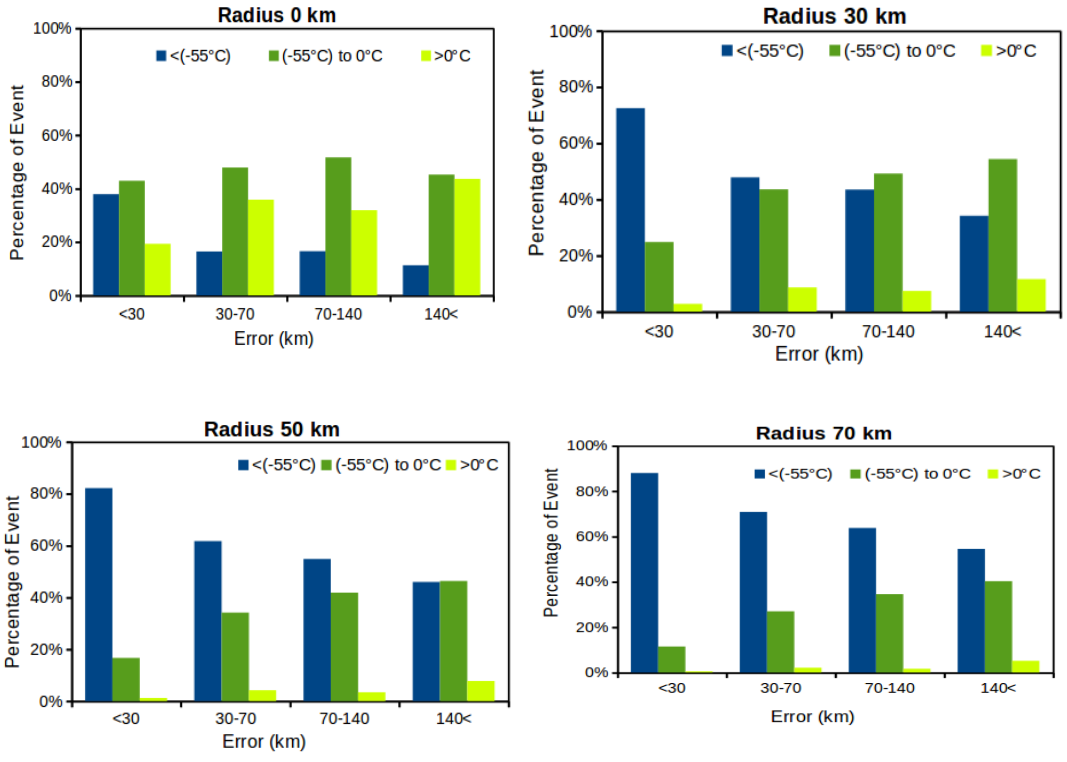

Figure 2.18. Percentage of lowest cloud top temperature (CTT) measured by Himawari 8 band 15 (12µm) in radius 0km, 30 km, 50 km, and 70 km.

2.3.2.2. AVON lightning geolocation result

Figure 2.19 shows the one hour example of geolocation estimation on June 20th, 2019, at 15:00 UTC. The background color is the Himawari 8 Band 15 (12.3 µm), which shows the cloud top temperature (CTT). For that image, we can see the thunderstorm cloud growth with lightning in around Bengkulu-Indonesia, Riau Islands, and Natuna sea, the south of Vietnam, north part of Kalimantan Island, North Sulawesi, and South part of Philippines. Around the south part of the Philippines, there is much lightning, even though the clouds are relatively small. The error, as described in sub-chapter 2.3.3, also represents the sensitivity of the AVON detection networks. The different sensitivity of lightning detection will cause the difficulty and error of thunderstorm cloud analysis.

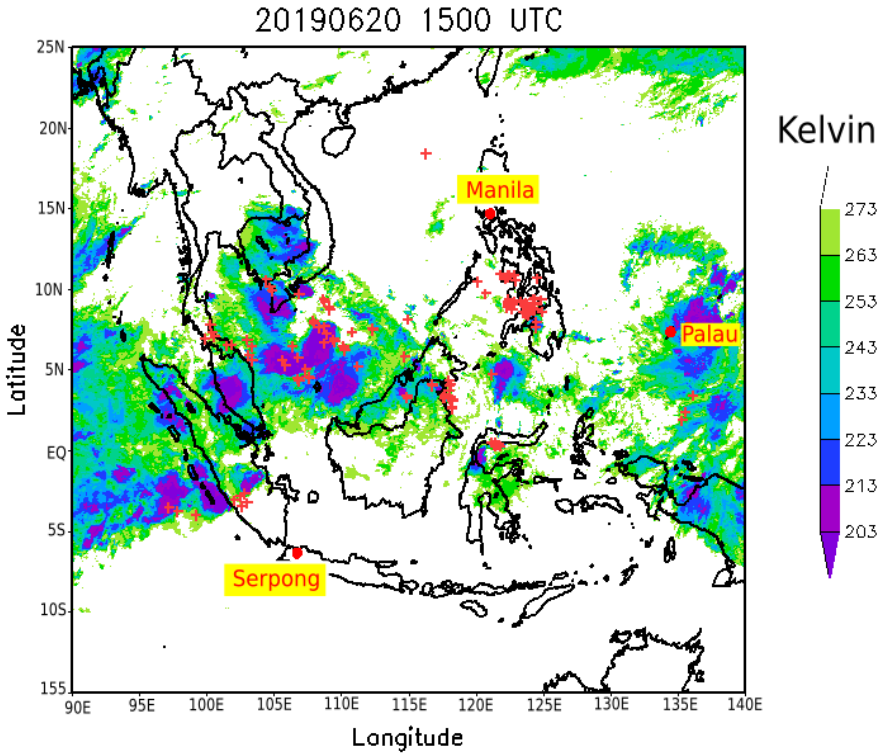

Figure 2.19. Lightning geolocation estimated using Manila, Serpong, and Palau time of arrival data on June 20th, 2019 15:00 UTC. The red cross is the lightning location estimation. The background color is the cloud temperature of Himawari 8 band 15 (12.3 µm).

To check the reliability of the lightning geolocation result, we compare the AVON lightning geolocation result with Blitzortung. Blitzortung We take lightning geolocation in the square area ~1100 km x ~1100 km for the location longitude 120ºE to 130ºE and latitude 0º to 10ºN. Based on the lightning geolocation simulation, the sampling area has an error estimation of around 30 km – 40 km. From June 20th, 2019 to March 31st, 2020, The lightning detected by AVON and Blitzortung in the sample area is 47762 and 16072. The AVON is about three times of Blitzortung, meaning that the AVON is more sensitive than Blitzortung in the sampling area. We also count the time and distance relative to both lightning detection.

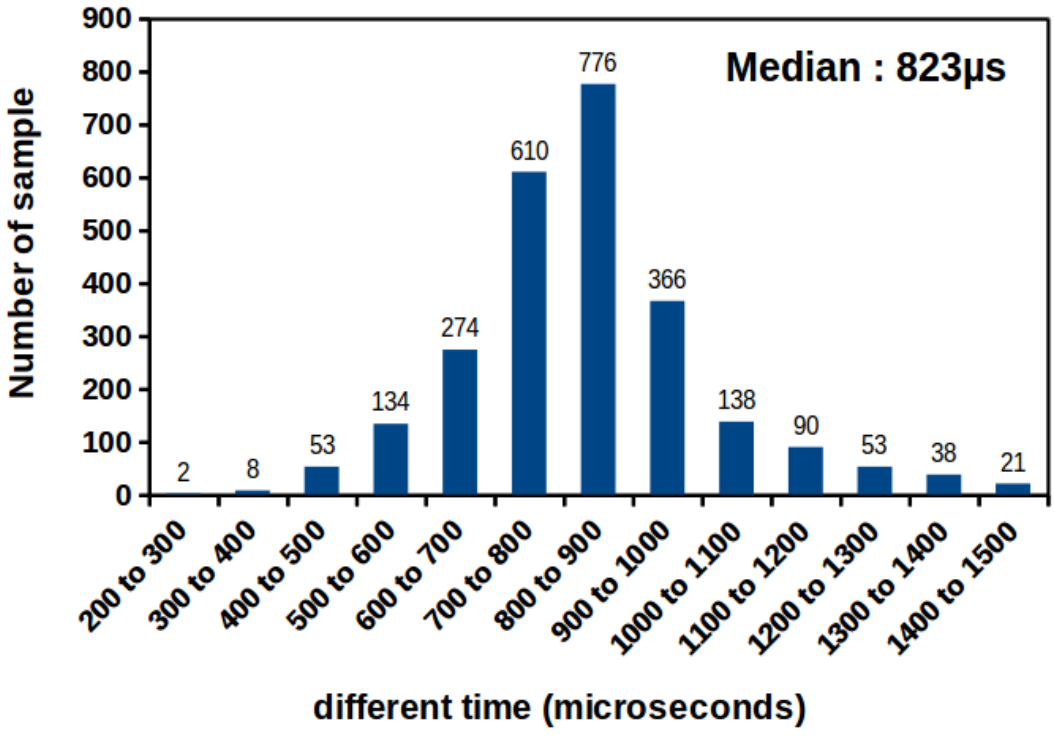

Figure 2.20. The number of lightning events in the absolute different times detected by AVON and Blitzortung in the sample area ~1100 X ~1100 km and 286 days.

Figure 2.20 is the number of lightning events in the absolute value of different time in microseconds. Based on figure 2.20, the same lightning detection between AVON and Blitzortung is ~823µs, which is the median value of the sample distribution. We take the sample with the time similarity 700 to 900µs to estimate the relative distance between AVON and Blitzortung. About 8.7% (1397 events) of the Blitzortung data can be the same lightning detection with the AVON. We count the absolute relative distance of the 1397 samples. Then, we plot it with an interval of 10 km, as shown in figure 2.21. The median value of the relative distance is 37 km.

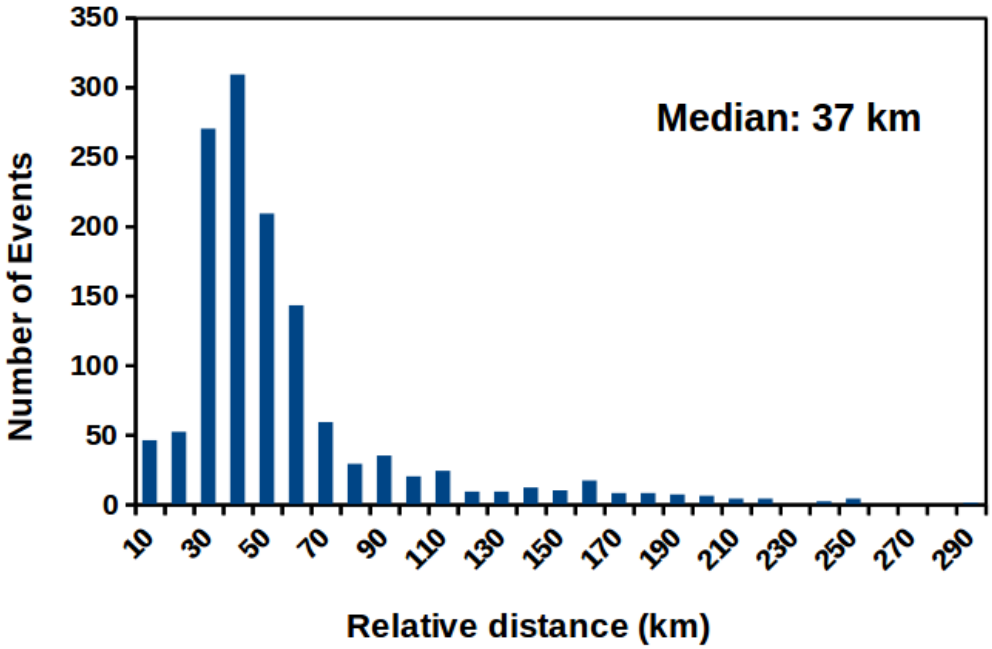

Figure 2.21. The number of lightning events in relative distance between AVON and Blizortung

2.3.3. Philippines Nation-wide Network geolocation estimation

In this work, we estimate the lightning geographic location using the time of group arrival (TOGA). We modify the time of arrival method (ToA) used for AVON, and we change to use TPS, not TPP. From the ToA cross-section result, we estimate the time received for the fourth and the next station, as illustrated in figure 2.22.

Unlike the AVON lightning detection network, we apply a more fine grid of ToA lines 0.01º(1 km). As mentions in sub-chapter 2.3.2, the result of ToA lines is the area formed by a group of the coincident grid. Then, we estimate the time of arrival of every point to the next V-POTEKA station. If the estimated time matching with the actual signal with tolerance ±10μs (±1 of TPS number), the stations are assumed to contribute to the lightning geolocation result. Then, we apply this procedure to the next stations. Additional stations will decrease the error because it will cut the ToA cross-section area, as described in figure 2.22 (right).

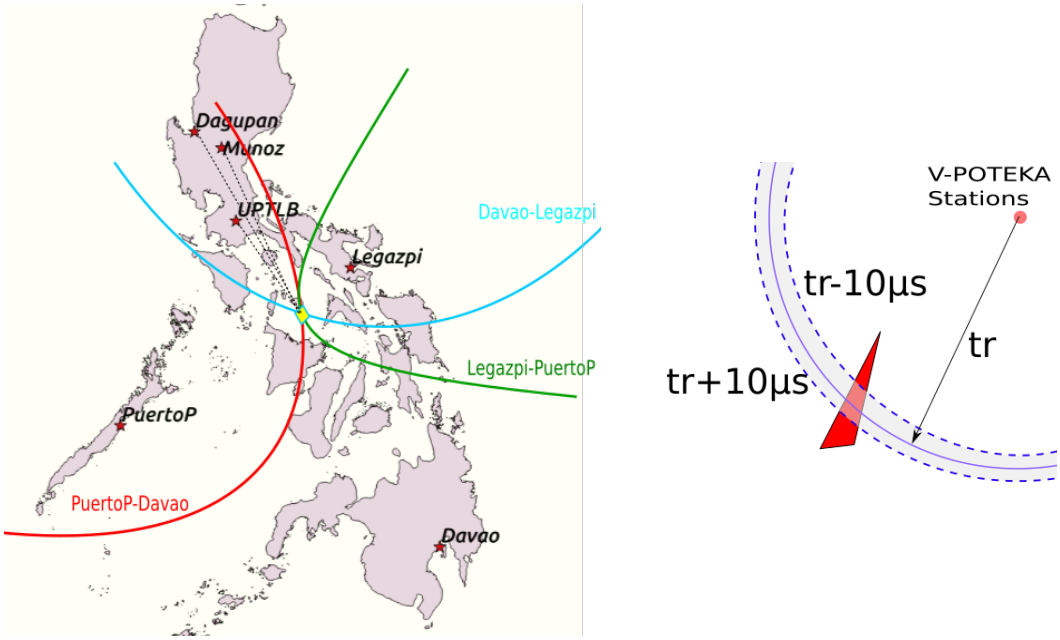

Figure 2.22. Toga illustration with the main station Puerto-Davao-Legazpi (left). Illustration of increasing number of station will decrease the error of lightning geolocation(right). Red triangle is the ToA lines cross-section.

Figure 2.23 shows the example of lightning geolocation results using the VLF receiver installed in the Philippines with three main stations Puerto-Davao-Legazpi.

The result shows matching the location of the clouds shows by the CTT below < 0ºCelsius. For the quantitative comparison, we will compare the Philippines Nation-wide Network with the Blitzortung. We take lightning event samples in the rectangle area ~1100km x ~1650km (Latitude: 120ºE to 130ºE and Latitude: 5ºN to 20ºN). The period is October 1st, 2019 to March 22nd, 2020 (174 days). In this sample area, we get the 33132 and 6794 lightning data detected by the Philippines Nation-wide Network and Blitzortung, respectively. The number of lightning detection shows the Philippines Nation-wide Network more sensitive than Blitzortung in the sampling area.

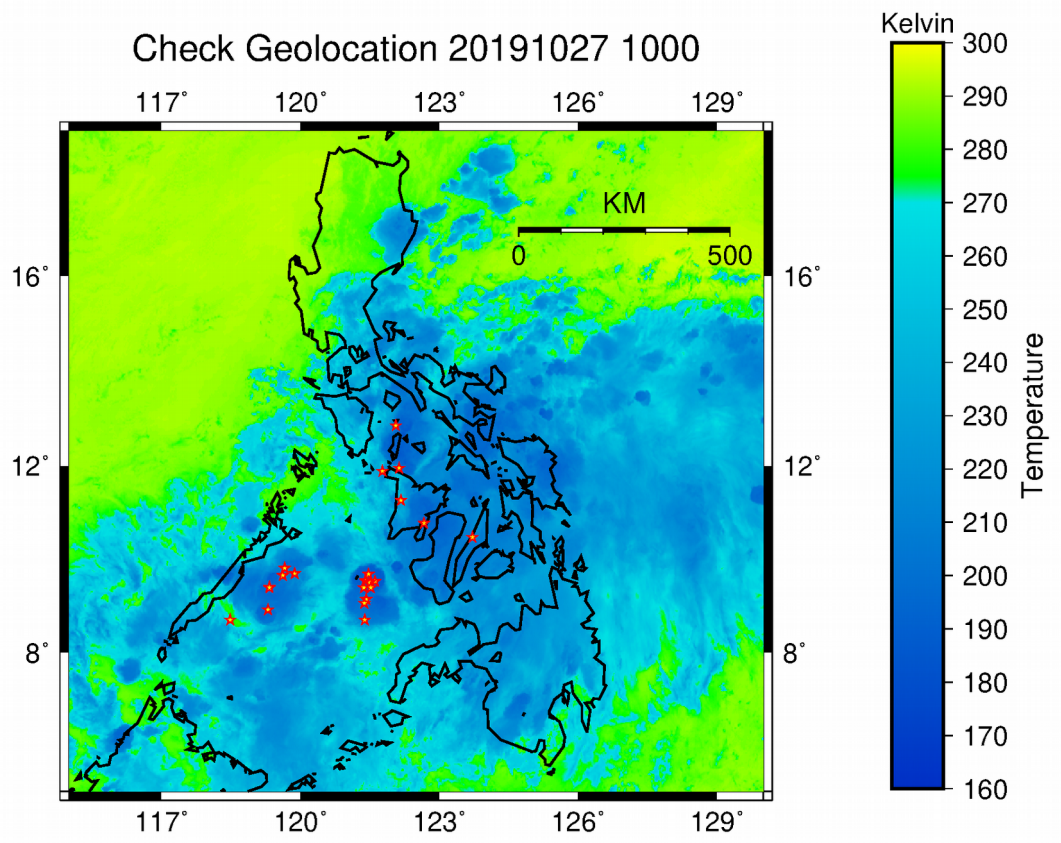

Figure 2.23. Example lightning geo-location result for 10 minutes duration and overlay with Himawari 8 band 15 (12.4 µm)

Figure 2.24 shows the number of lightning events in the absolute value of different times in seconds. Figure 2.24 shows that the same lightning detection between the Philippines Nation-wide Network and Blitzortung is ~1 seconds, which is the median value of the sample distribution. We take the sample with the time similarity 0.9 to 1.1 seconds to estimate the relative distance between the Philippines Nation-wide Network and Blitzortung. We get a 425 sample of the lightning data, the range of the time similarity. Then, we count the absolute relative distance of the 425 samples. Finally, we plot it with an interval of 10 km, as shown in figure 2.25. The median value of the relative distance is 35 km. Even the median value is 35 km, the relative distance < 20 km more frequently occur.

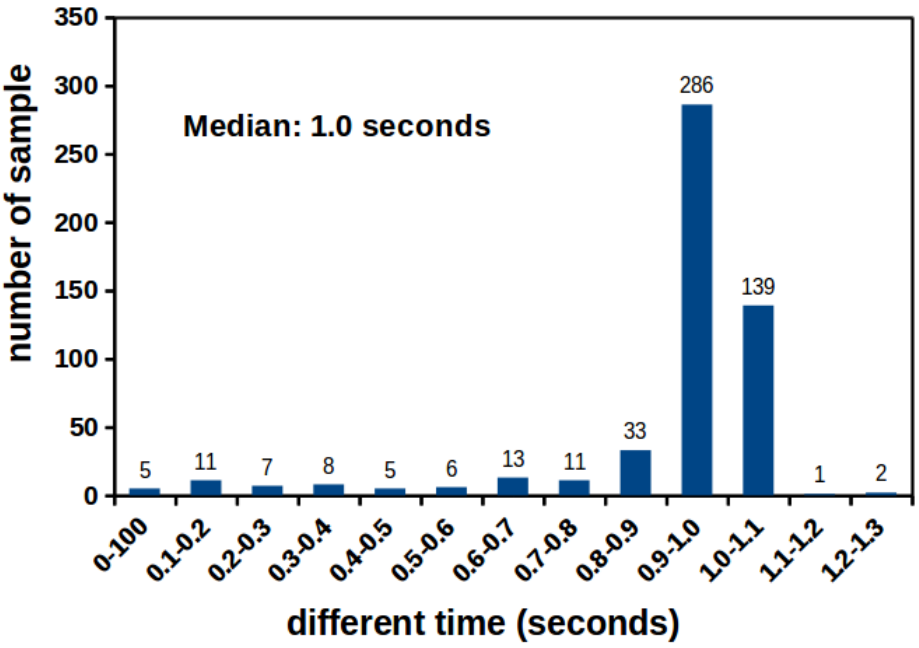

Figure 2.24. The number of lightning events in the absolute different times was detected by the Philippines Nation-wide Network and Blitzortung in the sample area ~1100 X ~1100 km and 178 days.

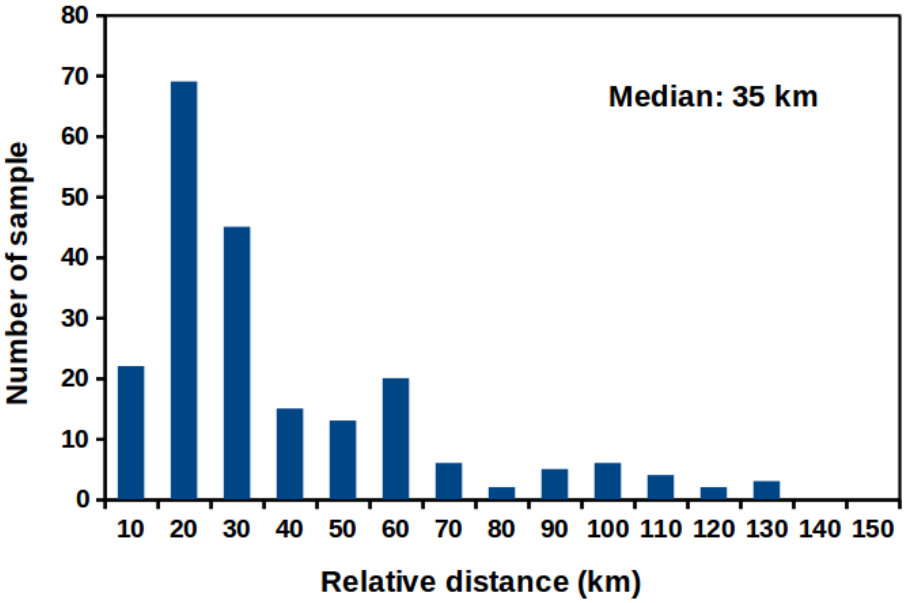

Figure 2.25. The number of lightning events in relative distance between Philippines Nation-wide Network and Blizortung

2.4. Results

In this sub-chapter, we will show the utilization of the lightning geolocation data. We are doing some natural phenomena analysis in the area covered by the AVON lightning detection network and V-POTEKA networks. Some previous study has mentioned that lightning phenomena have a correlation with thunderstorm cloud evolution and severe weather such as torrential rainfall, small tornadoes, and lightning itself [4-8,21,22,30,31]. In this study, we utilize the lightning data to analyze thunderstorm height and rainfall, diurnal lightning in Kalimantan, Taal Volcano ash cloud, and the typhoon maximum wind speed.

2.4.1 Thunderstorm cloud study

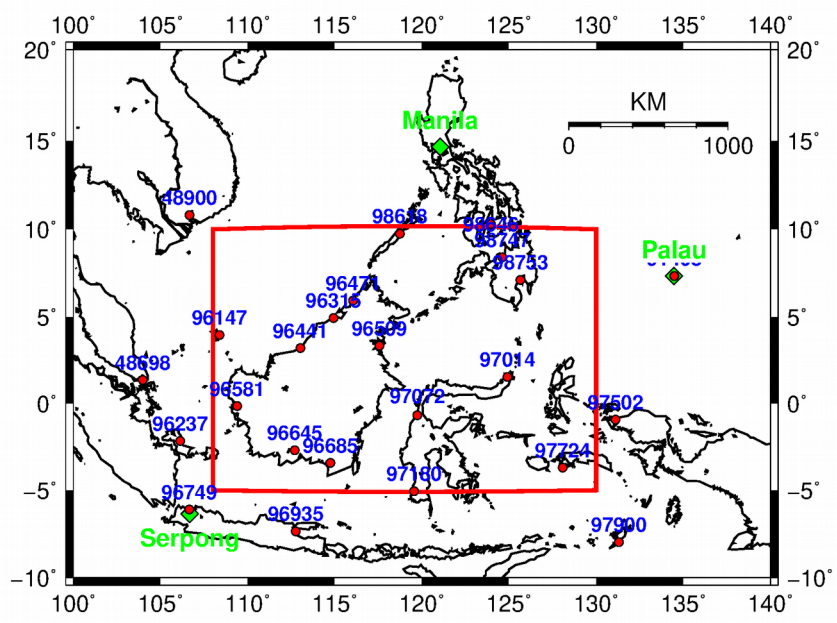

Figure 2.26. Observation area (red rectangle), ground CG lightning detector location (green diamond), and radiosonde launched station(red circle).

In this study, we investigate the relationship between the lightning produced by thunderstorms with its top temperature, top height, and the rainfall. We take sample areas around the north part of Indonesia and the south part of the Philippines, as shown by the red rectangle in figure 2.26. Using this sample area with longitude 108° to 130° and latitude -5° to 10°, we will observe the tropical thunderstorm. This observation area is covered by the Asia VLF Observation Network (AVON) V-POTEKA instrument installed in Manila, Palau, and Serpong to detect the lightning signal in the very-low-frequency range (VLF). These AVON instruments are time synchronize by GPS and connected to the server by a 3G Internet connection. The signal data is sent to the server every minute. Using at least three stations of V-POTEKA instrument, we can observe and estimate the geographical location of lightning using the time of arrival method. For this work, we use the lightning location to indicate the thunderstorm cloud's existing and area.

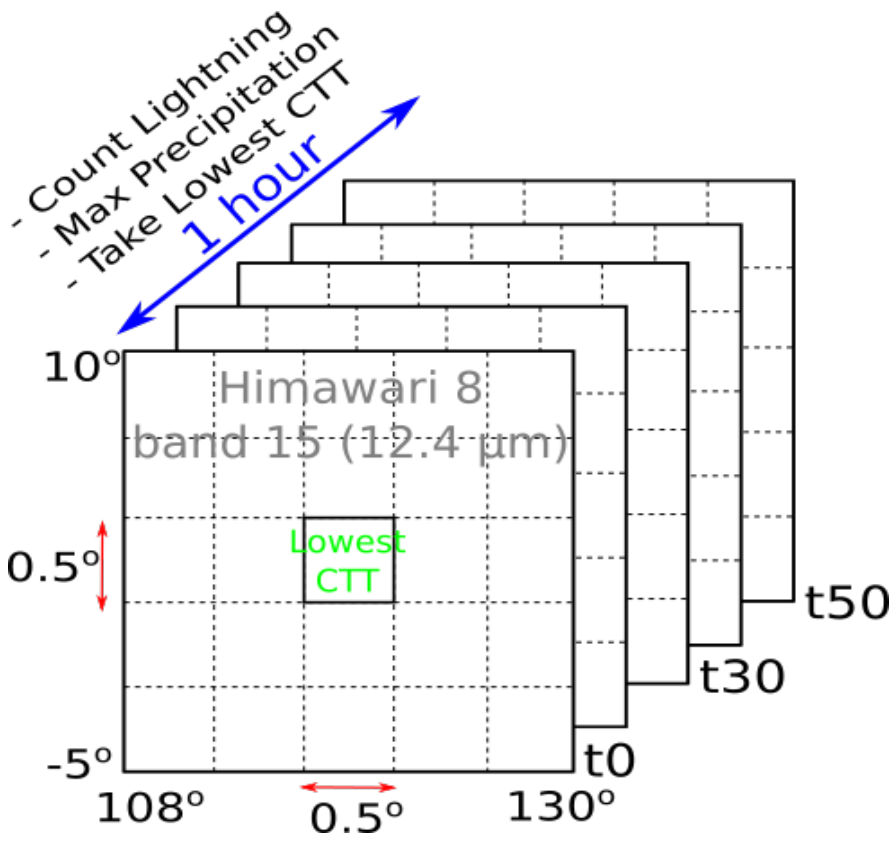

Figure 2.27. Processing data schematic

Table 2.2. Data distribution and sorting result

Number of Lightning	with lightning	Temp < 273 K	Lapse rate and 0°C isotherm
1	31064	27740	27027
2	5492	4902	4766
3	1814	1601	1568
4	819	727	717
5	441	386	384
6	278	247	247
7	171	152	152
8	109	101	100
9	87	74	74
10	60	55	54

We take the observation period from July 1, 2019, to January 31, 2020. The Himawari 8 and 15 (12.4 μm) provided by Jaxa with temporal resolution every 10 minutes and spatial resolution 2 km is used to provide cloud top temperature (CTT). Radiosonde data downloaded from Wyoming University data archived is used to convert CTT to cloud top height (CTH). The radiosonde data availability is every 00 and 12 UTC. For the rain rate, we use TRMM precipitation product Standard V7 with temporal resolution and spatial resolution 1 hour and 0.1° (~10 km), respectively.

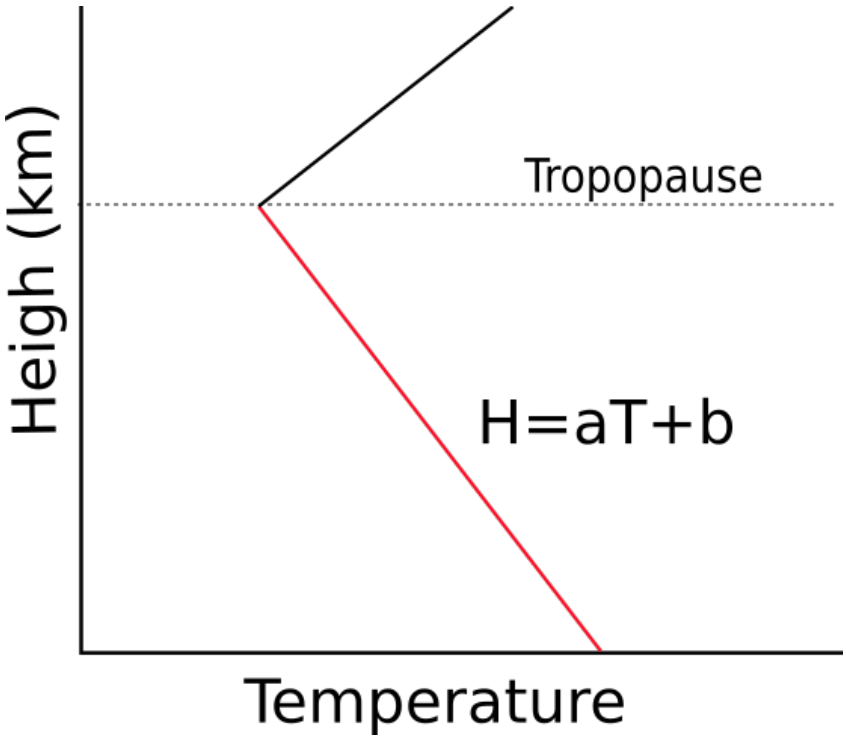

Figure 2.28. Radiosonde air temperature profile

For this work, we use the data that has different time and spatial resolution. So, we create grids 0.5° x 0.5º for the sample area in figure 2.26 and temporal resolution data for 1 hour. Himawari 8 data is the highest temporal and spatial data used in this work. For this data, we take the lowest temperature of each grid for one

hour. Lightning data is counted every hour in each grid. We also take the highest rain rate in each grid. The data processing is illustrated in figure 2.27.

In this method, we used area lightning density rather than thunderstorm cell density. This methodology is more simple compare to the previous study, which makes the correlation between every cell of the thunderstorm [8]. By defining the specific dangerous area as a static observation area, we believe that this methodology is the easy way and applicable to observe the dangerous area from the flood or landslide caused by torrential rainfall from the thunderstorm cloud.

In this work, we sort the grids using three steps:

1) We take the grids, which is at least one lightning exist; the result is shown by distribution data in column 2 in table 2.
2) From the result of step one, we take the grid with the temperature below 0° Celsius (273 Kelvin). The distribution of data and the sorting result is shown in table 1, column 3.
3) From the CTT in step 2, we convert it to its height using the nearest place and time of the radiosonde air temperature profile. The average distance of the whole sample grid to the nearest radiosonde station used for height calculation is 272 km. To estimate the cloud top height (CTH), we make a trend line of temperature versus altitude before reaching the inversion level, as shown in figure 2.28. *a* and *b* represent the air temperature lapse rate and 0ºC isotherm level, respectively.

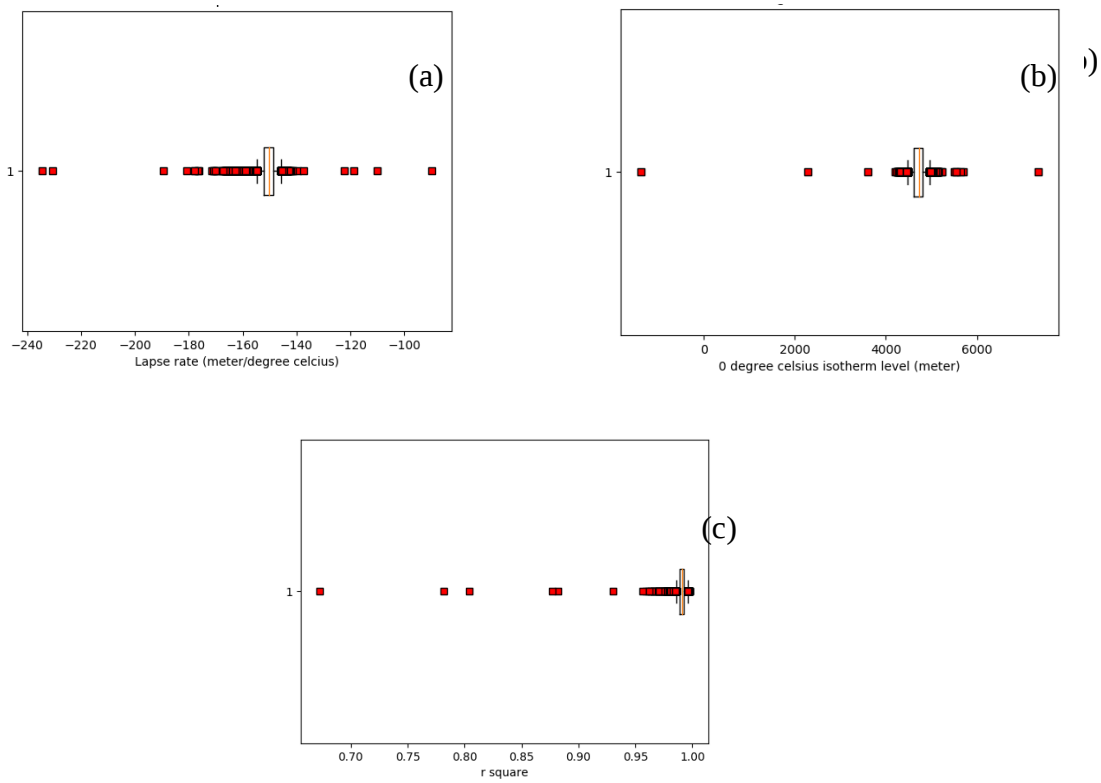

Figure 2.29. Radiosonde temperature profile distribution data (a) lapse rate (b) 0ºC isotherm level (c) linear correlation coefficient (r^2).

The data distribution of air temperature lapse rate and 0ºC isotherm level are shown by whisker and box plot in figure 2.29. We exclude the data with fliers *a* and *b*. From this work, we get a range *a* and *b*. From this work, we get a range of *a* must be -143 m/ºC to -158 m/ºC. The range of *b* should be 4330 meters to 5107 meters. The average r^2 is 0.99.

The data distribution of CTT performs in figure 2.30. The x-axis is the number of lightning per hour per grid, and the y-axis is the cloud top temperature. We perform the data as the mean value of every number of CG lightning, shown by the blue dot. The mean value is looked smooth with the logarithmic trend line $f(x)=-7.95\ ln(x) - 54.57$ with $R^2=0.95$. *Meanwhile, t*he error bar of every dot shows the standard deviation of the sample. Based on that image, the thunderstorm cloud's temperature must be less than -30ºC to produce at least 1 CG lightning, which can be detected by AVON V-POTEKA.

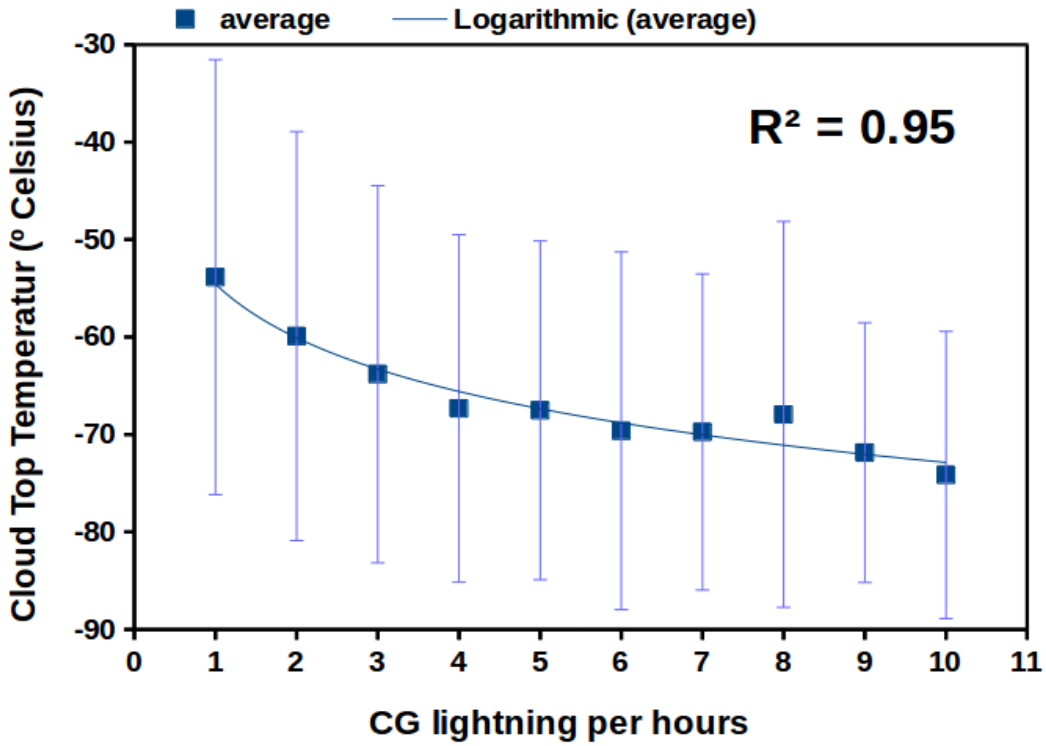

Figure 2.30. Cloud top temperature (CTT) for every number of CG lightning per hours in a grid size ~50 km x 50km. The error bar shows the standard deviation.

Like CTT distribution data, the distribution CTH is shown by the median value of every number of CG lightning per hour in a grid size ~50 km x 50km. The plot of CTH is performed in figure 2.31. The average data plot shows that CTH is the logarithmic function of the CG lightning f(x)=1203 ln(x) + 12957 with R^2=0.95. If the x and y-axis are changed reverse, the curve will become an exponential relationship with exponential slope 0.6. Meanwhile, Ushio et al. (2001) show the exponential relationship between CTH of thunderstorm and lightning activity with exponential slope 6.0 and 48 for land and ocean of broad tropics area, respectively[5]. Moreover, Ushio et al. (2001) used TRMM lightning data from space that does not consider the type of lightning. However, in this study, only CG lightning detected by AVON V-POTEKA in the maritime continent is used in the relationship between CTH and lightning.

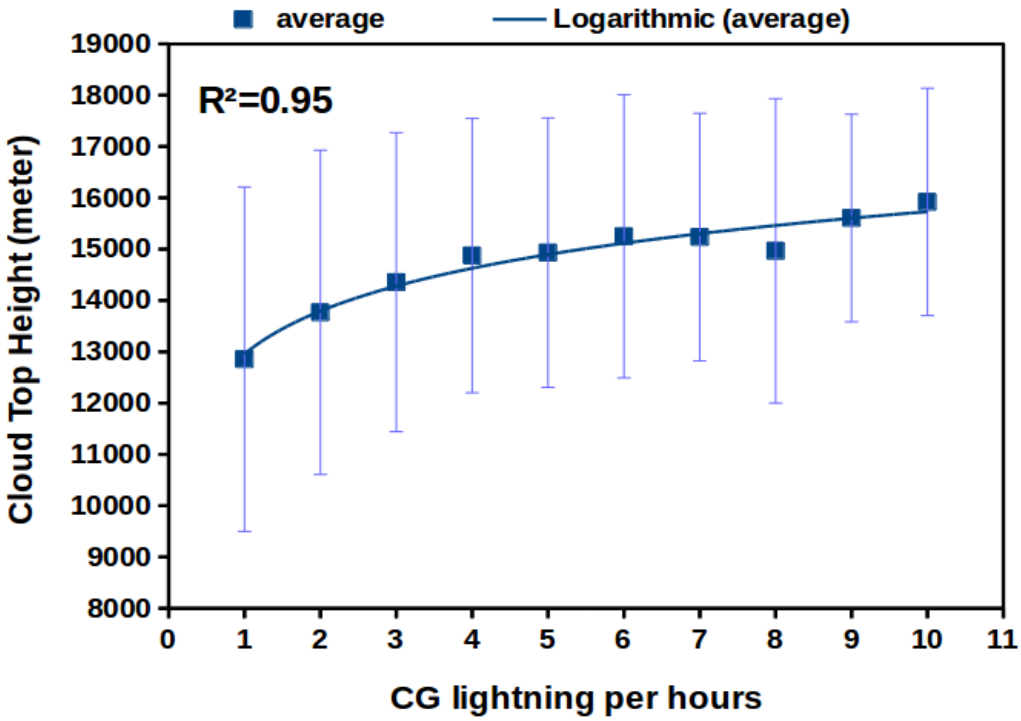

Figure 2.31. Cloud top height for every number of CG lightning per hour in a grid size ~50 km x 50km. The error bar shows the standard deviation.

For rain data, we use TRMM precipitation product standard V7 hourly gauge-calibrated rain rate data to get a broad sample. This data has a one-hour time resolution and spatial resolution 10 km. The error bar shows the upper and lower standard deviation, which shows the skewed data to the low value of rain intensity. Even though the distribution data is quite broad, the participation data focus on the median value of the data. The mean value of the precipitation rate for each CG lightning number is shown in figure 2.32. The data is fitted with a power trend line $f(x)=0.96\,x^{0.48}$ and $R^2=0.92$.

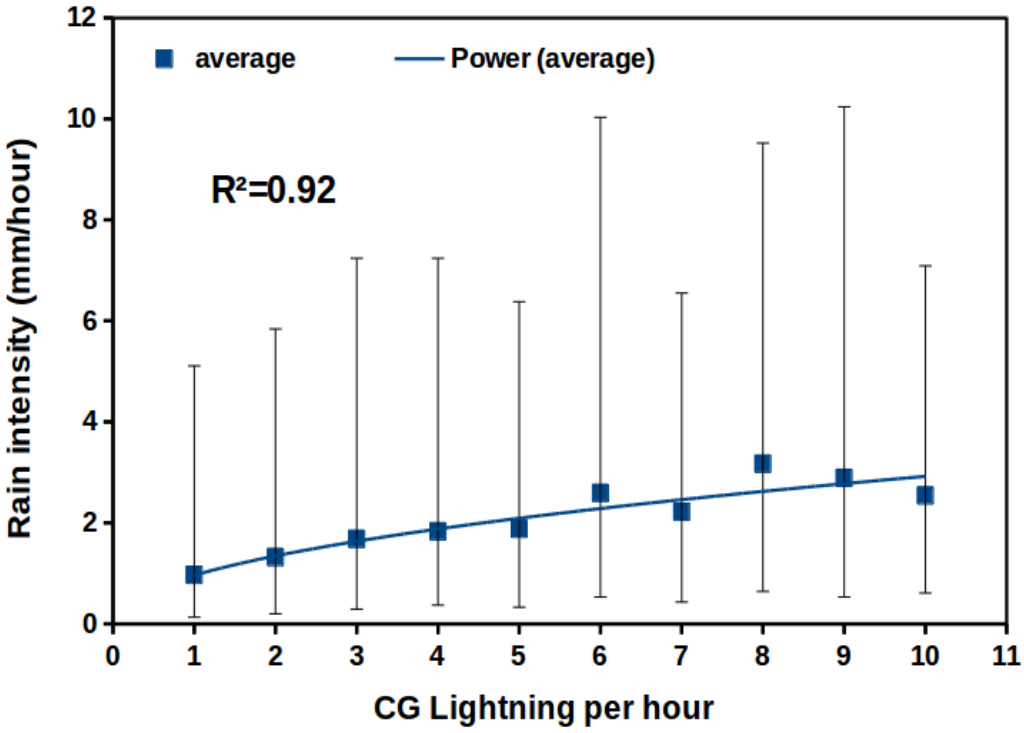

Figure 2.32. Rain intensity as a function of lightning number detected by AVON. The error bar shows the upper and lower standard deviation.

Precipitation volume (PV) of the thunderstorm cloud is the thunderstorm cloud parameter correlated to lightning numbers by many previous studies [8]. In this study, we also make a correlation between PV and the CG lightning stroke detected by AVON. We calculate the PV from the TRMM precipitation data. As explained at the beginning of this subchapter, the TRMM used in work has spatial and temporal resolution ~10 km and 1 hour. We multiply the precipitation rate to the spatial resolution of TRMM data to get the PV. We sum 25 PV data inside the gird size 50 x 50 km. The pattern of PV distribution the figure 2.33, shown by error bar, is almost similar to the rain intensity distribution. The PV is fitted with power trend line $f(x)=(3.36E6)x^{0.32}$ with $R^2=0.8$.

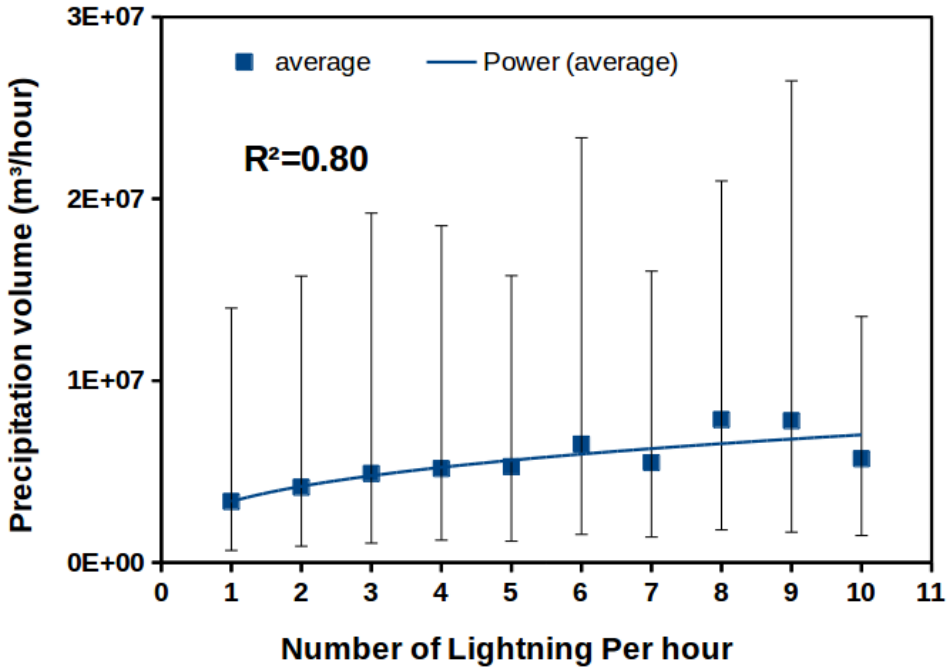

Figure 2.33. Precipitation Volume (PV) as a function of lightning number detected by AVON. The error bar shows the upper and lower standard deviation.

For the relationship between CTT and rainfall, we examine the rainfall during the dry season in Manila, December 2019, to May 2020. The 30 P-Poteka, which is equipped with automatic weather station (AWS) and rain gauge, has been deployed in Metro Manila and become the densest in Southeast Asia. It can record the rain rate every minute. For the CTT, we take from Himawari 8 band 15 (12μm) with resolution every 10 minutes. So in this relationship, use time resolution of 10 minutes for both rainfall and CTT data. We take the maximum rainfall from all stations, and we take the minimum CTT over the P-Poteka installation area. The exponential relationship between CTT and rain rate with R^2=0.50 is achieved in this study.

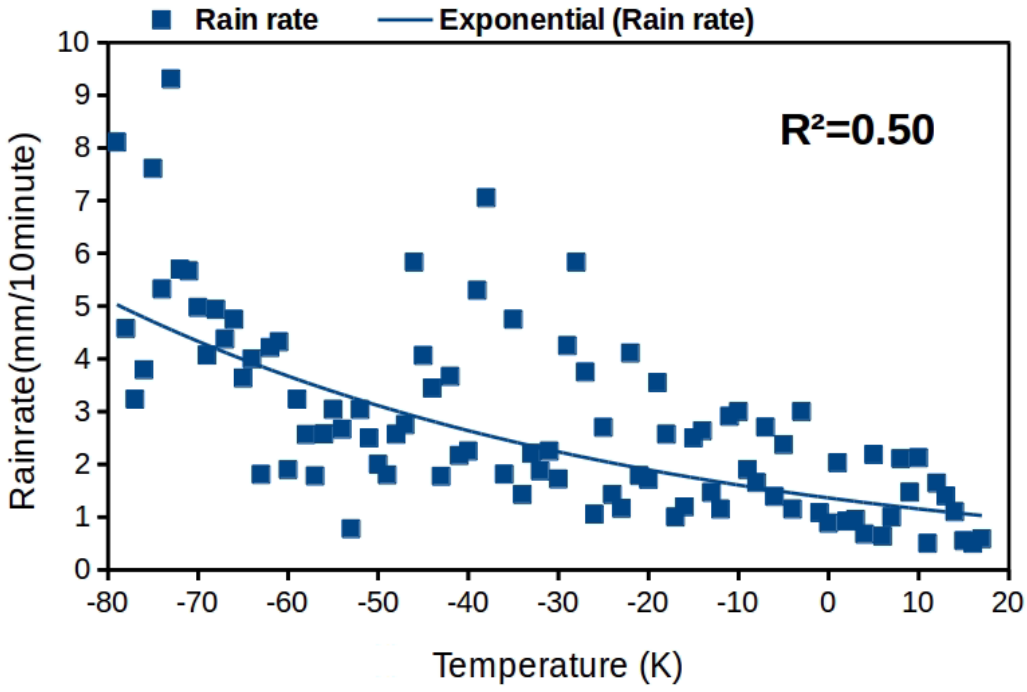

Figure 2.34. Relationship between cloud top temperature (CTT) and rain rate.

2.4.2. Diurnal convection activities in Kalimantan

The thunderstorm cloud is the result of the convection process in the atmosphere. Strong convection is mostly followed by a strong dynamical process inside the thunderstorm cloud. The dynamical process inside the thunderstorm cloud increases the probability of the friction between ice crystal and grouple, which makes charge separation and different potential electricity inside the thunderstorm cloud or to the ground. The lightning will occur if the air isolation between the two parts has been break by the different potential energy of electricity. So, we think that lightning can represent the convection level of the area.

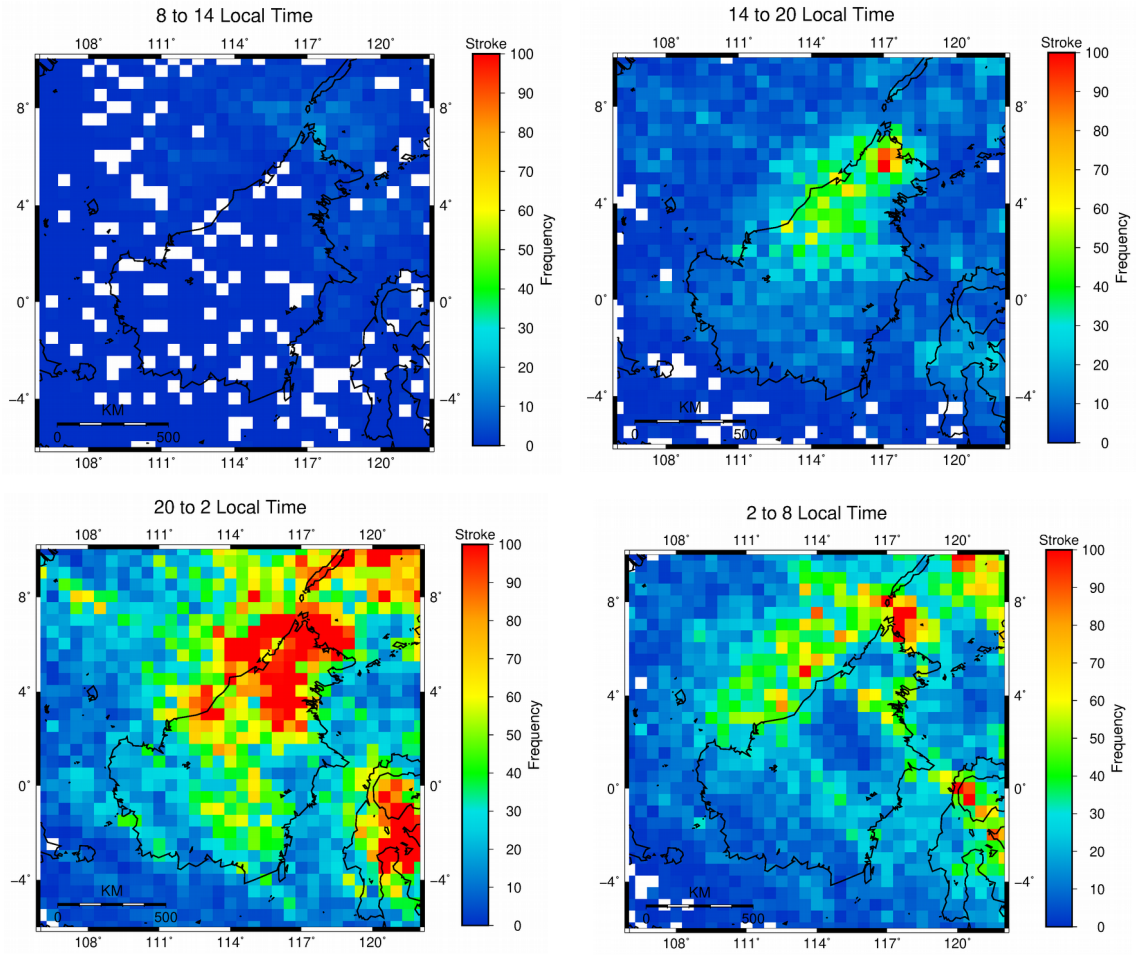

Figure 2.35. The ten months lightning event detected by the AVON lightning detection network from June 20th, 2019 to April 21nd, 2020. Each panel shows the 6-hourly accumulated lightning event with grid 0.5º x 0.5º during the period.

Using lightning data, we will show the diurnal variation of convection over Kalimantan Island. We use AVON V-POTEKA data from June 20th, 2019, to April 21nd, 2020. We make lightning density during that period with the grid 0.5º x 0.5º, as shown in figure 2.35. The lightning mostly occurs in the afternoon and evening along the coast island. Moreover, in the central region of Kalimantan island and the sea adjacent to the coast, the lightning mostly occurs at night and early morning.

For the comparison, we make the ten months mean near-surface rain detected by the TRMM Precipitation in the same period with the lightning data. Generally, the

pattern of the rain diurnal variation is the same as the diurnal lightning occurrence. The rain mostly occurs in the afternoon and evening along the coast island. Meanwhile, night time and in the early morning, the rain occurs over plains of the central island region and the sea adjacent to the coast. However, the high rain intensity in the afternoon and evening along the west coast of Kalimantan is not followed by the high intensity of the rain. On the contrary, the high lightning density on the northeast coast of Kalimantan is not followed by a high intensity of rain.

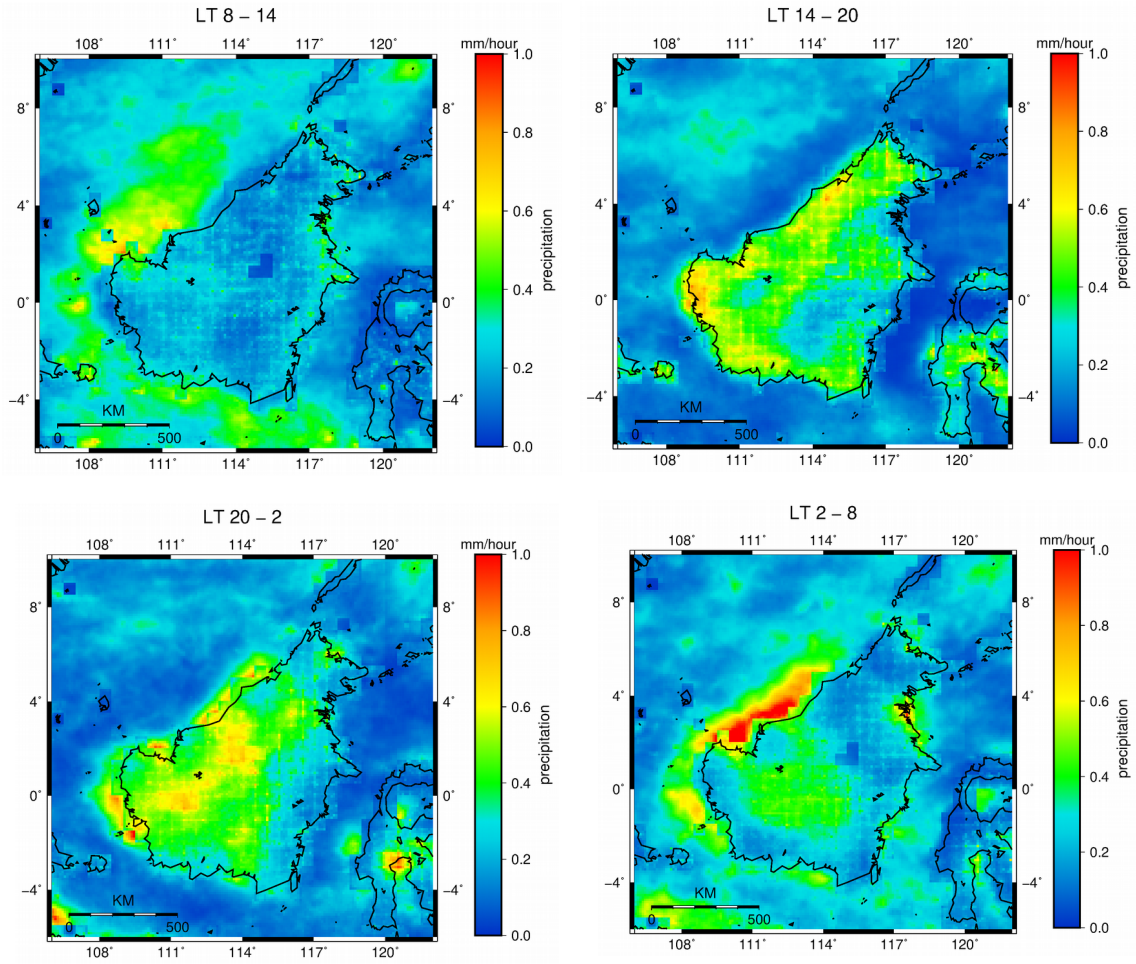

Figure 2.36. The ten months mean near-surface rain detected by the TRMM Precipitation standard V7 for the period June 20th, 2019, to April 21nd, 2020. Each panel shows the 6-hourly mean rainfall rate for the indicated period.

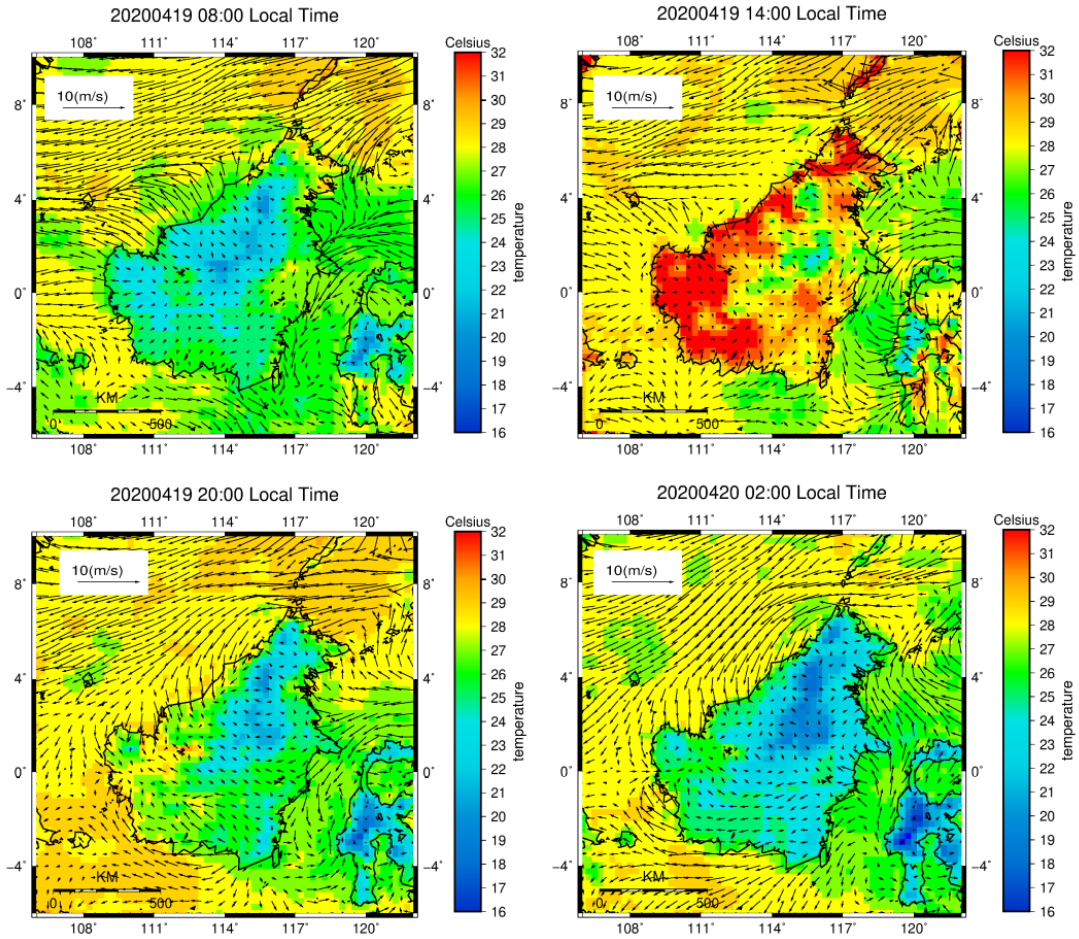

Figure 2.37. The surface air temperature and wind vector on April 19th, 2020 at 08:00, 14:00, 20:00, and 02:00 local time.

To understanding the convection mechanism over Kalimantan, we plot the surface air temperature and wind vector on April 19, 2020, at 08:00, 14:00, 20:00, and 02:00 local time. In the morning, when the land temperature is less than the sea temperature, the land breezes occur in the west part of Kalimantan. As a result of the rising air over the sea, the sea's surface pressure becomes lower than the land. The opposite condition happens in the afternoon when the land temperature is warmer the sea. The convection over land is stronger than the sea, making the pressure over the land lower than the sea. The sea breeze start occurs, and the clouds over the coast are growing. With the temperature over the land reach 32ºC, convection over land is

stronger than convection over the sea in the morning. The sea breeze continues at night, even though the land's temperature is lower than the sea.

2.4.3. Typhoon

Price et al., 2009 analyzed the evolution of maximum winds and total lightning frequency every six hours. They found that in all hurricanes, lightning frequency and maximum sustainable wind speed are significantly correlated with a correlation coefficient of 0.82 with the lag time ~30h[21]. Whittaker et al., 2015, enhance the Price work by increasing the number of tropical cyclones and changing the lightning collection window. Whittaker et al. increase the number of tropical cyclones from the previous study of 58 storms by Price to be 144 cyclones in an 8-year dataset. They did the same way, with a 10^{o} square window, as Price did, and they got a similar result to the smaller data set. Then they change the lightning collection window by the radial shape. They confirm that using radial lightning collection windows of < 500 km, the lag time between lightning and maximum sustainable wind speed is ~1 day — both studies using WWLLN lightning data[22].

The previous study done by Price and Whittaker is inspiring us to investigate why the lightning in a distance of their collection window has a significant correlation with the maximum sustained wind of the cyclones with the almost constant lag time. To do this, we make the initials assumption as:

1) The number of lightning activity around the hurricanes is proportional to heat energy.
2) This heat energy moves to enter the cyclones as the speed and direction of the wind.

Based on the initial assumption, that the energy brings by the wind, we did back-tracing using the wind data of ERA5 reanalysis at the pressure level 1000 to 400 Mb with the interval 100 Mb and typhoon data from Joint Typhoon Warning Center (JTWC). First, we make symmetrical of 60 initial points in the radius of 100 KM surrounding the center. Then we trace the points with the speed and opposite

direction of the wind. The new position is calculated using the 30 minutes interval time and up to 48 hours before. The result of back-tracing every pressure level is shown in figure 2.38. As shown in figure 2.38, the back-tracing is like a different radius size of spiral for different pressure levels. Temporary conjecture, the spiral's radius size corresponds to the lag time between lightning and maximum wind speed in the previous lightning collection windows.

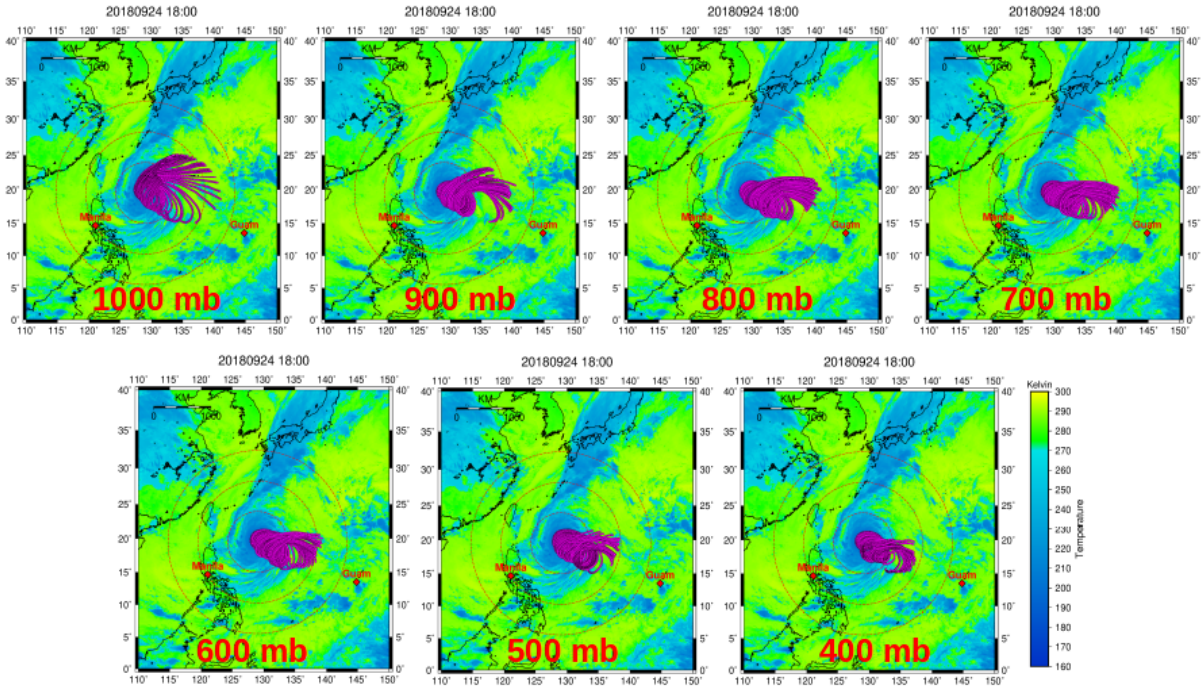

Figure 2.38. The back-tracing technique was applied for typhoon Trami on September 24, 2018, 18:00 UTC up to 48 hours before for different altitudes.

Figure 2.39 shows the back-tracing for several initial time locations for the wind data at the height level of 900 hPa. Based on figure 2.39, the source of energy area is varied during the typhoon Trami development.

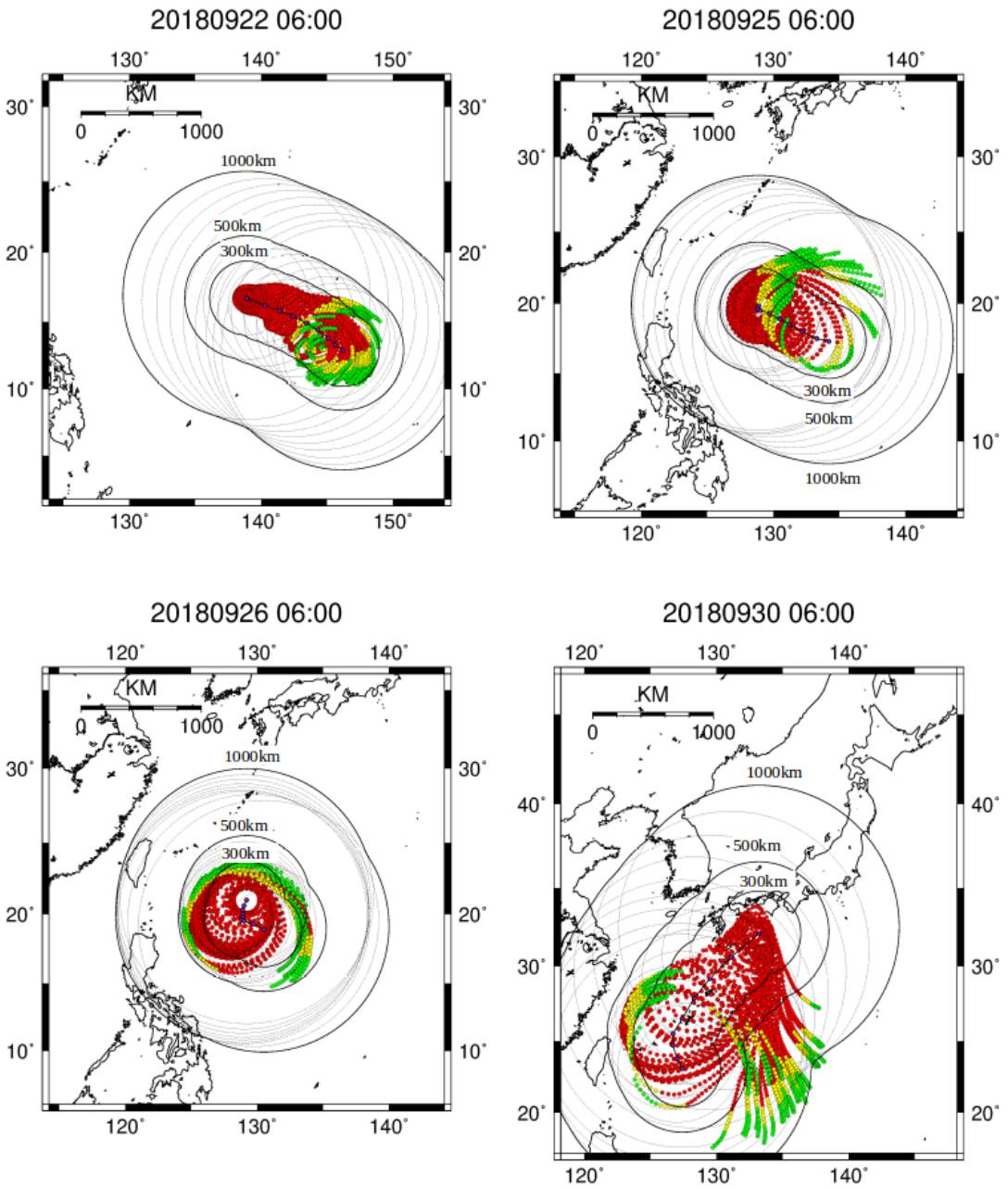

Figure 2.39. Back-tracing for several initial time at 900 hPa height level. The red, yellow, and green dot are the -36, -42, -48 hours tracing, respectively. The purple is the typhoon eye tracking.

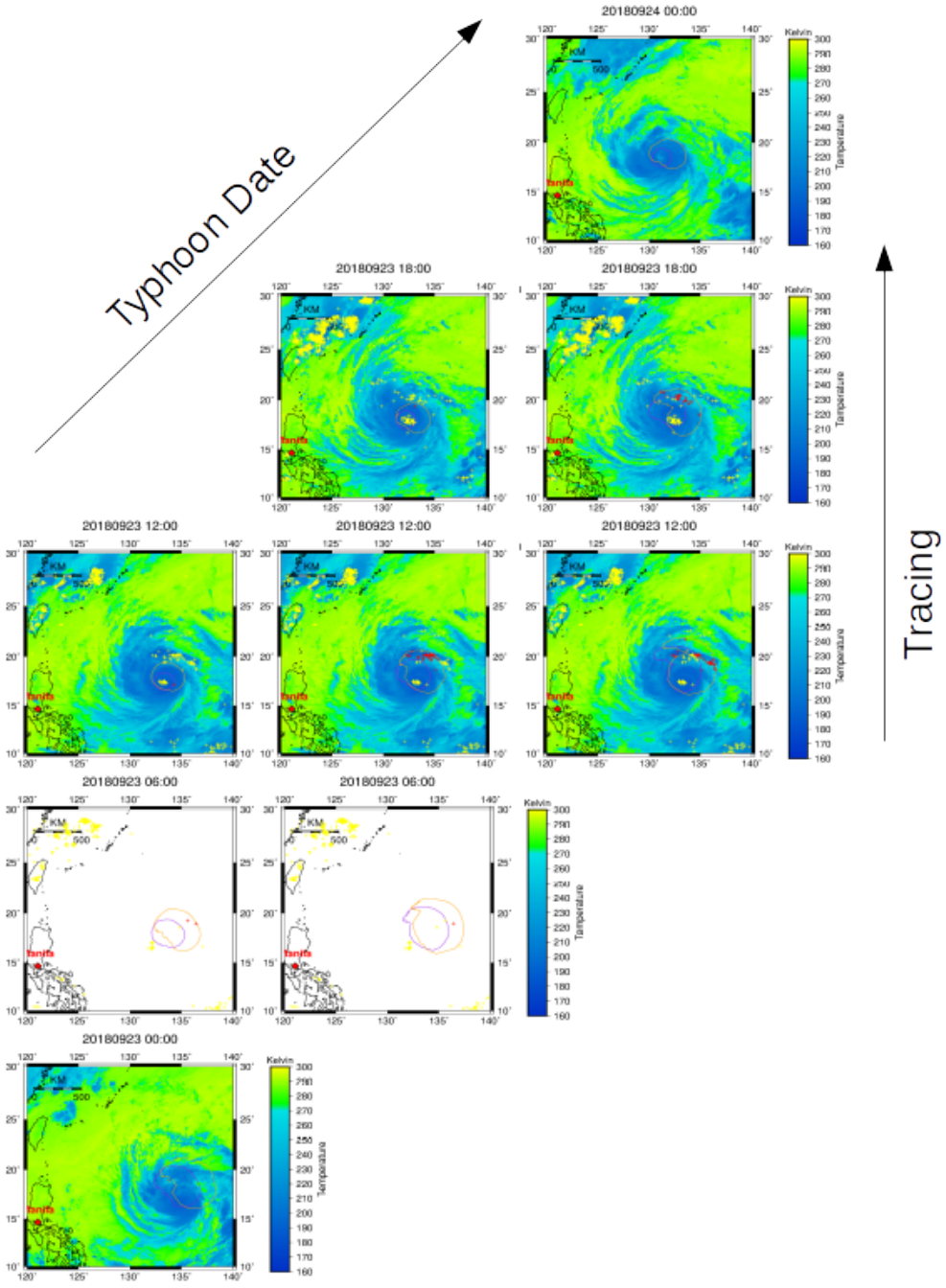

Figure 2.40. Back-tracing lightning collection window. The red cross is the counted lightning, and the yellow cross is uncounted lightning.

After we get the back-tracing point, every point with a similar time is connected and forms the polygon area as our lightning collection window. Then, we only count the lightning occurrence between the two polygon areas with an interval of 6 hours at the desired time. The example of our lightning collection windows is shown in figure 2.40. The lightning collection windows on September 23, 2018, 12:00 UTC in figure 2.40 show that the lighting collection windows are different if the initial time is different. Ideally, every initial time of back-tracing will take different lightning strokes.

The result of lightning collection is shown in figure 2.41. We show the lightning collection for different pressure levels on a separate chart and variation of initial time in one chart with a different color. We also show the maximum sustainable wind speed taken from the Joint Typhoon Warning Center (JTWC). For the first analysis, we can compare qualitatively between BT and a circle radius of 300 km and 500 km. Qualitatively, the lightning number counted using BT is more matching with the maximum wind speed curve data than the lightning number counted using circle windows. Moreover, the shape of the lightning collection chart almost similar to the shape of the maximum wind speed chart at pressure level 800 hPa, 700 hPa, and 600 hPa. The stopping time from -30 to -48 hours is looked acceptable to a similar chart pattern with the maximum wind speed chart.

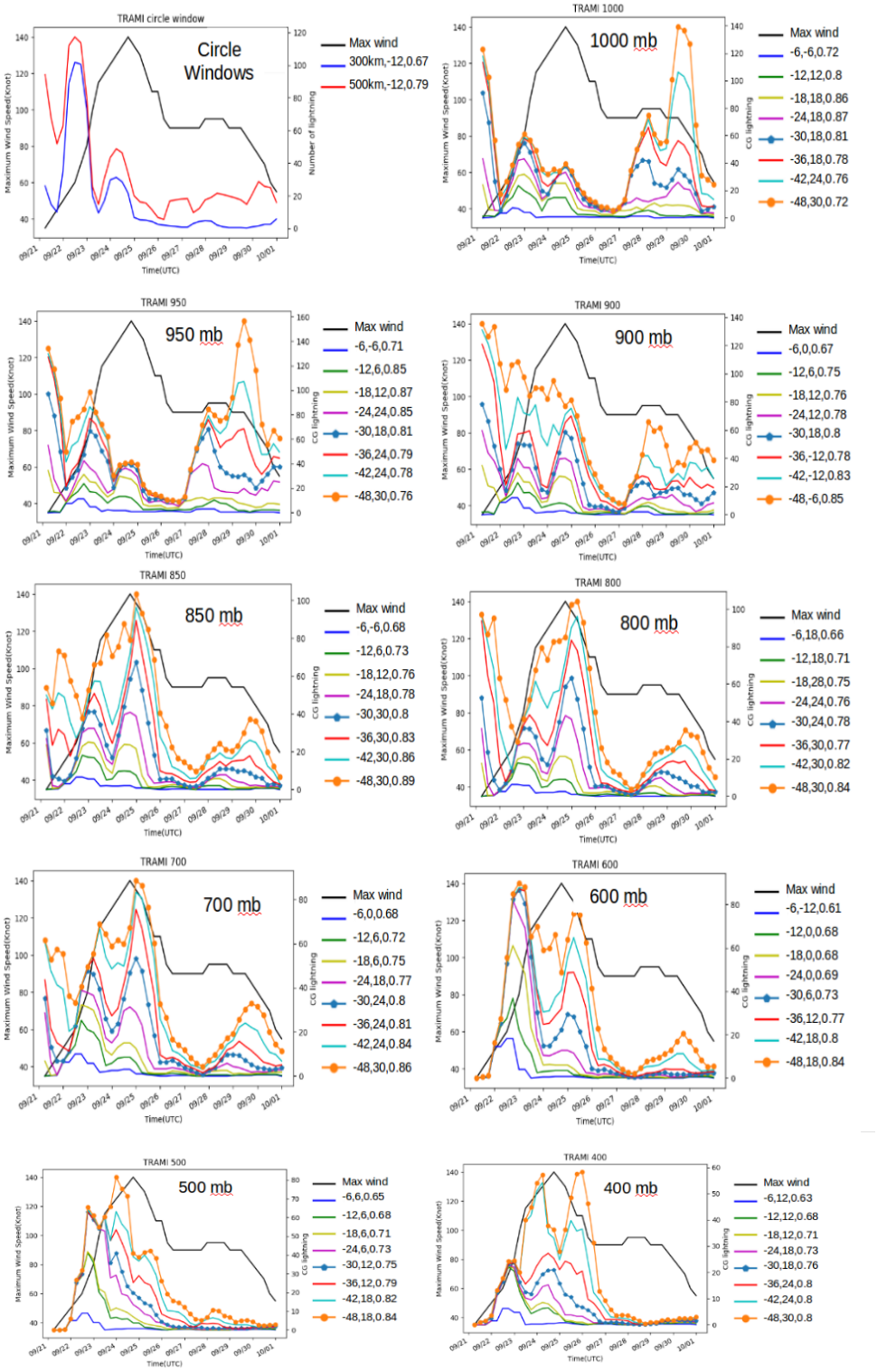

Figure 2.41. Cross-correlation between the lightning swept by the wind and the maximum sustained wind speed of Typhoon Trami. The lightning data is smoothing using 24 hours moving average.

For quantitative comparison, we calculate the cross-correlation of this result. As the previous study did, we apply a moving average for every 24 hours [21,22]. The result of the moving average is looked like making smooth of the lightning data curve. We apply cross-correlation for both works to estimate the lag time between lightning activity and maximum sustainable wind speed. The best cross-correlation is taken to get the lag time. The lag time estimation and its correlation coefficient are performed on the image legend. Minus lag time shows that the lightning activity occurs before the maximum sustained wind speed of typhoons.

Based on figure 2.41, for the wind in level 600 Mb to 400 Mb, there is no lightning before or during the beginning increasing of maximum sustainable wind speed. Logically, the typhoon needs much energy to increase the maximum wind speed. The maximum wind speed is the result of the latent heat conversion to the kinetics energy. Then, the latent heat energy, as described as the number of lightning, must exist before or during the maximum wind speed increase. So, we think that the wind in level 600 Mb to 400 Mb is not possible for the typhoon's energy carrier.

Based on the cross-correlation coefficient and the lag time, the level 900 Mb for the first locations -36 hours to -48 hours shows the reasonable level path and initial location of the energy. Qualitatively, it also shows the similarity of the chart's shape pattern with the maximum wind speed chart.

2.4.4. Taal volcano eruption produce lightning

Volcanic lightning is prevalent in explosive eruptions, which happens during most intermediate or more massive explosions. As the magma rises to the surface, it can become frothy and bubbly and break itself apart. The water bubbles expand and blow themselves up. That breakage process is highly electrifying. Once those tiny rock particles volcanic ash are shooting up into the atmosphere at high speed, they are colliding, exchanging electrons, and creating a charge right at the base of the volcanic plume. Then once the plume rises high enough to freeze, the ice particles help to generate even more lightning by separating more charges [38-0].

a)

b)

Figure 2.42. a)Aerial view of the volcano taken from the NE showing the Taal MCL (TMCL) (Hernandez et al, 2017). b) Taal Volcano eruption on January 12, 2020 produce ash cloud and lightning (Photo: Bataan Weather Page's official Facebook account)

The Taal Volcano is located in the middle of Taal Lake, in province Batangas, Philippines. Taal Volcano is the second most active volcano in the Philippines. Acid crater lakes form when volcanic or hydrothermal fluids enter a volcanic lake filled with meteoric water[41].

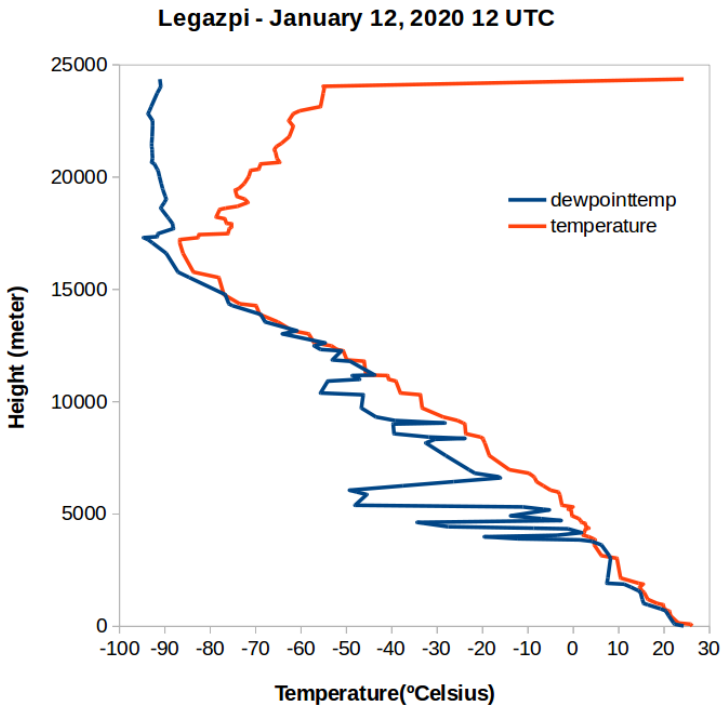

Figure 2.43. Atmosphere profile temperature measuring by radiosonde balloon in Legazpi, ~312 km from Taal Volcano. Dew point temperature(blue) and temperature (red)

The last Taal Volcano erupted on January 12th, 2020, which produced cloud ash and lightning. The Philippines Nation-wide lightning detection network detects some flashes of lightning in around the Taal Volcano eruption. On the other hand, the cloud ash was also detected by Himawari 8 geostationary satellite. This study will show the evolution of the Taal Volcano cloud ash using the V-POTEKA lightning detection network and Himawari 8 Band 15 (12µm). The Himawari 8 Band 15 (12µm) will detect the CTT. By assuming the temperature of the CTT follow the environment temperature, we estimate the height of every pixel of the Taal Volcano ash cloud and perform it as a 3D image.

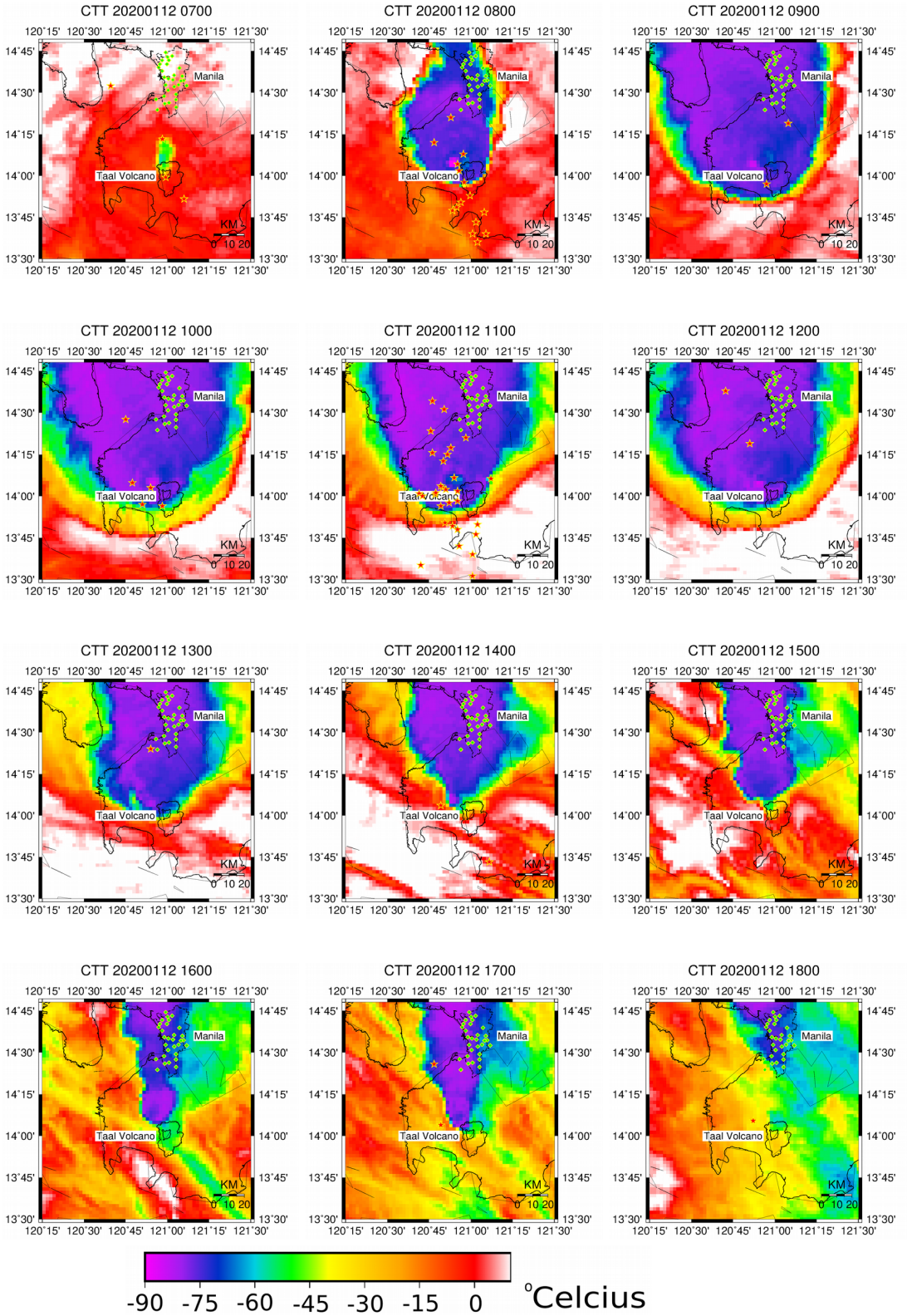

Figure 2.44. Taal volcano eruption detection from space by Himawari 8 Band 15 (12µm) And the lightning detected by V-POTEKA network (red star). Green diamond is the P-POTEKA location in Metro Manila.

Before the eruption, the Taal Volcano area is covered by the cloud layer in height around 5000 meters, as shown in figure 2.44. This condition agrees with the atmosphere temperature profile by radiosonde measured by Legazpi station, which shows the inversion layer at the level 5000 meter. The Taal volcano eruption has enough energy to break through this inversion level. So the cloud produce by the Taal volcano eruption can grow higher than this level. The minimum temperature detected by Himawari 8 Band 15 (12μm) is ~90ºC and agrees with the minimum temperature atmosphere profile measured by radiosonde. From figure 2.44, we can see that the material of eruption directed to the north.

Moreover, if we look more detailed in image 2.44, warmer areas are surrounded by cold areas, making ambiguity in estimating the CTH. The warmer area can be the lower area of the minimum temperature. However, it can also be the part of the cloud that passes the inversion layer in the tropopause. We use a single band of Himawari 8, which may have difficulty detecting the overshooting thunderstorm (OT). Based on figures 2.44 and 2.45, the lightning's peak occurs at 11:00 UTC (19:00LT). However, there is two explosions lightning event around 08:00 UTC and 11:00 UTC.

We plot the minimum CTT and CG lightning stroke every ten minutes for temporal analysis. We take the minimum of CTT in rectangular area size 40 km x 40 km covering the Taal Volcano area. For the lightning data, we only use the lightning with the ambiguity geolocation at least 20 km from the Taal Volcano. Figure 2.47 shows the temporal evolution of cloud ash and the lightning occurrence with the resolution 10 minutes. Figure 2.47 shows that there are two majority groups of lightning activities at 8 UTC and 11 UTC. The first group occurs ~1 hour after the big explosion, as mention in some news that the big explosion occurred around 15:00 local time (07:00 UTC). We also estimate the cloud growth speed, which shows the maximum growth speed ~50m/s at around 15:00 local time (07:00 UTC), which is closed to the big explosion, as mentioned in the online media. The first CG lightning occurs after the maximum growth speed and near the maximum height.

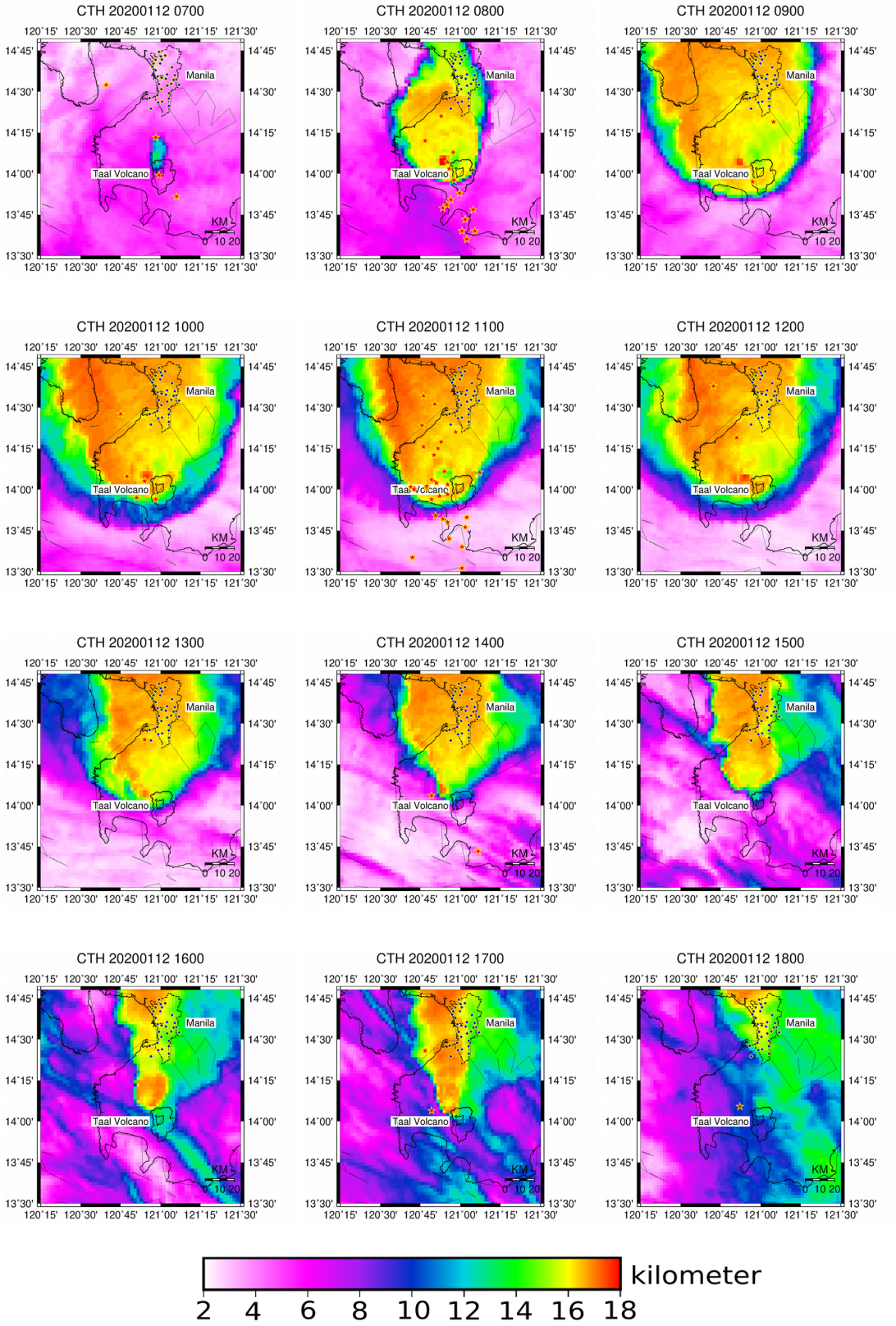

Figure 2.45. Cloud ash height estimation of Taal volcano eruption and the lightning detected by V-POTEKA networks. Green diamond is the P-POTEKA location in Metro Manila.

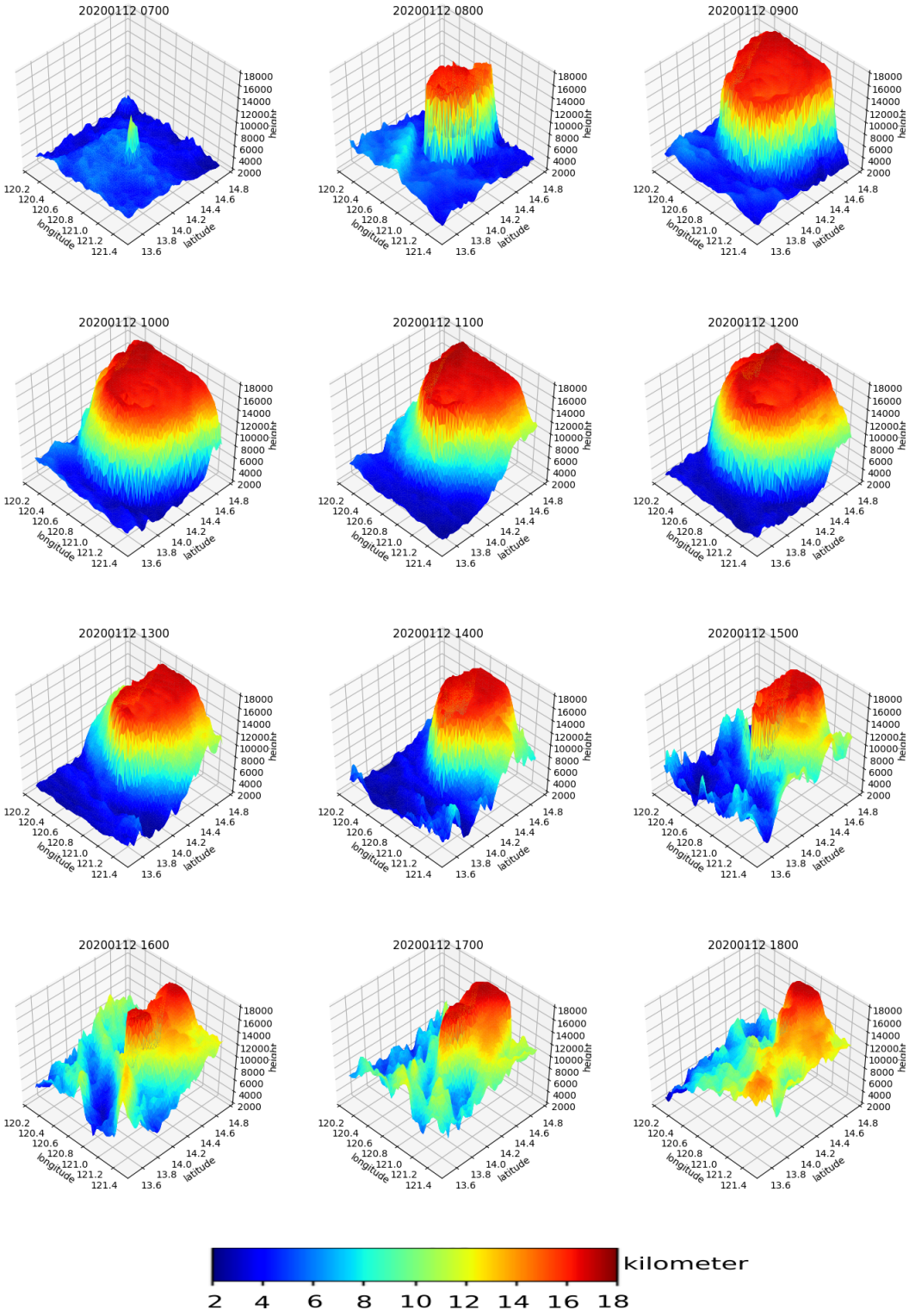

Figure 2.46. Cloud ash evolution produce by Taal Volcano eruption perform in 3D.

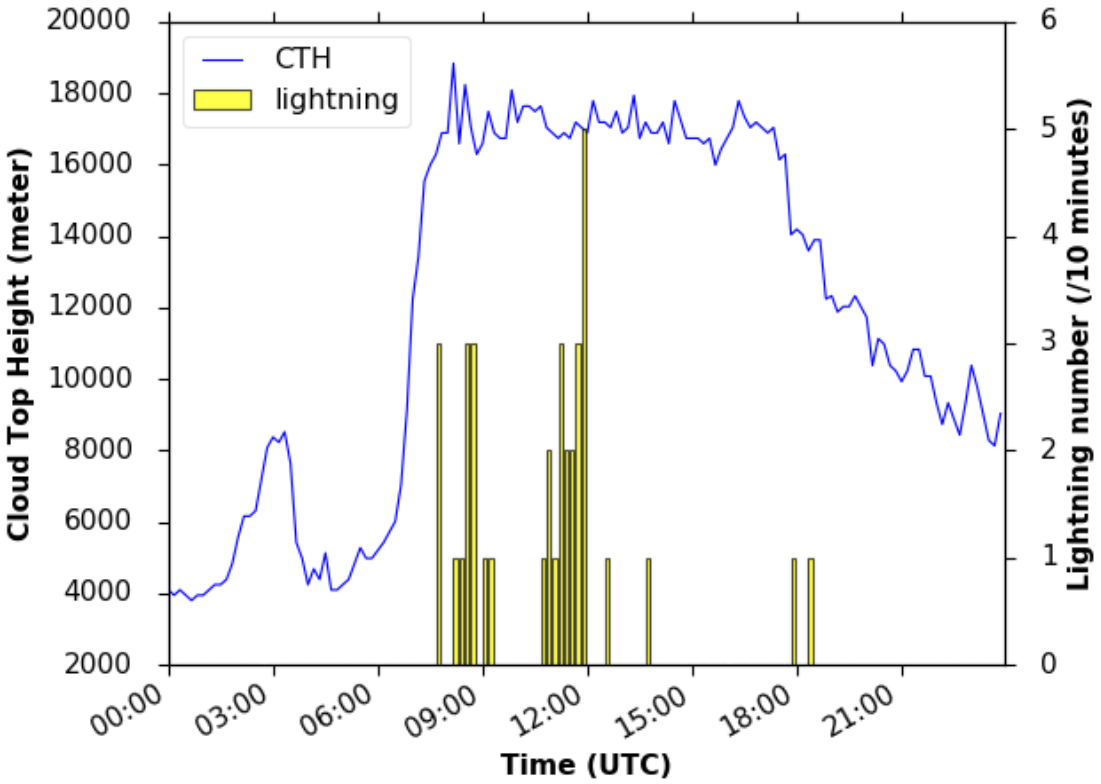

Figure 2.47. The Taal volcano cloud ash height and the lightning event detected by V-POTEKA lightning detection networks in Philippines.

2.5. Discussion

2.5.1. Thunderstorm clouds study

Much research has been conducted to study convection cloud over the Maritime Continent (MC)[36]. Intense latent heating accompanies heavy rainfall during Maden-Julian-Oscillation (MJO) is the global issue attracting the object of the study over the MC because it is a significant heat source for global atmospheric circulation. A local topic such as the characteristic lightning discharge in Indonesia, such as

lightning spatial and temporal distribution, and the relationship between lightning and severe weather have been conducted using different instrumentation and methodology[4].

In this research, we investigate the relationship between lightning with other thunderstorm parameters over MC, namely CTT, CTH, ran rate, and precipitation volume. The AVON with the V-POTEKA instrument has been deployed and operated for around ten months. During around ten months, many lightning data have been collected in a broad area over MC. The result of the relationship with the static area sampling method is performed in sub-chapter 2.4.1. As described in some result in sub-chapter 2.4.1, the distribution of the data is quite broad. The MC, which consist of many island and sea, has many variations of the local characteristic. Besides that, MC also has seasonal and intraseasonal characteristics, which also affect the thunderstorm cloud's character. The local characteristic, which also depends on the seasonal and intraseasonal, may influence the thunderstorm cloud's characteristics.

Recently, the relationship between the flash rate and cloud top height (CTH) has been studied by many researchers. The study has done by Ushio et al., 2001 shows that the flash rate increases exponentially with storm height[5]. He states that the fifth power dependency derived from scaling laws, done by William[1985] who modify the scaling laws by Vonnegut [1963], is not inconsistent with, but necessarily required by, the observed data[5]. The physical basis to support the relationship comes from the theory that flash rate is strongly affected by the strength of the charge separation and the charge distribution geometry, in which vertical air motion plays a fundamental role. Hence the flash rate is expected to depend on the intensity of vertical air motion closely related to the storm height[5. In his study, Ushio et al., used lightning data from the Tropical Rainfall Measuring Mission (TRMM) satellite and did not mention the type of lightning.

As explained in sub-chapter 2.4.1, all of the relationships between the lightning and other parameters of the thunderstorm cloud shows the logarithmic as a function of lightning number per grid area per hour. For the comparison with Ushio et al., 2001, result, which mentions that the flash rate increases exponentially with

storm height, we reverse the x-axis and y-axis, as shown in figure 2.48. The result shows that the relationship between the CTH and CG lightning of the Thunderstorm cloud is an exponential function with R^2=0.95.

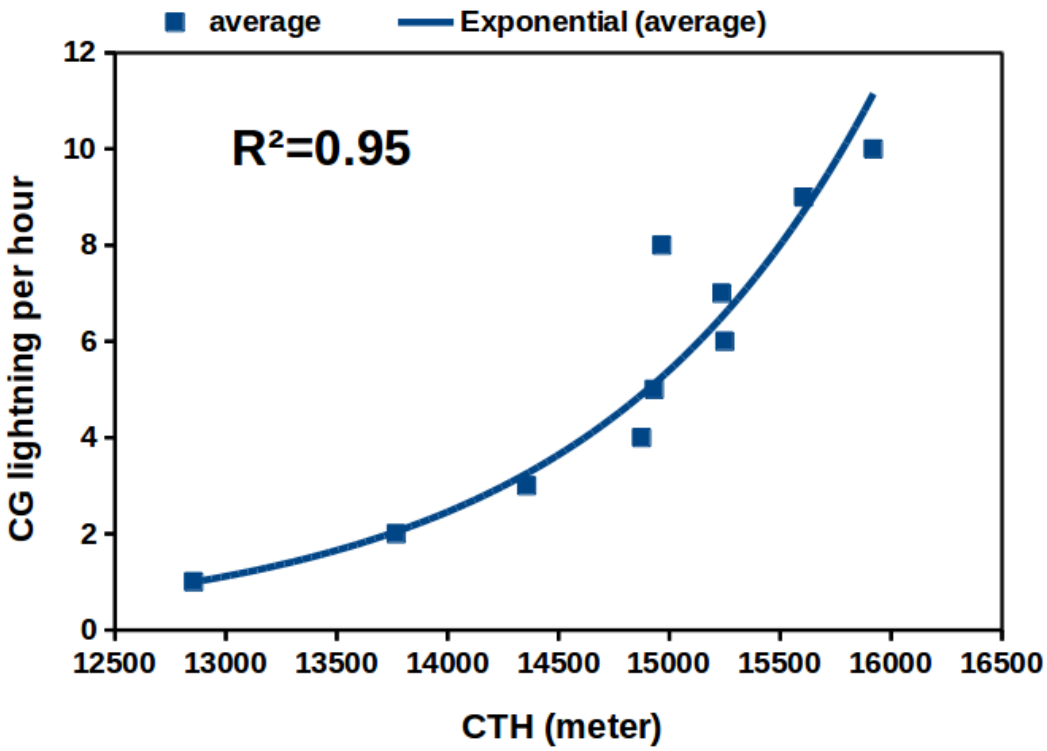

Figure 2.48. The relationship between the CTH derived from Himawari 8 band 15 (12µm)and CG lightning detected by AVON with V-POTEKA instrument

Gungle and Krider, 2006, summarize the previous study about the relationship between CG lightning flash rate and precipitation volume (PV)[8]. In their summary, they noted about 28 studies made the report on this topic. Compare to our result, Gungle and Krider, 2006 show the linear relationship between lightning and PV, shown in figure 2.49, while our result shows a logarithmic relationship for PV and maximum rain rate. However, in their works, they use a thunderstorm area rather than a static grid area. So, the increase in lightning number is followed by the linear increase in precipitation volume. We think, even though not mention by Gungle and Krider in their study, that the PV is also the result of the increasing

precipitation area. If the PV per unit time is divided by rain intensity, we get a number with the unit of area. As shown in figure 2.49, the result of linear PV divided by rain intensity is a power relationship with a different grade of power. So, the correlation between the CG lightning number and precipitation water area is possible to be a power relationship.

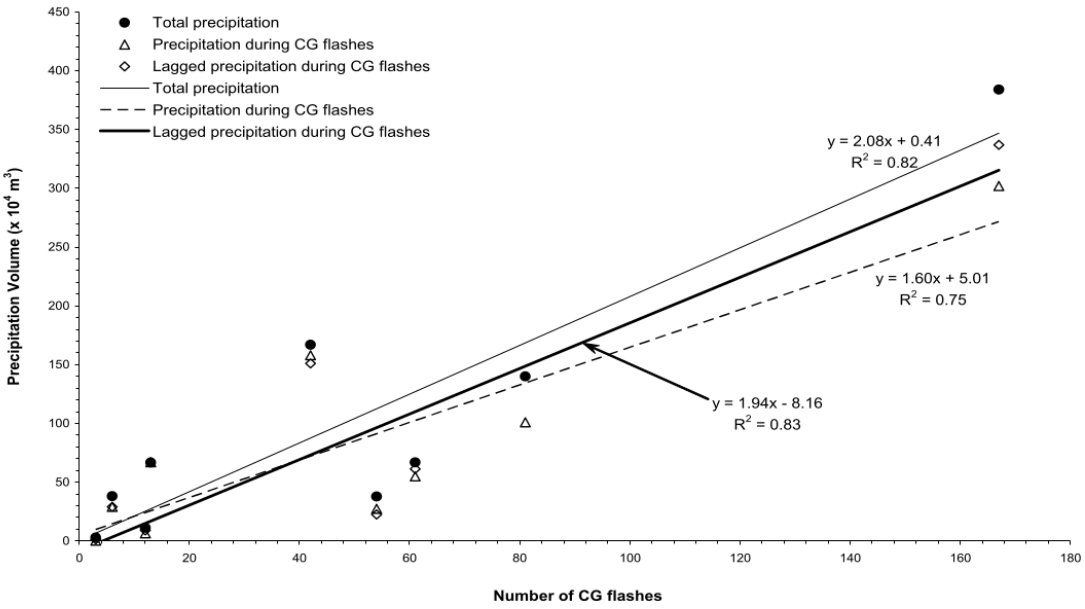

Figure 2.49. Linear regression of the precipitation volume computed using methods 1, 2, and 3 (see text) versus the total number of CG flashes in nine Florida thunderstorms. Gungle and Krider, 2006.

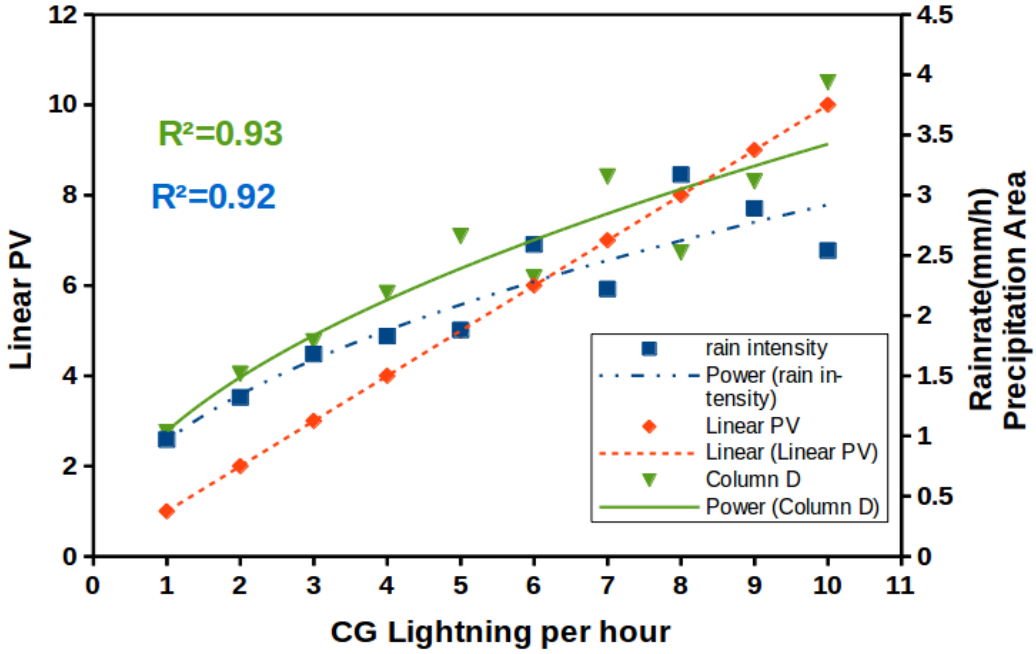

Figure 2.50. Schematic describe the relationship between CG lightning and the rain rate, PV, and precipitation area of thunderstorm clouds.

However, a recent study, Zheng et al. (2010), correlates between total lightning activity and precipitation particle characteristics from 34 thunderstorms around Shanghai and Wuhan of China[7]. They conclude that the spatial relationship between total lightning density and precipitation particles are not significant in the spatial grid of 0.1°x0.1°. They mention that the relationship between lightning density rainfall intensity is a power relationship that agrees with our result. On the contrary, we found a good relationship between CG lightning and the maximum rain rate of PV in the spatial grid of 0.5°x0.5°. This grid size is enough to cover the estimated error of geolocation of lightning.

In this study, the relationship between lightning density with other thunderstorm characteristics, namely Cloud Top Temperature (CTT), Cloud Top Height (CTH), rain rate, and precipitation volume (PV) in the grid area shows good correlation. The obtained fitting equation may use for the reference of the numerical prediction model assimilation to improve the accuracy of prediction. Moreover, the correlation in the grid area in size 0.5°x0.5° may use full and applicable for target

area observation. The combination method of ground lightning detection networks and thermal infrared camera onboard micro-satellite with its advantages and deficiency such as high-resolution but limited field of view (FoV) is suggested to use static target area observation method to predict the torrential rainfall caused by thunderstorms clouds.

2.5.2. Diurnal convection variation over Kalimantan

In the previous study, Wu et al., 2008, investigated the diurnal convection variation over western Kalimantan (Borneo) Island and adjacent seas. Using precipitation measurement from TRMM satellite, they found that rainfall mostly occurs in the afternoon and evening along the coast island, and at night and in the early morning over the plains in the central region of the island and the sea adjacent to the coast as shown in figure 2.51. They confirmed that the occurrence of afternoon and evening convection along the western coast of the island, and nighttime and morning convection over the sea west of the island is observed frequently in the infrared (IR) images from the GMS Satellite in the rainy season, especially when the prevailing winds are weak in the region [42]. Generally, the daily CG lightning occurrence around Kalimantan island and adjacent sea estimated using ten months of lightning data detected by AVON, as shown in figure 2.35, clearly represents the diurnal convective activity.

The diurnal variation of rainfall over Kalimantan, figure 2.36, is made using TRMM precipitation standard V7 data with the same period with AVON lightning data. So, it is comparable with the diurnal lightning result. Based on figures 2.35 and 2.36, the high rain intensity in the afternoon and evening along the west coast of Kalimantan is not followed by the high intensity of the rain. On the contrary, the high lightning density on the northeast coast of Kalimantan is not followed by a high intensity of rain.

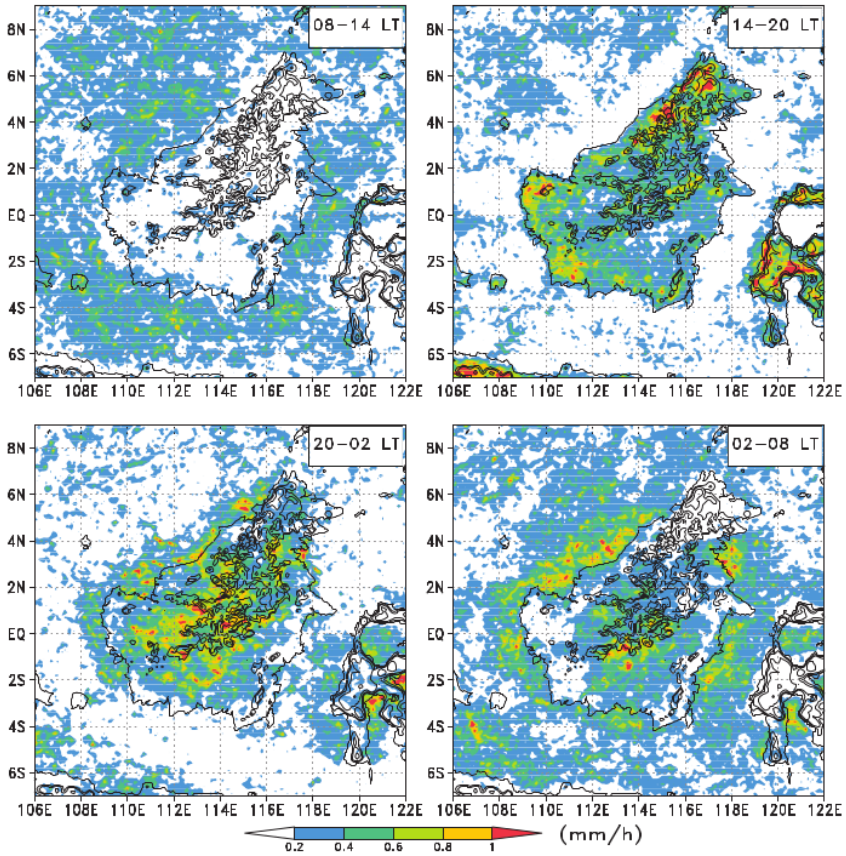

Figure 2.51. The annual mean near-surface rain detected by the TRMM Precipitation Radar (PR) for the six years from 1998 to 2003. Each panel shows the 6-hourly mean rainfall rate for the indicated time. Solid contours show terrain elevation in 500−m intervals. (Wu et al., 2008)

For other options, we make diurnal lightning density using Bliztzortung lightning data. Even though the Blitzortung detection networks' error and sensitivity are not known in this area, the number of lightning detector is more than AVON right now. Figure 2.52. shows the annual mean lightning density detected by Blitzortung for the three years from 2017 to 2019. The diurnal lightning event shows a similar pattern with the Wu et al. 2008, rainfall pattern which mostly occurs in the afternoon and evening along the coast island, and at night and in the early morning over the plains in the central region of the island and the sea adjacent to the coast.

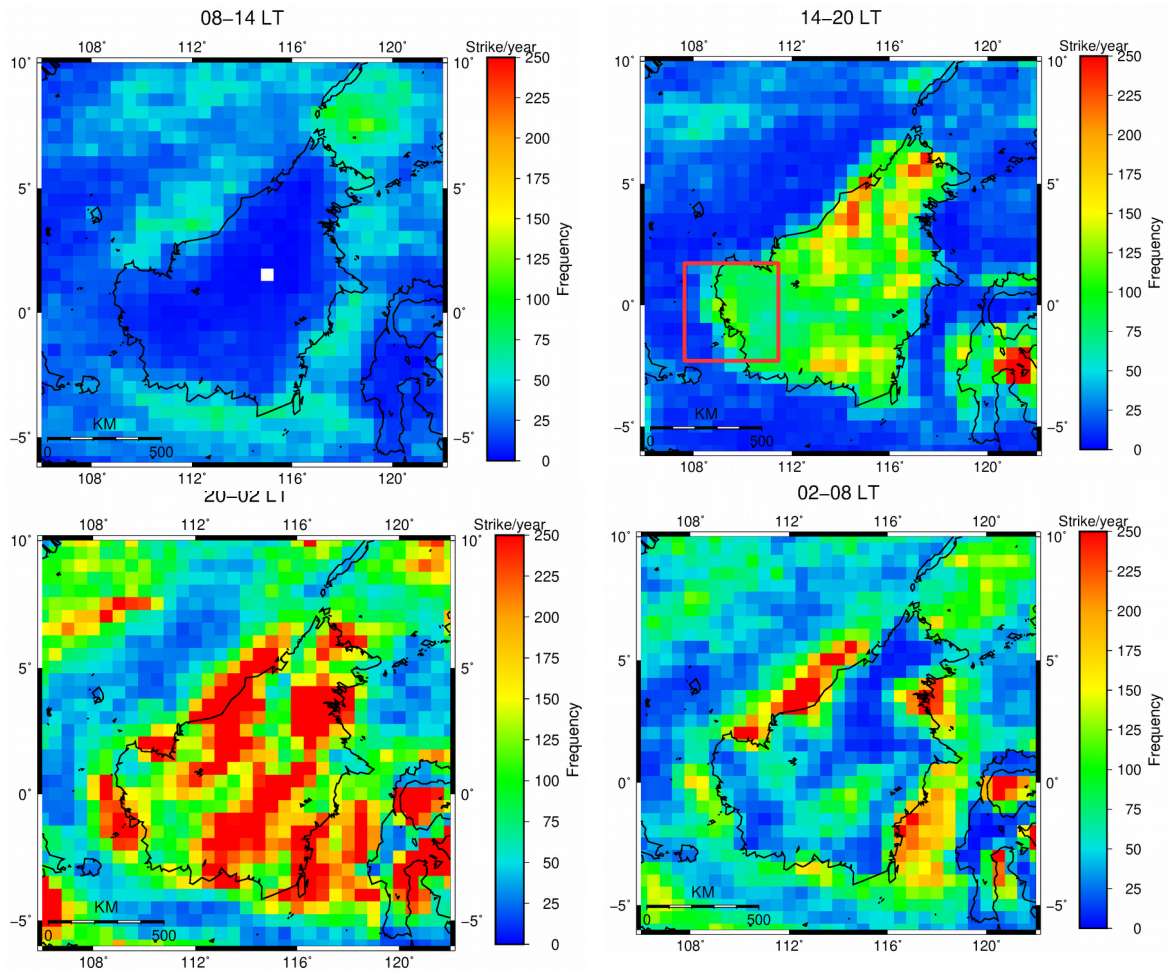

Figure 2.52. The annual mean lightning density detected by Blitzortung for the three years from 2017 to 2019. Each panel shows the 6-hourly accumulated lightning event with a grid 0.5ºx 0.5º during the period.

For the same three-year comparison, we are recreating the annual mean near-surface rain map using TRMM precipitation product standard V7. The result of this work is shown in figure 2.53. Based on figure 2.53, The diurnal pattern is still consistent with Wu et al., 2008, result and also generally consistent with the diurnal lightning pattern of Blitzortung. The case for Kalimantan's western coast in the afternoon to evening shown by the AVON lightning also appears in the diurnal lightning over Kalimantan using Blitzortung. In their study, Wu et al. 2008 mention that heavy rainfall mostly occurs in the late afternoon and evening.

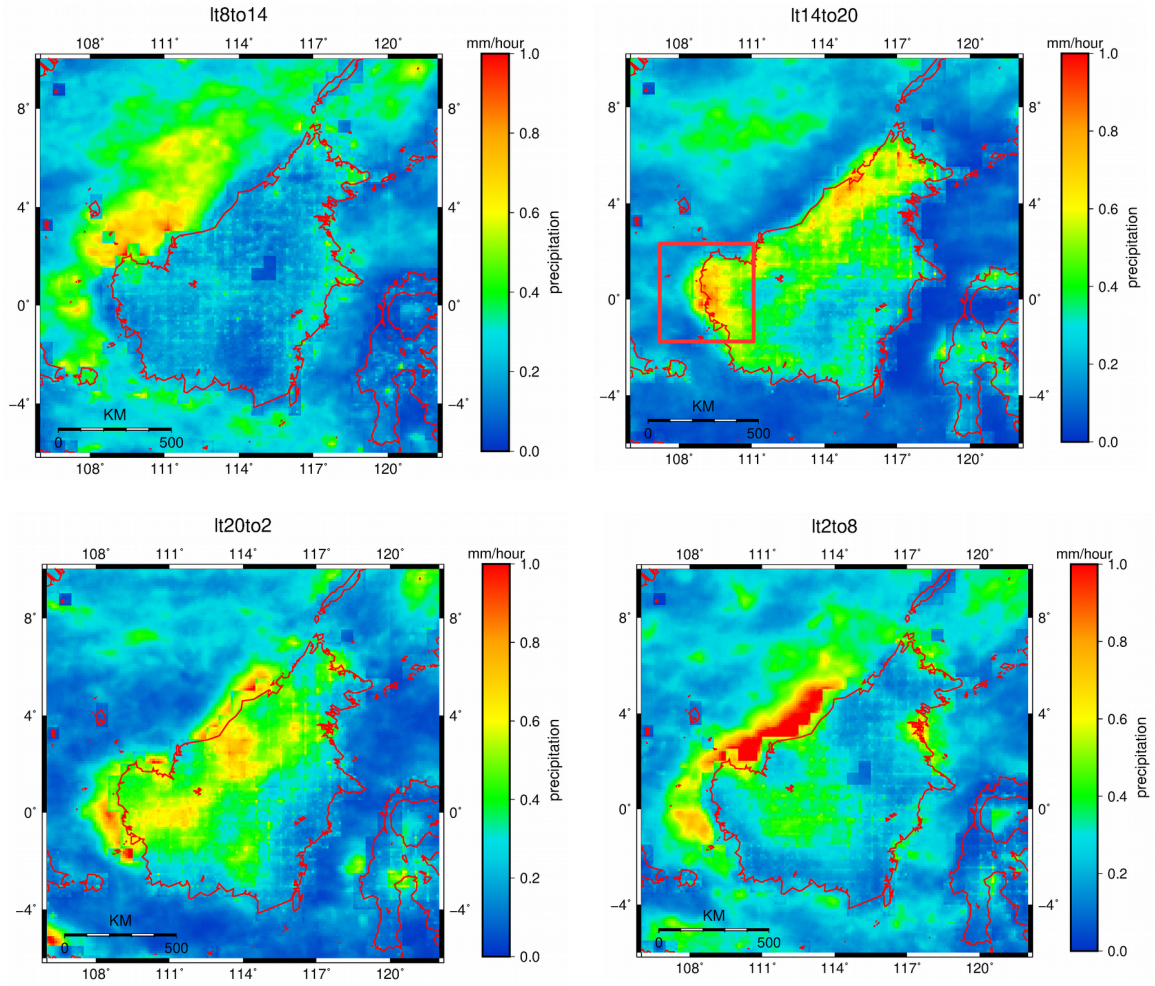

Figure 2.53. The annual mean near-surface rain detected by the TRMM Precipitation standard V7 for the three years from 2017 to 2019. Each panel shows the 6-hourly mean rainfall rate for the indicated period.

Moreover, we also perform the temporal graphic chart of the lightning data. Figure 2.54 shows the temporal data of AVON lightning, Blitzortung lightning, and area accumulation of CTT < -55ºC over Kalimantan Island. The lightning data is counted hourly of each month, July to December 2019. The CTT < -55ºC is used to indicate the thunderstorm cloud, which produces lightning. The CTT < -55ºC detected by Himawari 8 Band 15 is used to indicate the thunderstorm cloud's diurnal growth, which produces the lightning. The Himawari 8 Band 15, used in this study,

has 2 km spatial resolution and 10 minutes interval data. The area of the CTT < -55ºC is accumulated hourly of each month.

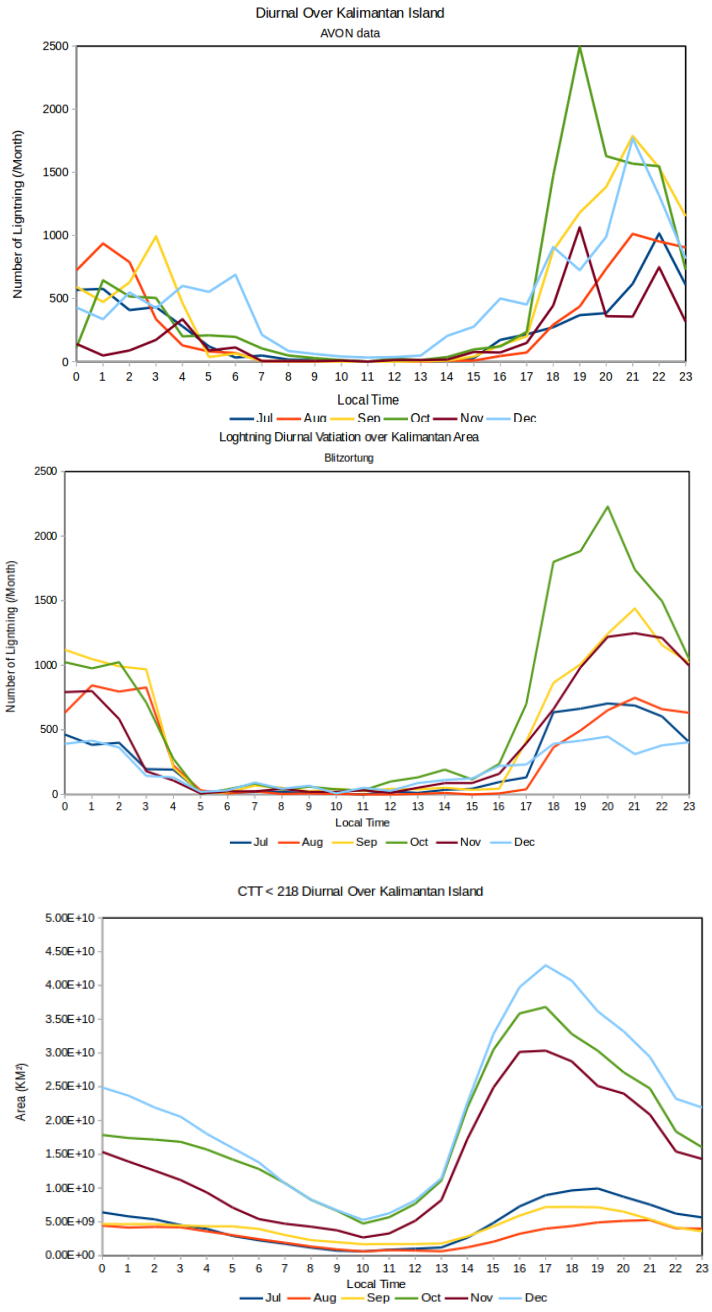

Figure 2.54. Diurnal Lightning and CTT < -55ºC over Kalimantan Island for July to December 2019.

Both lightning data in figure 2.54 show the slope and peak of lightning activity in the evening, which is not consistent with the accumulated CTT < -55ºC

area data. The accumulated CTT < -55ºC area starts raising in the afternoon and get a peak in ~17 local time, leading ~4 hours to the lightning peak. The drop number of lightning for both AVON and Blitzortung is around sunrise and sunset. Even though the CTT < -55ºC has ambiguity in describing the thunderstorm cloud, it is looked more reasonable diurnal variation of a thunderstorm cloud. So, we are suspicious that the lightning's detection is affected by the D region of the ionosphere condition, which is also affected by the sunlight. In this study, we will not discuss the lightning dependency on day and night. However, we must note that the number of lightning during the evening and morning can be more than the actual observations.

2.5.3. Typhoon

Price et al.; 2009, found that in all of the hurricanes, lightning frequency and maximum sustainable wind speed are significantly correlated with a correlation coefficient of 0.82 with the lag time ~30h. Whittaker et al., 2015, change the lightning collection of a 10° square window by the radial shape. They confirm that using radial lightning collection windows of < 500 km, the lag time between lightning and maximum sustainable wind speed is ~1 day. Both of them show a good correlation between lightning and sustainable wind speed. However, their result still misses the explanation of why this correlation happens.

By doing the back-tracing technique using wind speed at different levels of height and lightning is assumed to be proportional to latent heat energy, we could trace the typhoon's energy source. From the typhoon Trami case, we found that the energy source comes from -36 to -48 hours of wind travel in level 900 hPa (~1km). The reasonable conversion energy process is about -12 to -6 hours. However, this study still shows one analysis of typhoons. More sample is needed to get better conclusions of the explanation about the relationship between lightning and maximum sustainable wind speed of the typhoon.

2.5.4. Taal volcano eruption produce lightning

Volcanic plumps differ from thunderstorm clouds in the presence of tephra volcanic, aerosol, and gas content, as well as temperature profiles and convection methods. The addition of silicate particles plays another electrification mechanism. Besides, initially higher temperatures, seen in the close ventilation section of volcanic fur, inhibit the development of graupels. Then, the mechanism of ice filling becomes important to boast of lightning, which develops in the upper regions of the volcanic plume, where sub-freezing temperatures can increase ice formation [23-25].

Based on the news in online media, the big explosion of Taal Volcano is around 15:00LT (07:00 UTC)[37]. The cloud ash's temporal evolution shows that the maximum cloud growth speed is ~50 m/s at around 07:00 to 07:10 UTC, close to the big explosion time. The first CG lightning detected by V-POTEKA Nation-wide Network occurs at 07:47:25.15725 UTC. 34 V-POTEKA Nation-wide Network detects CG lightning during the Taal Volcano eruption on January 12th, 2020. Based on the temporal evolution, the lightning occurs after the maximum growth speed, and the high of the cloud almost reach the maximum height or in the low temperature below the freezing level. This work agrees with the previous study that the ice crystals are needed in the electrification mechanism. The crucial level observation of early thunderstorm cloud for target area must be focused on the cloud growth speed in the level 0°C to -40°C.

Chapter 3
Cloud Imaging

3.1. Introduction

Thunderstorm clouds can be identified as big and tall clouds and strong updraft at the beginning of thunderstorm cloud formation. Strong updraft inside the thunderstorm cloud increases the collision, coalescence, and friction between water droplets, groupel, and ice crystal. This process increases the particle size and the separation of electric charge, resulting in torrential rainfall and lightning stroke, respectively. Zipser, 1994, mentions that the occurrence of lightning in a thunderstorm requires strong updraft (7 m/s) at a temperature colder than 0°C to -20°C [30]. The study result in chapter 2 also shows that AVON can detect the CG lightning need CTT < -30°C. Observing the CTT and estimating the cloud growth speed becomes essential for observing the early formation of the thunderstorm cloud using a TIS camera.

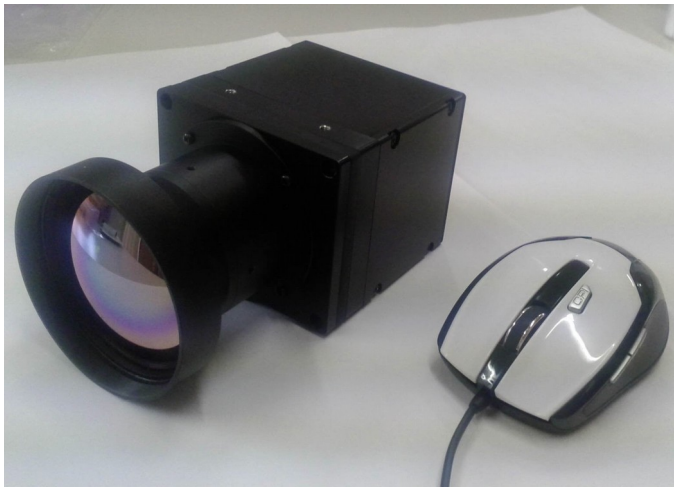

Figure 3.1. Hokkaido TIS camera size compare with a computer mouse

In this study, the TIS camera with the specs to observe the early beginning of thunderstorm development is developed. The physics behind the thunderstorm development and the atmosphere behavior in light absorption is the basis for choosing the filter and band of the camera. Besides that, the TIS camera must be robust again in the condition during storing, launching, and operation. In this study, we did some environmental testing, namely, thermal chamber test, vibration test, vacuum chamber test, and electromagnetic compatibility (EMC) test. All the testing is conducted at Hokkaido University.

3.2. LAPAN-A4 micro satellite

LAPAN-A4 is the micro-satellite developed by the Indonesian National Institute of Aeronautics and Space (LAPAN). LAPAN-A4 will be launched 3rd quarter of 2020. It has some missions, namely: earth observation using optical line scanner imager and TIS camera, global maritime traffic monitoring using AIS Space Receiver, a scientific mission using a space-based magnetometer. TIS camera design by Hokkaido University will be one of the payloads of this LAPAN-A4 microsatellite. Another payload that will bring by this micro-satellite is Automatic Identification System (AIS), Space-Based Magnetometer, Medium Resolution Imager (MRI), and High-Resolution Imager (HRI).

With all payload, power system, computer, and communication, the size and weight of the LAPAN-A4 microsatellite are simulated to be 744 mm x 700 mm x 520 mm and ~150 kg, respectively. The LAPAN-A4 is designed as a low earth orbit (LEO) microsatellite with the orbit 500 km and inclination 97°. The LAPAN-A4 is planned to be launched in the 3rd quarter of 2020 using the India rocket satellite. The LAPAN-A4 is designed to have the ability to rolling during flying in its orbits. Not only observe at nadir, but LAPAN-A4 can also be controlled to point some target areas.

3.3. Thermal infrared camera development

The Hokkaido University (HU) TIS camera is designed to detect the spectral radiance from 8 to 14 μm with lens filter 12μm. Using this spectrum that focuses on 12μm, the HU TIS camera can detect the clouds top with a small effect of the atmospheric absorption. The spatial resolution of the 0.294 mrad or 176 m surface resolution from orbit 500km. Using the HU TIS camera, the thunderstorm cloud could be observed in more detail than Himawari 8. In 500km orbit, the field of view (FoV) on the earth's surface becomes 56 x 42 km.

Table. 3.1. HU TIS camera specs

Wavelength	8-14 um (lens filter 12μm)
Spatial Resolution	0.294 mrad
	176 m
Field of view (FoV)	(H)5.4°x (V) 4.0°
	(H)56.3 x (V) 42.2 km
Measurement Temperature range	min: -60°C, max:+100°C
Temperature accuracy	< ±4°C
Temperature different resolution	< 100 mK
Frame rate per seconds	60 fps

The TIS camera is designed to have a minimum temperature of -60°C. With accuracy less than ±4°C, the accuracy of CTH will be less than ~400 meters. In the other hand, the different temperature resolution < 100mK will gives detailed information on the cloud's surface. As mentioned in some previous study, the electrification process occurs in range 0°C to -20°C with the updraft > 7 ms-1 so that the HU TIS camera can detect the early formation of thunderstorm clouds. Using the HU specs, the early formation of thunderstorm clouds could be grasped.

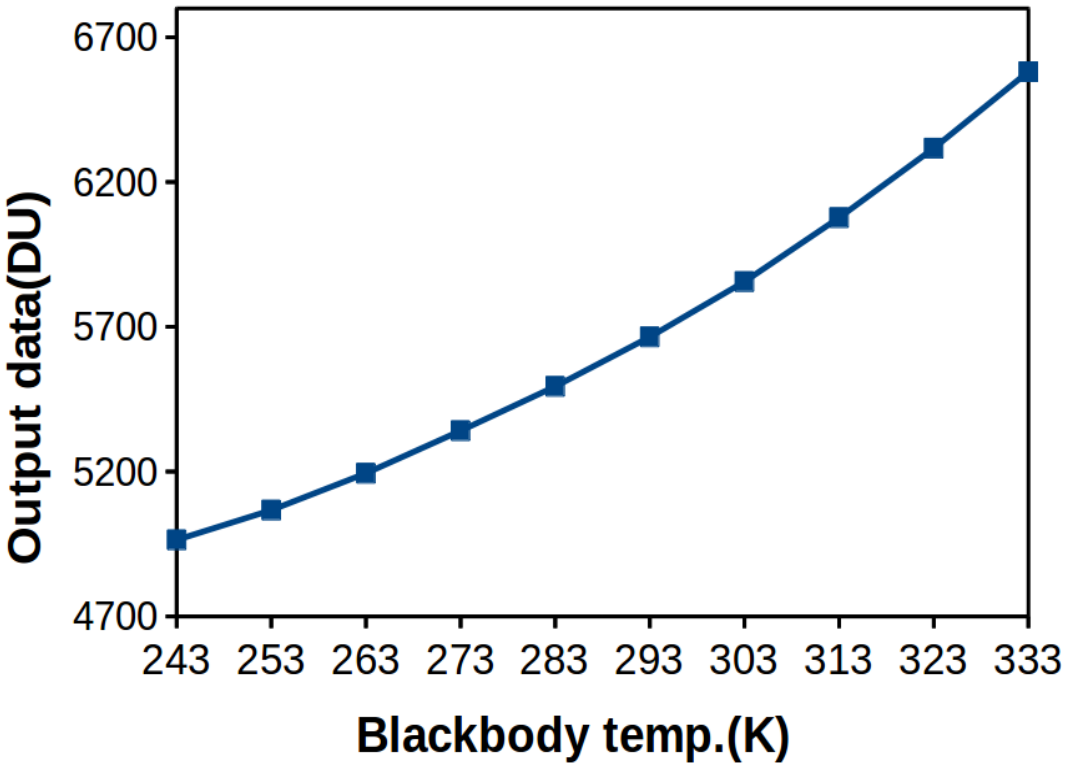

Figure 3.2. Calibration of HU TIS camera using black body temperature from 100°C to 30ºC.

3.3.1 Thermal chamber test

The HU TIS camera will get some various temperatures after it produced until its operation in space. During storing, testing, and installation on micro-satellite, the TIS camera will get room temperature, typically 25°C. The temperature produced by the electronic device is estimated at ~55 °C. The temperature in the rocket vehicle during launching is simulated to give the temperature ~80°C. After the LAPAN-A4 release from rocket vehicle, the micro-satellite temperature is simulated to be -40°C. After the LAPAN-A4 starting operation, the maximum temperature that produces whole

electronics in space is predicted to be ~55°C. The variation of the temperature during day and night in space operation is predicted to be ~55°C and -20°C, respectively. The thermal test is applied to the TIS camera to predict the robustness against the whole environment temperature condition, t. Besides the various temperature apply to the camera, the on and off condition also apply as the real condition. The camera will be off in the rocket vehicle and on during operation, and testing. The temperature profile during thermal tests is shown in figure 3.3.

Figure. 3.3. Temperature profile during thermal tests

The thermal vacuum chamber is done in the Space Mission Center (SMC) of Hokkaido University. The vacuum test is done from September 27th to October 1st, 2018. The electrical test is done by checking the voltage drop in the camera device. After getting the thermal treatment, the functionality of the camera is no chance. So, we conclude that the camera will remain robust again the thermal condition which will be passed by the TIS camera.

Figure. 3.4. TIS camera inside thermal chamber during thermal test in SMC

3.3.2 Vibration test

The space instruments are subjected to random vibration and shock along all three orthogonal axes during the launching process in rocket vehicles. The TIS camera must pass a vibration test that is used to simulate conditions at rocket launcher to reduce failure during the launch process with a rocket vehicle. The random vibration testing applied to the TIS camera at all frequencies within the specified bandwidth, namely 20 to 2000 Hz. For this random vibration analysis, units of g2 Hz^{-1} are used for the PSD of acceleration. The acceptance PSD value is determined by LAPAN.

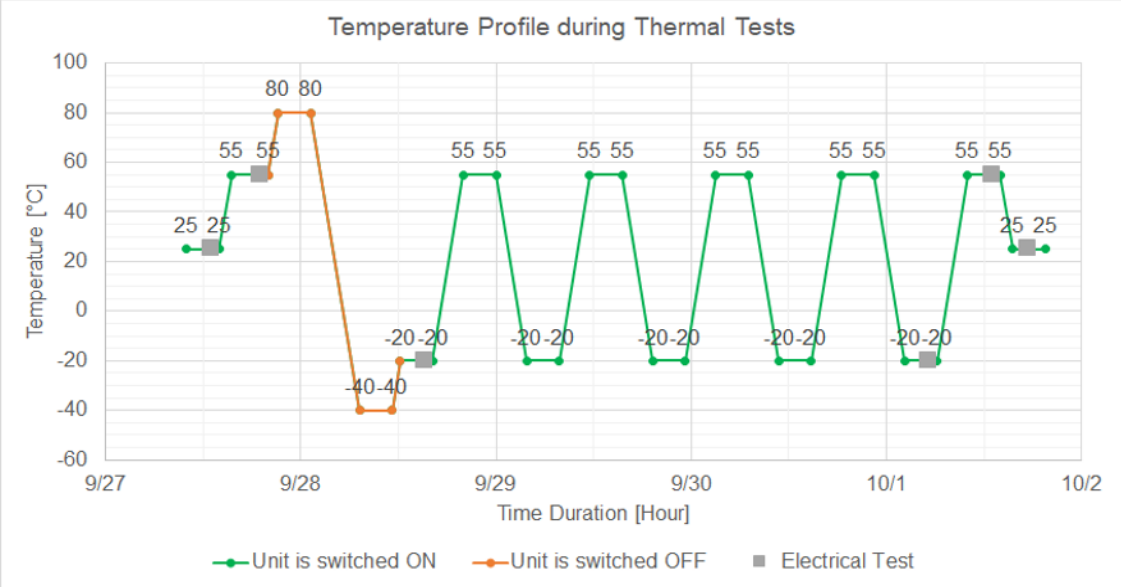

Table. 3.2. Random vibration test levels

Frequency	Acceptance PSD (g^2/Hz)
20	0.001
110	0.001
250	0.015
1000	0.015
2000	0.004
gRMS	4.47
Duration	1 min/axis

itation that either sweeps across a frequency band or dwells on a single frequency. Two types of

sinusoidal, namely longitudinal axis and lateral axis. The frequencies range and the acceptance level is described in table 3.3.

Table. 3.3. Sine vibration test levels

Sine Vibration test levels

	Freq. Range (Hz)	Acceptance level
Longitudinal axis axis	4-10	8 mm (0 to Peak)
	10-100	3 g
Lateral axis	2-8	8 mm (0 to Peak)
	8-100	2 g
Sweep rate		4 Oct / min

For both tests, the TIS camera was off. After both vibration testing, the camera has tested the functionality and showed working correctly.

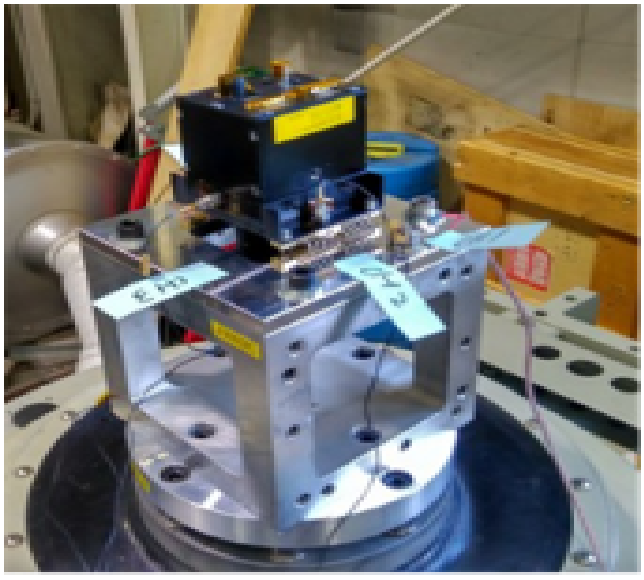

Figure. 3.5. TIS camera on the vibration machine

3.3.3. Vacuum chamber test

In space where this camera will be operated, the air temperature pressure almost zero. The hard vacuum of space (10^{-6} to 10^{-9} torr) will cause outgassing, which is the release of volatiles from materials. The outgassed molecules then deposit on line-of-sight surfaces and are more likely to deposit on cold surfaces. This molecular contamination can affect the optical properties of vehicle and payload surfaces and spacecraft performance, particularly for sensitive optics[43]. The vacuum test is done inside the SMC laboratory, with the pressure reach < 1 Pascal.

Figure. 3.6. TIS camera is tested in vacuum chamber

3.2.4. EMC Test

Space instrumentation is the subject of electromagnetic radiation overexposure. Electromagnetic radiation may come from cosmic radiation or the electromagnetic wave produced by electronic components in spacecraft. Electromagnetic radiation overexposure may cause some degradation of an electronic component in spacecraft. The HU TIS camera will be installed in LAPAN-A4 and other sensors, power systems, computers, and communication devices. Every device spacecraft may produce electromagnetic, which exposes the HU TIS camera. Moreover, cosmic ray

floods may hit the LAPAN-A4 and expose the HU TIS camera. So, we did the electromagnetic compatibility (EMC) test to recheck the HU TIS camera robustness these phenomena.

Table. 3.4. Frequency band and the type of antennas

Frequency Band	10kHz~30MHz	30 MHz~8.4 GHz	6 GHz~18GHz
Antenna	Loop Antenna	Trilog Antena	Horn Antenan

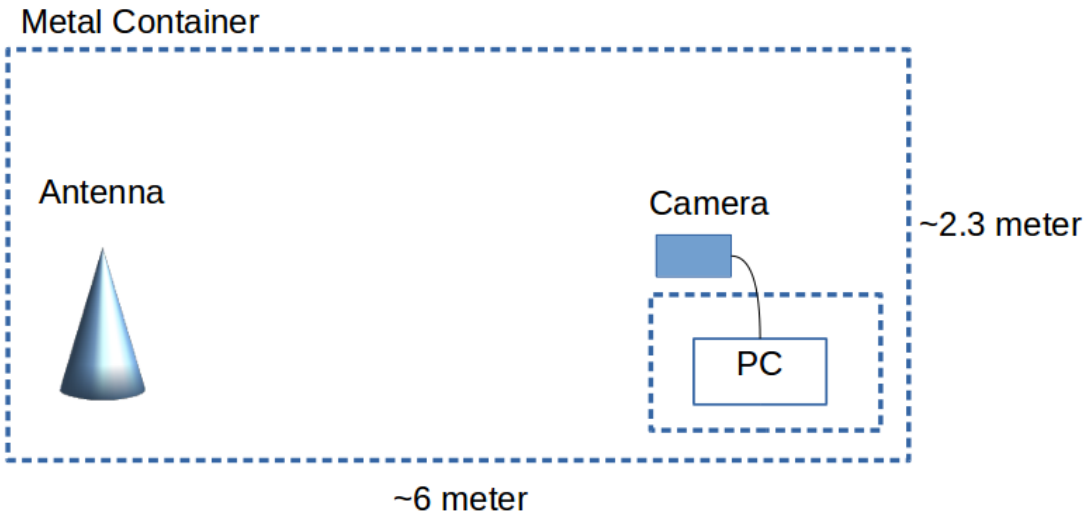

Figure. 3.7. Schematic of EMC test

We expose the camera with some various frequencies band inside the metal chamber. Different type of antenna is used to produce a maximum electromagnetic wave in different frequencies. The range frequency band and the type of antenna are shown in table 3.4. During the test, the HU TIS camera was on. The computers and cables are covered by metal to reduce the electromagnetic wave produced by other devices, . After the EMC test, the HU TIS camera has checked the functionality. The result HU TIS camera sustain this test again. So, the HU TIS camera is predicted to be robust against the electromagnetic exposure in space during operation.

3.4. Discussion

As shown in the previous study, the occurrence of lightning in a thunderstorm requires strong updraft (7 m/s) at a temperature colder than 0°C to -20°C[30]. The cloud growth speed at the beginning of thunderstorm formation is essential information to predict the result of thunderstorm clouds such as lightning and rainfall. Using the minimum temperature specs of the HU TIS camera, the camera can detect the early formation of thunderstorm clouds. The HU TIS camera has temperature accuracy < ±4°C, which means the accuracy of CTH estimation is 400 meters for the ideal environmental lapse rate 100m/°C. The HU TIS camera design to have the temperature difference resolution 100mK and frame rate per second 60fps. Using these specs and assuming the environmental lapse rate 100m/°C, the maximum and minimum cloud growth speed detected by the HU TIS camera is 600m/s and 10m/s. So, the HU TIS camera can detect thunderstorm clouds that are more active than the smallest thunderstorm clouds in the Zipser, 1994, study.

Chapter 4

Conclusion and suggestion for future work

4.1 Conclusion

This study evaluates the relationship between lightning activities and other thunderstorm clouds parameters such as CTT, CTH, and rainfall. This evaluation aims to create a suggested method for the real-time thunderstorm observation application using ground-based lightning detection networks and thermal infrared camera onboard microsatellite. During the Understanding of Lightning and Thunderstorm (ULAT) Project and e-Asia Joint research Project, 2017 to 2019 FSY, some VLF receiver with sampling frequencies 100 μs was deployed to cover cloud to ground (CG) lightning in Asian countries such as Northwest Pacific and southeast (AVON). Moreover, VLF receiver with sampling frequencies ten μs was deployed in the Philippines to cover lightning observation in that country (Nationwide Network). Both of VLF receiver is manufactured by Meisei Company-Japan and developed together with Hokkaido University. It can be and mostly combined with automatic weather stations (POint TEnki KAnsoku = POTEKA), so it is called V-POTEKA.

During the research period, the instrument was tested and operated. The lightning VLF signal received for every station shows matching with the general diurnal cycle of clouds. The lightning VLF signal received also shows the attenuation as the distance, which is typical in VLF signal propagation. Moreover, the lightning geolocation estimation software for both AVON and nationwide network is created using time of arrival (ToA) method. The result of the lightning geolocation estimation shows a consistent result which is matching with the cloud pattern. The comparison of the lightning geolocation estimate by the V-POTEKA lightning

detection networks and Blitzortung shows the relative distance 35km and 37 km for the V-POTEKA with sampling frequency 10μs and 100 μs, respectively. The absolute different time of detection between both types of V-POTEKA and Blitzortung for the same lightning is estimated to be 1 second and 823μs for the V-POTEKA with sampling frequency 10μs and 100μs, respectively.

The relationship between lightning and other thunderstorm cloud characteristics such as cloud top temperature (CTT), cloud top height (CTH), and precipitation has been conducted using AVON lightning data and static grid method. All the relationship shows that the CTT, CTH, and rainfall is a logarithmic function of lightning stroke. For the lightning and CTH relationship, the result is agreed with the previous work, which mentions that the total lightning is an exponential function of CTH. Using the grid 0.5ºx0.5º lightning density detected by AVON, we could draw the daily thunderstorm activities over Kalimantan and its adjacent sea. The lightning mostly occurs in the afternoon and evening along the coast island. Moreover, at night and early morning, lightning mostly occurs in the central region of Kalimantan island and the sea adjacent to the coast.

Generally, the result agrees with the diurnal rainfall pattern of TRMM precipitation standard V7 average, in the same period. The static target area observation method is suggested to predict torrential rainfall caused by thunderstorm cloud using a combination method of ground lightning detection networks and thermal infrared camera onboard micro-satellite.

During the operation, the V-POTEKA Nationwide Network in the Philippines detects the lightning produce by Taal Volcano eruption the cloud ash on January 12th, 2020. The evolution of development Taal Volcano eruption the cloud ash is detected using Himawari 8 band 15 (12μm) and performed in 2D and 3D. Based on the news in online media, the big explosion of Taal Volcano is around 15:00LT (07:00 UTC). The cloud ash's temporal evolution shows that the maximum cloud growth speed is ~50 m/s at around 07:00 to 07:10 UTC, which is closed to the big explosion time. The first CG lightning detected by V-POTEKA Nationwide Network occurs at 07:47:25.15725 UTC. V-POTEKA Nationwide Network detects CG lightning during

the Taal Volcano eruption on January 12th, 2020. Based on the temporal evolution, the lightning occurs after the maximum growth speed, and the high of the cloud almost reach the maximum height. The result of this work agrees with the Goodman, 1988 result. The crucial level observation of early thunderstorm cloud for target area must be focused on the cloud growth speed in the level 0°C to -40°C.

Moreover, the back-tracing technique has been applied for the first time in the world to investigate the relationship between typhoons' lightning and maximum sustainable wind speed. The lightning is assumed proportional to the energy and the wind to be the carrier of the energy. We did the back-tracing of the 60 points in radius 100 km to the typhoon eye. The speed and direction are taken from the ERA5 reanalysis at the pressure level 1000 hPa to 400 hPa with spatial resolution 0.25°x0.25°. We calculate a new point with interval time 30 minutes with the speed and direction updated to be the closest place and time of data. The lightning is counted using the back-tracing point windows with interval time 6 hours. This study shows that the wind in level 900 hPa is the most reasonable path to carry the energy to the typhoon Trami from place with the distance-time 36 hours to 48 hours from the typhoon Trami eye. The lag time in the maximum cross-correlation value between reaching center time and increasing maximum wind speed is 6-12 hours, which is assumed to be the conversion time of energy from latent heat to the kinetics energy.

Hokkaido University has designed the thermal infrared sensor (TIS) camera during this study. This TIS camera will be installed in the LAPAN-A4 satellite designed by LAPAN and launched in the third quarter of 2020. The thermal calibration has been done for the range of 100°C to -30°C, which is sufficient to observe the thunderstorm cloud in the early formation. The earth surface resolution in the LAPAN-A4 orbit, 500 km, is estimated to be ~176m, which is better than the existing geostationary satellite. The environmental testing such as thermal chamber test, vibration test, vacuum chamber test, and EMC test has been conducted to guarantee that the HU TIS camera will sustain against the condition in storing, launching, and operating. Using the HU TIS specs, the maximum and minimum thunderstorm growth speed is 600m/s and 10m/s, respectively.

4.2. Suggestions for future works

4.2.1. Semi real-time torrential rainfall alert applications

The empirical relationship achieved by this study can be used for the weather hazard alert or data assimilation for the numerical forecast. However, Some areas may have a specific local and seasonal characteristic of the thunderstorm cloud formation. However, this study result is done for the broad area and random season. The study for local and seasonal for a specific area is needed to get more precisely alert.

4.2.2. TIS camera space calibration

The TIS camera has been calibrated before launching. However, The calibration done on the ground may change when operating in space. The space calibration of TIS camera is recommended to do after the satellite LAPAN-A4 launched.

4.2.2. More typhoon analysis

However, in this work, we analyzed only for typhoon Trami analysis. In order to prove the back-tracing technique, we need to apply this method to other typhoons.

Bibliography

[1] Anonymous. “Hydro-meteorological Hazards.” Disaster Risk Reduction, Unesco, 2017, http://www.unesco.org/new/en/natural-sciences/special-themes/disaster-risk-reduction/natural-hazards/hydro-meteorological-hazards/#topPage

[2] Brooks, C.E.P. 1925. The distribution of thunderstorm over globe. Geophys. Mem. 24:147-64

[3] Krehbiel P.R. 1986 The electrical structure of thunderstorms, in The Earth's Electrical Environment (E.P. Krider et al., eds. Washington, DC: National Academy Press, pp 263)

[4] Gatlin and Goodman (2010), A total lightning trending algorithm to identify severe thunderstorm, Journal of atmospheric and oceanic technology, vol 27.https://doi.org/10.1175/2009JTECHA1286.1

[5] Ushio T., Heckman S.J., Boccippio D.J., Christian H.J., Kawasaki Z. 2001. A survey of thunderstorm flash rates compared to cloud top height using TRMM satellite data. Journal of geophysical research, Vol. 106, No. D20, pages 24.

[6] Williams, E. 2014. The Lightning Flash 2nd Edition: Charge structure and geographical variation of thunderstorm, IET, PP 1-15

[7] Zeng, D. 2010. Correlation between total lightning activity and precipitation particle characteristics observed from 34 thunderstorm. Acta Meteorological sinica. Vol24

[8] Gungle, B and Krider, E.P. 2006. “Cloud-to-ground and surface rainfall in warm-season Florida thunderstorms”, Journal of Geophysical research, Vol. 11, doi: 10.1029/2005JD006802

[9] Pirtilla J., Lehtinen M.S., Huuskonen A.,Markkanen M.. 2005.A Proposed Solution to the Range–Doppler Dilemma of Weather Radar Measurements by Using the SMPRF Codes, Practical Results, and a Comparison with Operational Measurements, American Meteorological Society, vol. 44, Page 1375-1390

[10] Hiroshi Kikuchi Mitsuteru Sato Tomoo Ushio Takeshi Morimoto Masayuki Kikuchi Atsushi Yamazaki Makoto Suzuki Ryohei Ishida Yuji Sakamoto Ting Wu Zen Kawasaki. 2017. Simultaneous observations of optical lightning from space and LF band lightning waveforms from the ground.geophysical research letters,vol. 44, pages 1123-1131 https://doi.org/10.1002/2016GL071783

[11] Yamashita K, Takahashi Y, Sato M., Kase H. 2011 Improvement in lightning geolocation by time-of-arrival method using global ELF network data Journal of Geophysic Research 116 pp 1-12

[12] Said R. K, Inan U.S., and Cummins K. L. 2010 Long-range lightning geolocation using a VLF radio atmospheric waveform bank Journalof Geophysics Research 115

[13] Kudo T 2014 A Study of lightning magnitudes and thunderstorm activity based on the observation of VLF sferics (Hokkaido University, Faculty of Science)

[14] Tapia A., Smith J. A., Dixon M. 1998. Estimation of Convective Rainfall from Lightning Observations. Journal Applied Meteorology 37 pp 1497-1509.

[15] Carey L. D, Rutledge S. A. 2000 The relationship between precipitation and lightning in tropical island convection: A C-band polarimetric radar study Mon. Wea. Rev. 128 pp 2687-2710.

[16] Soula S, Chauzy S. 2001 Some aspects of the correlation between lightning and rain activities in thunderstorms Atmospheric Research 56 pp 355–373.

[17] Seity Y, Soula S Tabary P and Scialom G 2003 The convective strorm system during IOP 2a of MAP: Cloud-to-ground lightning flash production to dynamics and microphysics Quarterly Journal of the Royal Meteorology Society 129 pp 523-542

[18] Williams E, Boldi B, Matlin A., Weber M., Hodanish S., Sharp D., Goodman S., Raghavan R., Buechler D. 1999 The behavior of total lightning activity in severe Florida Thunderstorms Atmospheric Research 51 pp 245-265.

[19] Goodman S J, Blakeslee R., Christian H., Koshak W., Bailey J., Hall J., McCaul E., Buechler D., Darden C., Burks J., Bradshaw T., and Gatlin P. 2005 The North Alabama Lightning Mapping Array: Recent severe storm observations and future prospects Atmospheric Research 76 pp 423-437

[20] MacGorman D. R, Burgess D.W., Mazur V., Rust W.D., Taylor W.L., and Johnson B.C. 1989 Lightning rates relative to tornadic storm evolution on 22 May 1981 Journal of Atmospheric Science 46 pp 221-250.

[21] Price C., M. Asfur, and Yair. Y. 2009. Maximum huricane intencity preceded by increase in lightning frequency. Nat. Geosci.,2,329-332, doi:10.1038/NGEO477

[22] Whittaker I.C, Douma E., Craig J. Rodjer, Marshall T. J.C.H. 2015. A quantitative examination of lightning as a predictor of peak winds in tropical cyclones. Journal of Geophysical Research: Atmosphere. Page 3789-3801.doi:10.1002/2014JD022868

[23] Van Eaton, A.R., Amigo, A., Bertin, D., Mastin, L.G., Giacosa, R.E., Gonzalez, J., Valderrama, O., Fontijn, K., Behnke, S.A., 2016. Volcanic lightning and plume behavior reveal evolving hazards during the April 2015 eruption of Calbuco volcano, Chile. Geophys. Res. Lett. 43 (7), 3563–3571. https://doi .org /10 .1002 /2016GL068076.

[24] Van Eaton, A.R., Mastin, L.G., Herzog, M., Schwaiger, H.F., Schneider, D.J., Wallace, K.L., Clarke, A.B., 2015. Hail formation triggers rapid ash

aggregation in volcanic plumes. Nat. Commun. 6, 1–7. https://doi .org /10 . 1038 /ncomms8860.

[25] Smith , C.M., Van Eaton A.R., Charbonnier S., McNutt S.R., Behnke, S.A, Thomas, R.J , Edens, H.E , Thompson, G. 2018. Correlating the electrification of volcanic plumes with ashfall textures at Sakurajima Volcano, Japan. Earth and Planetary Science Letters. 492. 47–58

[26] Lutz H.J, Inoue T., and Schmetz J.,. 2003. Comparison of a split-window and multi-spectral cloud classification for MODIS observation. Journal of the Meteorological Society of Japan, vol 81, page 623-631. https://doi.org/10.2151/jmsj.81.623

[27] Hamada A, Nishi N., Iwasaki S., Ohno Y., Kumagai H., and Okamoto H. 2008 Cloud type and top height estimation for tropical upper-tropospheric clouds using GMS-5 split-window measurements combined with cloud radar measurements Journal of Applied Meteorology and Climatology 4 pp 57–60

[28] Hamada A, Nishi N. 2010 Development of a Cloud-Top Height Estimation Method by Geostationary Satellite Split-Window Measurements Trained with CloudSat Data Journal of Applied Meteorology and Climatology 4 pp 2035–2049, doi:10.1175/2010JAMC2287.1.

[29] Zhe Wang, Zhenhui Wang, Xiaozhong Cao, Fa Tao. 2017. Comparison of cloud top heights derived from FY-2 meteoro-logical satellites with heights derived from ground-based millimeter wavelength cloud radar. Atmospheric Research, Doi:10.1016/j.atmosres.2017.09.009 (manuscript)

[30] Zipser E.J. 1994. Deep cumulonimbus system in the tropics with and without lightning, Mon. Weather rev, vol. 122, 1837-1851.

[31] Deierling W. and Petersen W.A. 2008. Total lightning activity as an indicator of updraft characteristic. Journal Geophysic Research. VOL. 113, D16210, doi:10.1029/2007JD009598

[32] Rakov V. A and M. A. Uman. 2003. Lightning Physics and Effects. Cambridge University press. The Eidenburgh Building, cambridge.

[33] Burke, C.P., and D.L. Jones 1992 On the polarity of and continuing currents in unusually large lightning flashes deduced from ELF event Journal of Atmospheric and Solar-Terrestrial Physics 54 pp 531-540

[34] Weidman C.D, Krider E.P 1986 The amplitude spectra of lightning radiation fields in the internal from 1 to20 MHz Radio Science 21 pp 964-970

[35] Kozo Yamashita.”AVON lightning observation in ELF and VLF range”. AVON winter school Feb. 5th 2015

[36] Katrina S. Virts and John M. Wallace, Michle L. Hutchins, Robert H. Holzworth. 2013. Diurnal lightning variability over Maritime Continent: impact of low-level wins, cloudines, and MJO. Journal of the atmospheric science. Vol 70, page 3128-3146. doi:10.1175/JAS-D-13-021.1

[37] Hidayat. S and Ishii M. 1996. Error in lightning location by time-difference and direction (TDD) technique-theory. T. IEE Japan, Vol. 116-B, No. 4

[38] https://en.wikipedia.org/wiki/2020_Taal_Volcano_eruption

[39] Berkowitz. R..”Q&A: Monitoring Volcanic Eruptions Using Lightning”. Physics 13, 44. March 27, 2020. https://physics.aps.org/articles/v13/44

[40] Genareau K., Gharghabi P., Gaford J. & Mazzola2 M., 2017. The Elusive Evidence of Volcanic Lightning. Scientific reports. 7, 15508 . DOI:10.1038/s41598-017-15643-8

[41] Hernandez, P. Melian G., Somoza L., Arpa M. C., Perez N.M., Bariso E., Sumino H., Padron E., Verekamp J.C., Albert-Beltran J., Solidum R.. 2017. The acid crater lake of Taal Volcano, Philippines: hydrogeochemical and hydroacoustic data related to the 2010– 11 volcanic unrest. Geochemistry and Geophysics of Active Volcanic Lakes. Geological Society, London, Special Publications, 437, https://doi.org/10.1144/SP437.17

[42] Wu P.,Yamanka M. D., Matsumoto J. 2008.The Formation of Nocturnal Rainfall Offshore from Convection over Western Kalimantan (Borneo) Island. Journal of the Meteorological Society of Japan, Vol. 86A, page 187-203. https://doi.org/10.2151/jmsj.86A.187